Reactivity of Nitrosyl Complexes of Co^{II}- and Mn^{II}-Porphyrinates with Reactive Oxygen Species: Putative Formation of Peroxynitrite Intermediates

A dissertation submitted to the
Indian Institute of Technology Guwahati as
Partial fulfillment for the degree of
Doctor of Philosophy in Chemistry

Submitted by

Baishakhi Mondal

(Roll No. 146122029)

Supervisor

Prof. Biplab Mondal

Department of Chemistry

Indian Institute of Technology Guwahati

September, 2019

Dedicated to My Family, Friends
&
Teachers

STATEMENT

I hereby declare that this thesis entitled "**Reactivity of nitrosyl complexes of Co^{II}- and Mn^{II}-porphyrinates with reactive oxygen species: Putative formation of peroxynitrite intermediates**" is the outcome of research work carried out by me under the supervision of Prof. Biplab Mondal in the Department of Chemistry, Indian Institute of Technology Guwahati, India.

In keeping with the general practice of reporting scientific observations, due acknowledgements have been made wherever the work described is based on the findings of other investigators.

September, 2019 **Baishakhi Mondal**

IIT Guwahati

भारतीय प्रौद्योगिकी संस्थान गुवाहाटी
INDIAN INSTITUTE OF TECHNOLOGY GUWAHATI
North Guwahati, Assam – 781039, India

Prof. Biplab Mondal
Department of Chemistry

Phone : + 91-361-258-2317
Fax: + 91-361-258-2349
E-mail: biplab@iitg.ernet.in

Certificate

This is to certify that **Ms. Baishakhi Mondal** has been working under my supervision since July, 2014 as a regular Ph.D. student in the Department of Chemistry, Indian Institute of Technology Guwahati. I am forwarding her thesis entitled "**Reactivity of nitrosyl complexes of Co^{II}- and Mn^{II}-porphyrinates with reactive oxygen species: Putative formation of peroxynitrite intermediates**" being submitted for the Ph.D. degree.

I certify that she has fulfilled all the requirements according to the ordinance of this Institute regarding the investigations embodied in her thesis and this work has not been submitted elsewhere for a degree.

September, 2019 **Biplab Mondal**

Acknowledgement

Through continued guidance and tremendous assistance from a lot of people, I am extremely privileged to have successfully completed my thesis. It would be a humble attempt on my part to gracefully thank all such people, who have been by my side in this endeavour.

First and foremost, I would like to express my sincere gratitude to my thesis supervisor, Prof. Biplab Mondal, for his continued support in my Ph.D. study and research. His patience, motivation, immense knowledge and guidance have been the key factors in submission of this thesis. No words on my behalf can ever be sufficient to express my thankfulness, which I owe to my thesis supervisor.

Alongside, I would like to thank the rest of my thesis committee members, Prof. Jubaraj Bikash Baruah, Prof. Gopal Das and Dr. Debapratim Das whose valuable suggestions have been instrumental in submission of my thesis.

My revered thanks to the teaching and non teaching staff of Department of Chemistry, IITG for their unhindered help. To Central Instrument Facility, IITG for providing instrument facility and to IITG for the financial support which is the prime backbone of any research.

To my lab seniors and lab mates Aswini Da, Vikash Da, Kanhu da, Hemanta Da, Somnath Da, Soumen Da, Kuldeep Da, Dibyajyoti Da, Rakesh, Shankhadeep, Bapan, Riya, Sayani and Anisha who have always been like a family to me during these 5 years, I owe you all my respect and love. Their immense help and support have always seen me through, even when the situation was tough. I have spent the most wonderful days of my research life with them.

To my Ph.D. colleagues, Upasana, Soumi, Ashalata, Renu, Koninika, Subas, Sayanta, Gourab, Utsab, Pinaki, Prasenjit, Suresh, Kalicharan and Archana I thank you for your support and staying by my side at all times.

To all my teachers, at every stage of life, I can never ever thank them enough with my words. Their teachings and guidance has helped me reach the stage, where I belong today.

To my family and friends-

My parents Mr Nilkanta Mondal and Mrs Nilmoni Mondal, who have been the backbone of my existence with their everlasting support, affection and encouragement in all my ventures.

To my dear sister, Susmita, I love you with my all heart and thank you for being by side. My heartiest thanks to Saumava, it was his companion and encouragement which help me to deal with the challenges that came across the journey and to proceed with more enthusiasm.

It is never possible to thank everybody, so if I have missed someone, I extend my humble apologies.

I am extremely honoured and grateful for the successful submission of my thesis and appreciate one and all, who have been involved in this journey of mine.

Baishakhi Mondal

Indian Institute of Technology Guwahati

Contents

Synopsis

The thesis entitled, **"Reactivity of nitrosyl complexes of Co^{II}- and Mn^{II}- porphyrinates with reactive oxygen species: Putative formation of peroxynitrite intermediates"** has been divided into five chapters.

Chapter 1: Introduction

Nitric oxide (NO) is synthesized in biological system by nitric oxide synthases (NOS) enzymes from L-arginine.[1] It plays major roles in controlling various physiological processes and only a submicromolar concentration of NO is required for its activity.[2,3] But overproduction results in cytotoxity through the formation of a secondary reactive species such as peroxynitrite ($ONOO^-$) (PN) ion and NO_2.[4-6] PN is proposed to form in the reaction of NO with superoxide (O_2^-) ion in a diffusion controlled rate. Alternatively, it can also be formed by the reaction of hydrogen peroxide (H_2O_2) and nitrite (NO_2^-) in the presence of the peroxidase enzymes.[7,8] Nitric oxide dioxygenase (NODs) enzymes are known to control the *in vivo* level of NO by converting it into the biologically benign nitrate (NO_3^-). This reaction is proposed to proceed through the formation of a Fe^{III}-PN intermediate in the reaction of Fe^{III}-superoxo [$Fe^{III}(O_2^-)$] species with NO.[9,10] It has been proposed that the O-O bond of Fe^{III}-PN intermediate homolytically cleaved to yield an oxo-ferryl, [$Fe^{IV}(O)$] species. In recent past, the reactions of dioxygenated complexes of oxymyoglobin (oxyMb) and oxyhaemoglobin (oxyHb) with NO to form their corresponding met forms and NO_3^- ion have been proposed to proceed through the corresponding Fe^{III}-PN intermediate.[9,11] But direct evidence for PN formation is still elusive due to their very unstable nature. In addition reports on the formation of high-valent metal oxo from metal PN intermediates are also rare. Model complexes like iron / manganese porphyrinates are reported to react with PN anion. These reactions were

proposed to go through Fe/Mn^{IV}=O species which formed by the homolytic cleavage of O-O bond of the proposed Fe/Mn^{III}-PN complexes.[12-16] For example it has been reported that the reaction of NO with a iron superoxo complex in heme system, [(THF)(F_8TPP)Fe^{III}(O_2^-)] (F_8TPPH_2 = tetrakis(2,6-difluoro-phenyl)porphyrin) lead to the corresponding NO_3^- complex *via* a putative PN intermediate formation.[17]

Classic examples of formation of oxo species *via* the formation of transient PN complexes are reported in two chromium complexes of 12-TMC and 14-TMC ligands. Spectroscopic evidence confirmed the formation of high-valent Cr^{IV}=O (Scheme S1).[18]

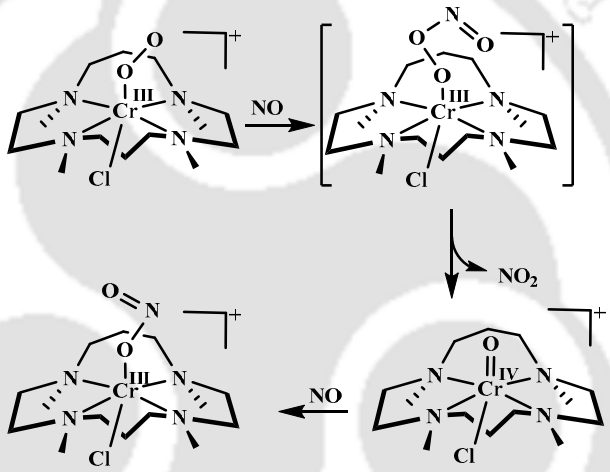

Scheme S1

Our group is also active in this area. We reported a cobalt peroxo complex in bis(2-ethyl-4-methyl-imidazol-5-yl)methane ligand reacts with NO to form Co^{II}-(NO_3^-) *via* putative PN complex formation.[19]

The reaction of a {CuNO}^{10} with H_2O_2 has been demonstrated to result in the formation of corresponding NO_3^- product where the involvement of a PN intermediate is presumed.[20]

In continuation, a nitrosyl complex of cobalt porphyrinate [(Cl_4TPP)Co], [Cl_4TPPH_2 = 5,10,15,20-tetrakis(4-chlorophenyl)porphyrin] was made to react with H_2O_2 to yield the Co^{III}-(NO_2^-) complex with the simultaneous release of O_2. The involvement of a Co^{III}-PN

intermediate was implicated (Scheme S2) in the reaction.[21]

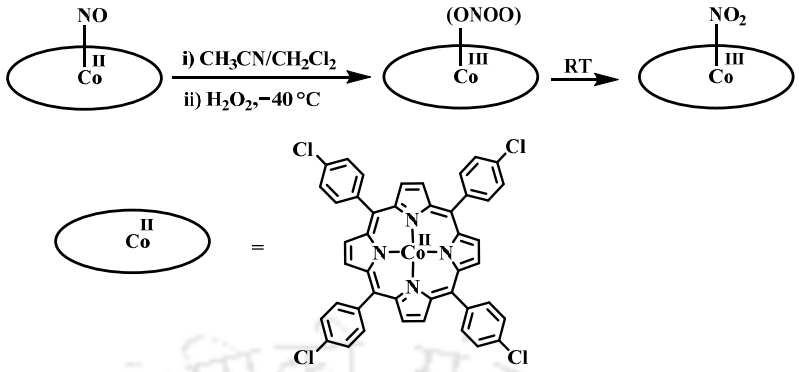

Scheme S2

However, none of these results demonstrate the direct evidence of the formation of metal-PN or metal-oxo intermediate as a result of homolytic O-O bond cleavage of the proposed metal-PN intermediate. This is perhaps because of the very fast recombination of metal-oxo species and NO_2 in the given reaction cage.

The present thesis work originated from our interest to identify the metal-PN as an intermediate in the reactions of metal nitrosyls with reactive oxygen species and to identify the involvement of high valent metal-oxo species in the decomposition or nitration reaction induced by metal PNs. The second chapter of the thesis describes reaction of a $\{CoNO\}^8$ complex of ligand, **L1H$_2$** (**L1H$_2$** = 5,10,15,20-tetrakis(2,6-difluorophenyl)porphyrin) and H_2O_2 and its successive decomposition to Co^{III}-(NO_3^-) *via* the corresponding Co^{IV}=O intermediate. The formation of a Co^{III}-PN was implicated. The third chapter demonstrates the reaction of [(L2)Mn^{II}(NO)] (**L2H$_2$** =5,10,15,20-tetrakis(4-chlorophenyl)porphyrin) with O_2^- to result in a NO_2^- complex *via* a putative Mn^{III}-PN intermediate. The fourth chapter describes the reactivity of [(L1)Mn^{II}(NO)] complex with O_2^- to result in a Mn^{III}-(NO_3^-) complex through a putative Mn-PN intermediate. The final chapter deals with the reaction of [(L3)Mn^{II}(NO)] (**L3H$_2$** = 5,10,15,20-tetrakis(pentafluorophenyl)porphyrin) complex with O_2^- to result in a Mn^{III}-(NO_3^-) complex *via* a putative Mn^{III}-PN intermediate.

Spectroscopic investigations revealed the formation of a Mn^{IV}=O in the course of the reaction.

Chapter 2: Nitric Oxide Dioxygenase Activity of a Nitrosyl Complex of Co^{II}-Porphyrinate in the Presence of Hydrogen Peroxide *via* Putative Peroxynitrite Intermediate

A cobalt(II) complex (**2.1**) was synthesized using ligand **L1H$_2$** (**L1H$_2$** = 5,10,15,20-tetrakis(2,6-difluorophenyl)porphyrin) by following reported procedure.[22] Complex **2.1** was characterized by various spectroscopic techniques. The corresponding nitrosyl complex (**2.2**) was prepared by bubbling NO gas into the dry and degassed dichloromethane solution of complex **2.1**. The nitrosyl complex, **2.2** was isolated and characterized spectroscopically. Structural characterization for complex **2.2** revealed that the Co^{II} is in square pyramidal geometry where the NO moiety is bonded axially (Figure S1(i)). In UV-visible spectroscopy complex **2.2** exhibited characteristic absorption bands at 404 (ε/M^{-1} cm^{-1}, 1.40 × 10^5) and 531 (ε/M^{-1} cm^{-1}, 1.53×10^4) nm. In the FT-IR spectrum, the strong stretching frequency at 1692 cm^{-1} in KBr is assignable to the coordinated NO group of complex **2.2** (Figure S2(i)).

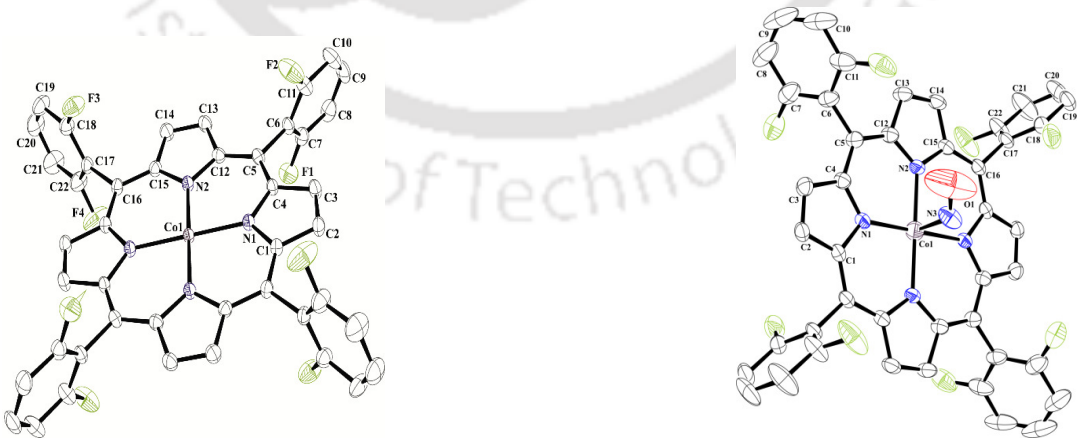

(i) (ii)

Figure S1. ORTEP diagrams of complexes **2.1** (i) and **2.2** (ii) (50% thermal ellipsoid plot, H-atoms and solvent molecules are omitted for clarity).

It was found to be EPR silent as expected due to antiferromagnetic coupling between the Co^{II} and NO moiety. The appearance of well resolved peaks at 8.95, 7.77 and 7.38 ppm in the ^{1}H NMR spectrum is also in agreement with the diamagnetic nature of complex **2.2**.

It was observed that complex **2.2** in dichloromethane solution is inert toward O_2. However, in acetonitrile solution it reacts with H_2O_2.

In UV-visible spectroscopy, the characteristic absorption bands of **2.2** at 404 and 531 nm disappeared with the formation of new bands at 430 ($\varepsilon/M^{-1}cm^{-1}$, 2.18×10^{5}) and 542 ($\varepsilon/M^{-1}cm^{-1}$, 1.77×10^{4}) nm, respectively (Figure S2(ii)). Complex **2.3** was isolated and characterized as the NO_3^- complex of the corresponding Co^{III}-porphyrinate, [(L1)Co(NO_3)], **2.3**.

In ESI-mass spectrometry complex **2.3** displayed peak at m/Z, 877.05 (calcd. m/Z 877.07) (Figure S3(i)). In the FT-IR spectroscopy, the observed stretching frequency at 1385 cm^{-1} is assignable to the NO_3^- stretching.

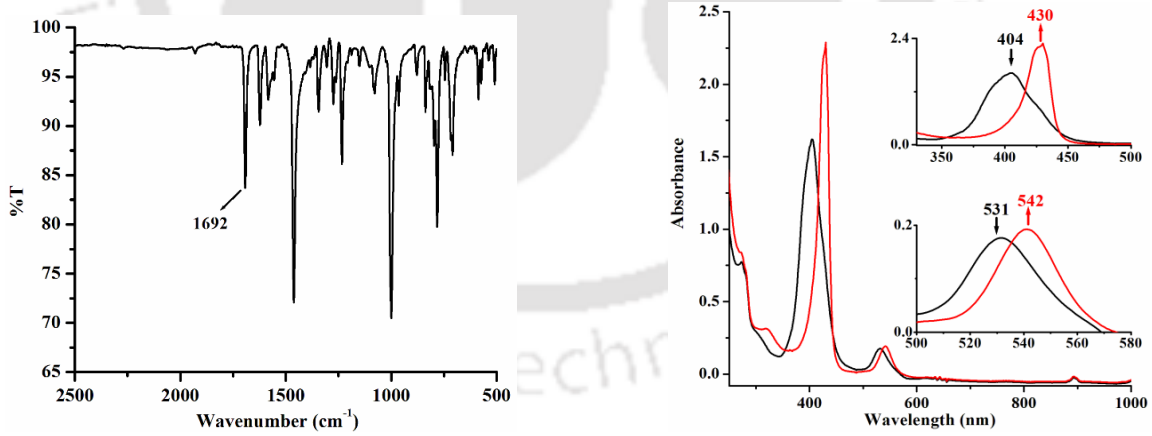

(i) (ii)

Figure S2. (i) FT-IR spectrum of complex **2.2** in KBr. (ii) UV-visible spectra of complex **2.2** (black) and after addition of H_2O_2 to result in complex **2.3** (red) in acetonitrile at –40 °C.

The reaction of complex **2.2** with H_2O_2 is proposed to go through a Co^{III}-PN intermediate

which could not be detected in UV-visible spectroscopy due to its transient nature. In X-band EPR spectroscopy the frozen reaction mixture shows a sharp peak at g = 2.002 at 77 K indicating the formation of new radical species (Figure S3(ii)). This has been attributed to the formation of a [(L1)Co^{III}-$O^{\bullet}$] radical complex (**2.2b**) which is formed from the O-O bond cleavage of the proposed Co^{III}-PN intermediate. (Scheme S3)

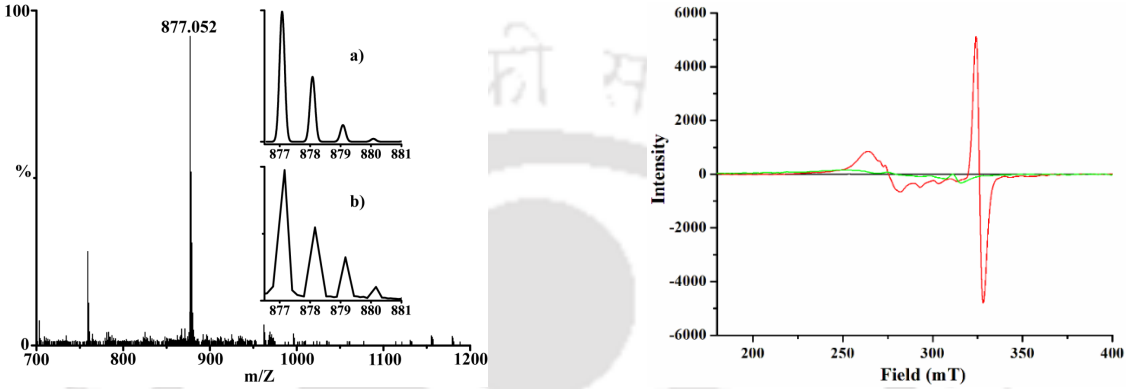

(i) (ii)

Figure S3. (i) ESI-mass spectrum of complex **2.3** in acetonitrile. [Inset shows the simulated (a) and experimental (b) isotopic distribution pattern in acetonitrile.] (ii) X-band EPR spectra of complexes **2.2** (black), **2.2b** (red) and **2.3** (green) in THF at 77K.

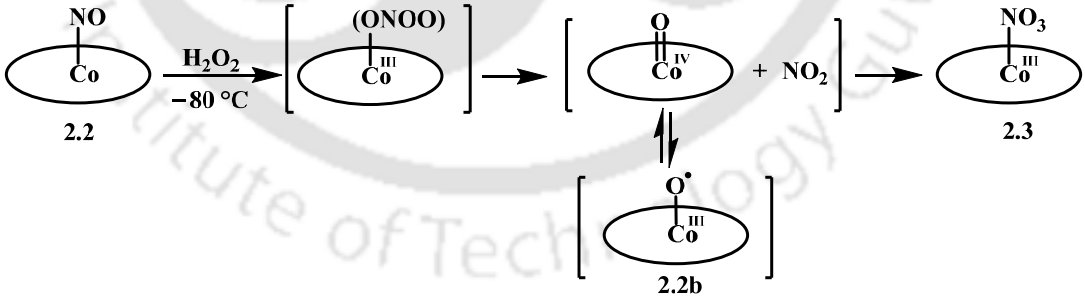

Scheme S3

Since we did not get any direct spectroscopic evidence for formation of Co^{III}-PN intermediate, we sought chemical evidence for the postulated species. Effective nitration (~50%) and corresponding Co^{III}-hydroxo product (~67%) were observed when 2,4-di-*tert*-butylphenol (DTBP) was added to complex **2.2** before the addition of H_2O_2.

Chapter 3: Reaction of a Nitrosyl Complex of Mn^{II}-(Cl_4TPP) Complex with Superoxide: Putative Formation of Peroxynitrite Intermediate

The nitrosyl complex of Mn^{II}-porphyrinate, [(L2)Mn(NO)], **3.2**, (**L2H$_2$** = 5,10,15,20-tetrakis(4-chlorophenyl) porphyrin) was prepared from the corresponding chloro complex, **3.1** following a reported procedure.[23] Red crystalline complex **3.2** was characterized by various spectroscopic techniques as well as single crystal structure determination. The ORTEP diagram reveals that complex **3.2** is in square pyramidal geometry where the NO group is bonded in linear fashion (Figure S4(ii)). The NO bond length is 1.096 (9) Å and the Mn-N-O bond angle is 180.0°. The complex **3.2** shows absorption bands at 426 (ε/M^{-1} cm^{-1}, 1.27×10^5) and 545 (ε/M^{-1} cm^{-1}, 1.60×10^4) nm in dichloromethane solution in UV-visible spectroscopy.

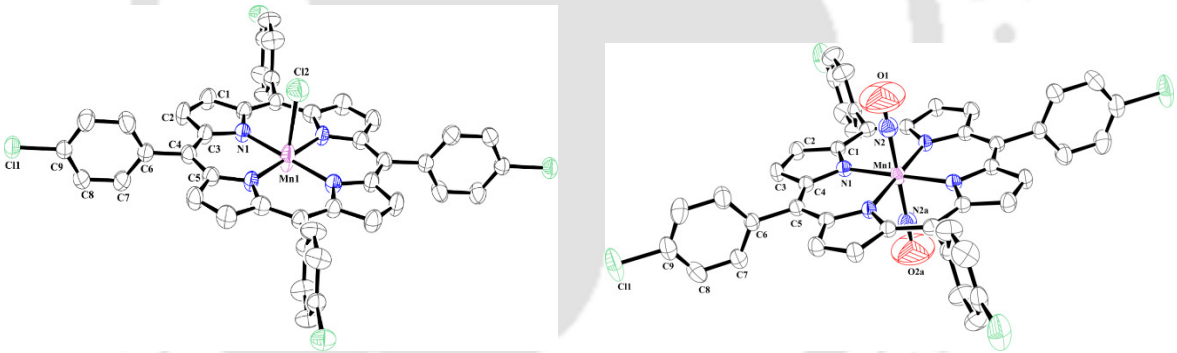

(i) (ii)

Figure S4. ORTEP diagrams of complexes **3.1** (i) and **3.2** (ii) (50% thermal ellipsoid plot, H-atoms and solvent molecules are omitted for clarity) (occupancy for both the NO is 50 %).

In the FT-IR spectrum, the NO stretching appeared at 1770 cm^{-1} (Figure S5(i)). Complex **3.2** is EPR silent as expected.

In UV-visible spectra, upon addition of KO_2 in C.E. (C.E. = 18-crown-6 ether) to the dichloromethane solution of complex **3.2** at −80 °C, characteristic bands at 426 and 545

nm gradually disappeared and new bands appeared at 478 (ε/M^{-1} cm^{-1}, 1.62 × 10^5), 582 (ε/M^{-1} cm^{-1}, 1.96 × 10^4) and 618 (ε/M^{-1} cm^{-1}, 2.07 × 10^4) nm. (Figure S5(ii))

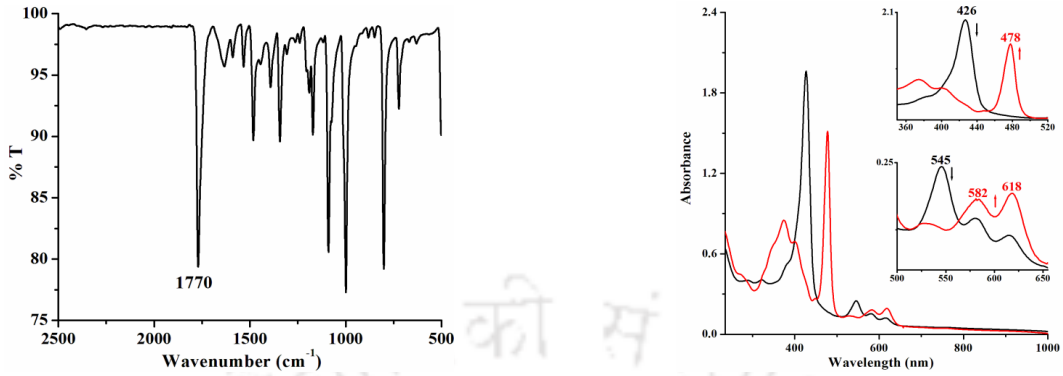

(i) (ii)

Figure S5. (i) FT-IR spectrum of complex **3.2** in KBr pellet. (ii) UV-visible spectra of complex **3.2** (black) and after addition of KO_2 in C.E. to result in **3.3** (red) in dichloromethane at −80 °C.

FT-IR spectrum displays formation of new peak at 1249 cm^{-1}, which is assignable to NO_2^- stretching frequency (Figure S6(i)). The final product was isolated and crystallized. The crystal structure revealed the final complex as the corresponding bridged NO_2^- complex, **3.3** (Figure S6(ii)).

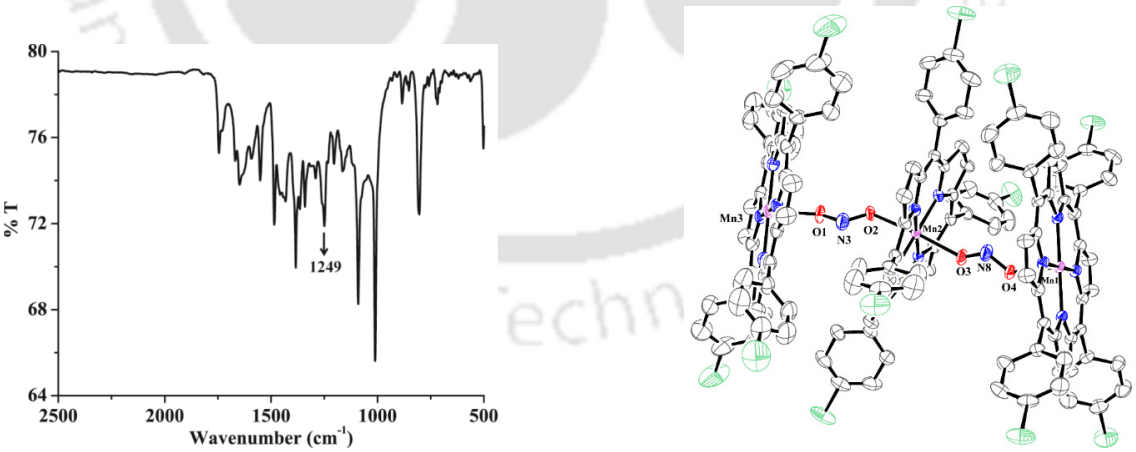

(i) (ii)

Figure S6. (i) FT-IR spectrum of complex **3.3** in KBr. (ii) ORTEP diagram of complex **3.3** (35% thermal ellipsoid plot, H-atoms and solvent molecules are omitted for clarity).

The formation of the complex **3.3** in the reaction of complex **3.2** with O_2^- proceeds through

the formation of a putative PN intermediate which was confirmed by phenol nitration reaction. When DTBP was added before the addition of KO_2 in C.E. to the solution of **3.2**, an appreciable nitration (~40%) along with corresponding bisphenol (~20%) formation was observed.

Chapter 4: Reaction of a Nitrosyl Complex of Mn^{II}-(F_8TPP) with Superoxide: Putative Formation of Peroxynitrite Intermediate

The ligand, **L1H$_2$** and its manganese complex, **4.1** were prepared following the reported procedure. The corresponding nitrosyl complex, **4.2** was synthesized by following the reported procedure with slight modification.[23] It was characterized by various spectroscopic techniques as well as single crystal structure determination. The crystal structure shows that **4.2** is a penta-coordinated nitrosyl complex (Figure S7(ii)).

In UV visible spectroscopy complex **4.2** exhibits characteristic absorption bands at 418 ($\varepsilon/M^{-1}cm^{-1}$, 1.43 × 10^5) and 535 ($\varepsilon/M^{-1}cm^{-1}$, 1.97 × 10^4) nm in THF. In FT-IR spectroscopy, the complex **4.2** in KBr displays nitrosyl stretching at 1762 cm^{-1} (Figure 8(i)).

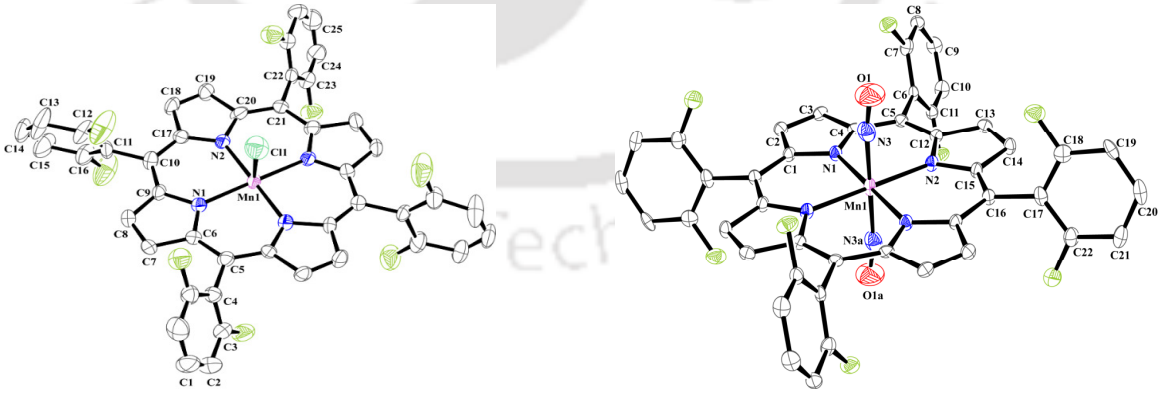

(i) (ii)

Figure S7. ORTEP diagrams of complexes **4.1** (i) and **4.2** (ii) (50 % thermal ellipsoid plot, H-atoms and are removed for clarity) (occupancy for both the NO is 50 %).

Complex **4.2** in THF solution was found to react with KO_2 in C.E. to result in the

corresponding Mn^{III}-(NO_3^-) complex, **4.3** where the involvement of a metal-PN intermediate is implicated.

In UV visible spectroscopy the absorption bands for complex **4.2** in THF solution at 418 and 535 nm disappears with the appearance of new peaks at 462 and 553 nm upon addition of one equivalent of potassium superoxide in C.E. at −80 °C (Figure 8(ii)). The appearance of the new peaks is attributed to the formation of complex **4.3**. It should be noted that even at −80 °C, no intermediate formation was observed.

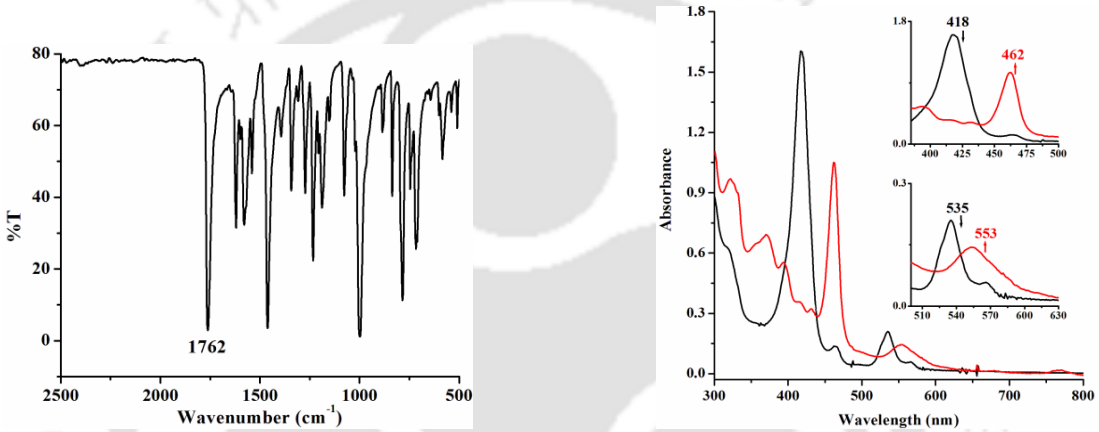

(i) (ii)

Figure S8. (i) FT-IR spectrum of complex **4.2** in KBr. (ii) UV-visible spectra of complex **4.2** (black) and after addition of KO_2 in C.E. to result in complex **4.3** (red) in THF at −80 °C.

In the FT-IR spectrum, complex **4.3** showed new stretching frequencies at 1384 and 1295 cm^{-1} which are attributed to the NO_3^- stretching.

The ESI-mass spectrum displays peak at m/Z value 873.03 [calcd. m/Z, 873.08] which corresponds to the [(L1)Mn^{III}(NO_3)]. Thus mass spectral results also support the formation of complex **4.3**.

Finally, the crystal structure revealed that the Mn^{III} center is bonded with four nitrogen atoms from the porphyrin ring and one axially bonded NO_3^- anion in a square pyramidal geometry (Figure S9).

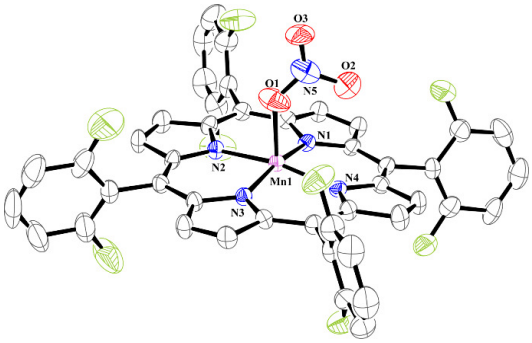

Figure S9. ORTEP diagram of complex **4.3** (50% thermal ellipsoid plot, H-atoms are omitted for clarity).

The formation of **4.3** can be envisaged through the formation of a putative PN intermediate in the course of the reaction. When DTBP was added before the addition of KO_2 to the solution of **4.2**, an appreciable nitration product (~45%) along with corresponding bisphenol (~10%) formation was observed.

Chapter 5: Nitric Oxide Dioxygenase activity of a nitrosyl complex of Mn^{II}-(F_{20}TPP) in presence of superoxide: Formation of a Mn^{IV}-oxo species through a putative peroxynitrite intermediate

The manganese nitrosyl complex, [(L3)Mn(NO)] (**5.2**) [**$L3H_2$** = (5,10,15,20-tetrakis(pentafluorophenyl)porphyrin)], was prepared from the reaction of [(L3)Mn(Cl], **5.1** with hydroxylamine following the reported procedure with slight modification.[23] It was characterized through various spectroscopic techniques as well as by single crystal structure determination. The ORTEP diagram of complex **5.2** shows that it is a five coordinated nitrosyl complex (Figure S10(ii)). In THF solution complex **5.2** shows absorption bands at 415 (ε/M^{-1} cm^{-1}, 1.04×10^5), 532 (ε/M^{-1} cm^{-1}, 1.02×10^4) and 564 (ε/M^{-1} cm^{-1}, 3.95×10^3) nm (Figure S11(ii)).

In FT-IR spectroscopy, the complex **5.2** displays nitrosyl stretching frequency at 1763 cm^{-1} (Figure S11(i)). After addition of a precooled THF solution of KO_2 in C.E. to the

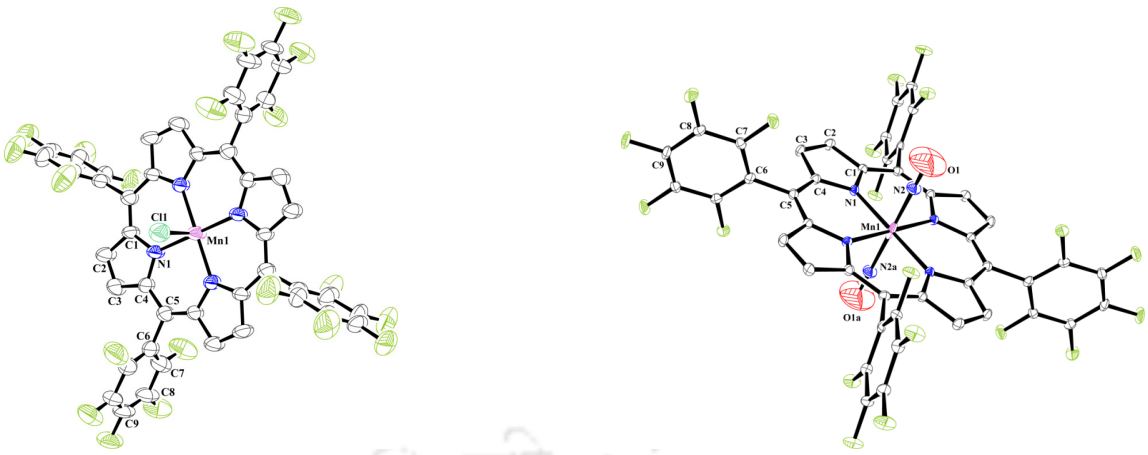

(i) (ii)

Figure S10. ORTEP diagrams of complexes **5.1** (i) and **5.2** (ii) (50 % thermal ellipsoid plot, H-atoms and solvent molecules are removed for clarity) (occupancy for both the NO is 50 %).

THF solution of **5.2** at −80 °C the characteristic soret band for complex **5.2** at 415 nm decreases along with a concomitant formation of new absorption bands at 426 and 458 nm. The 426 nm band was transient and disappeared but the intensity of 458 nm band increased (Figure S11(ii)). The isolated final complex **5.3** which is a NO_3^- complex of Mn^{III}-porphyrinate, showed soret band at 458 nm. The transient 426 nm band is attributed to the absorption of the corresponding Mn^{IV}-oxo species which is formed *via* the homolytic O-O bond cleavage of a presumed Mn^{III}-PN intermediate.

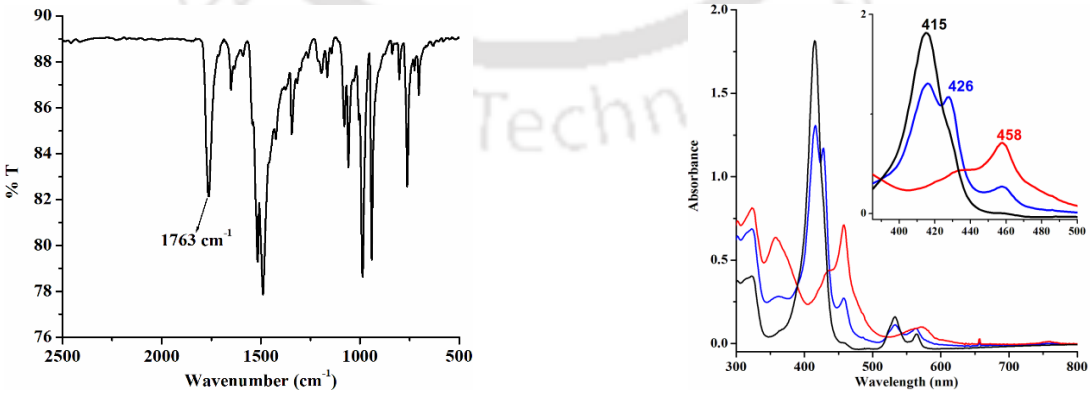

(i) (ii)

Figure S11. (i) FT-IR spectrum of complex **5.2** in KBr pellet. (ii) UV-visible spectra of complex **5.2** (black) and after addition of KO_2 to result in complex **5.3** (red) in THF at −80 °C.

The ESI-mass spectrum of the reaction mixture of complex **5.2** and KO_2 displays peak at m/Z 1043.07 which is assignable to the [(L3)Mn(O)] moiety (calcd. m/Z, 1042.98). After the completion of the reaction, peak at m/Z, 1088.88 corresponding to complex **5.3**, [(L3)Mn(NO_3)] (calcd m/Z, 1088.97) was observed (Figure S12(i)).

EPR silent nature of complex **5.2** is attributed to the anti-ferromagnetic coupling between the Mn^{II} center and the nitrosyl group. However, the frozen (at 77K) reaction mixture obtained from the reaction of complex **5.2** in THF at −80 °C with KO_2 displayed strong broad EPR signal with *g* ~5.26 and a weak one at 2.27, respectively. These are attributed to the presence of high spin Mn^{IV}=O center (S = 3/2) in a square pyramidal geometry (Scheme S4)(Figure S12(ii)).

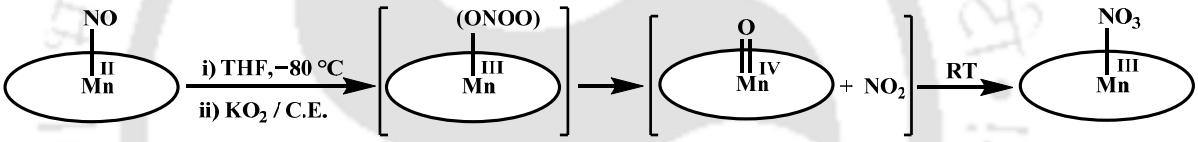

Scheme S4

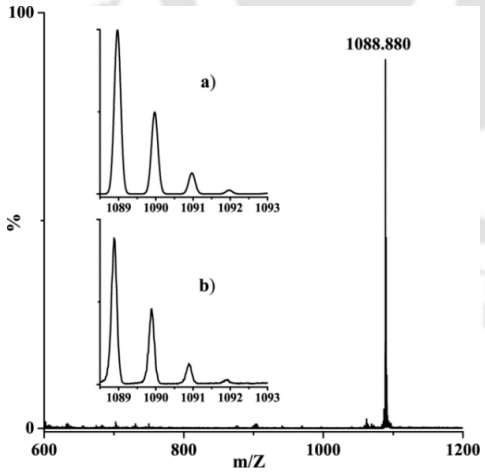

(i)

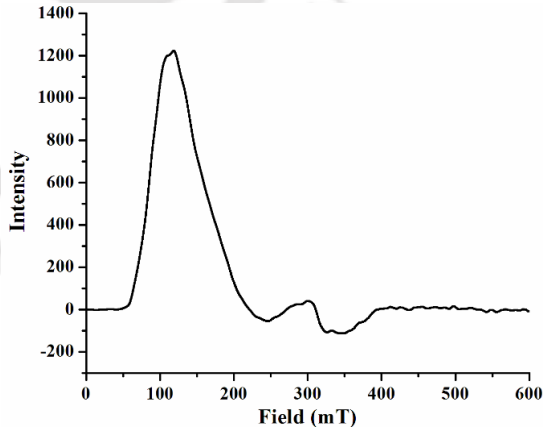

(ii)

Figure S12. (i) ESI-mass spectrum of complex **5.3** in acetonitrile. [Inset shows the simulated (a) and experimental (b) isotopic distribution pattern in acetonitrile.] (ii) X-band EPR spectrum of the intermediate formed during the reaction between complex **5.2** and KO_2 in THF at 77K.

The isolation and characterization of complex **5.3** as the decomposition product from the reaction of complex **5.2** and KO_2 also supports the formation of a Mn^{III}-PN intermediate.[24,25] As spectral characterization was precluded by the unstable nature of the intermediate, we sought chemical evidence. When the reaction was carried out in presence of 2,4-di-*tert*-butylphenol, nitration was observed leading to 2,4-di-*tert*-butyl-6-nitrophenol formation in ~40% yield with a fraction of oxidative product, bisphenol (~20%). Thus the involvement of a presumed Mn-PN complex is suggested in the reaction of complex **5.2** with KO_2 in THF.

References

1) (a) Ignarro, L. J. *FASEB J.* **1989**, *3*, 31. (b) Moncada, S.; Palmer, R.M.; Higgs, E.A. *Pharmacol. Rev.* **1991**, *43*, 109.

2) (a) Ignarro, L. J. *Nitric Oxide, Biology and Pathobiology* Ed. Academic Press, San Diego, CA, **2000**. (b) Richter-Addo, G. B.; Legzdins, P. *Metal Nitrosyls* Oxford University Press, New York, **1992**. (c) Feelisch, M.; Stamler, J. S. *Methods in Nitric Oxide Research* John Wiley and Sons, New York, **1996**.

3) (a) Furchgott, R. F. *Angew. Chem. Int. Ed.* **1999**, *38*, 1870. (b) Ignarro, L. J.; Buga, G. M.; Wood, K. S.; Byrns, R. E.; Chaudhuri, G. *Proc. Natl. Acad. Sci. U.S.A.* **1987**, *84*, 9265. (c) Murrad, F. *Angew. Chem. Int. Ed.* **1999**, *38*, 1856. (d) Ignaro, L. J. *Angew. Chem. Int. Ed.* **1999**, *38*, 1882. (e) Palmer, R. M. J.; Ferrige, A. G.; Moncada, S. *Nature* **1987**, *327*, 524.

4) Fang, F. C. *Nitric Oxide and Infection* Ed. Kluwer Academic/ Plenum Publishers, New York, **1999**.

5) Pacher, P.; Beckman, J. S.; Liaudet, L. *Physiol. Rev.* **2007**, *87*, 315.

6) Beckman, J. S.; Koppenol, W. H. *Am. J. Physiol.* **1996**, *271*, 1424.

7) Qiao, L.; Lu, Y.; Liu, B.; Girault, H. H. *J. Am. Chem. Soc*. **2011**, *133*, 19823.

8) Vliet, A.; Eiserich, J. P.; Halliwell, B.; Cross, C. E. *J. Biol. Chem.* **1997**, *272*, 7617.

9) (a) Doyle, M. P.; Hoekstra, J. W. *Inorg. Biochem.* **1981**, *14*, 351. (b) Cooper, C. E.; Torres, J.; Sharpe, M. A.; Wilson, M. T. *FEBS Lett.* **1997**, *414*, 281. (c) Tocheva, E. I.; Rosell, F. I.; Mauk, A. G.; Murphy, M. E. *Science* **2004**, *304*, 867.

10) Gardner, P. R.; Gardner, A. M.; Martin, L. A.; Salzman, A. L. *Proc. Natl. Acad. Sci. U.S.A.* **1998**, *95*, 10378.

11) Herold, S.; Exner, M.; Nauser, T. *Biochemistry* **2001**, *40*, 3385.

12) Stern, M. K.; Jensen M.P.; Kramer K. *J. Am. Chem. Soc.* **1996**, *118*, 8735.

13) Lee, J.; Hunt, J. A.; Groves, J. T. *J. Am. Chem. Soc.*, **1998**, *120*, 7493.

14) Shimanovich, R.; Groves, J. T. *Arch. Biochem. Biophys.* **2001**, *387*, 307.

15) Jensen, M. P.; Riley, D. P. *Inorg. Chem.* **2002,** *41*, 4788.

16) Lee, J. B.; Hunt, J. A.; Groves, J. T. *J. Am. Chem. Soc.* **1998**, *120*, 6053.

17) Schopfer, M. P.; Mondal, B.; Lee, D. H.; Sarjeant, A. A. N.; Karlin, K. D. *J. Am. Chem. Soc.* **2009**, *131*, 11304.

18) (a) Yokoyama, A.; Han, J. E.; Cho, J.; Kubo, M.; Ogura, T.; Siegler, M. A.; Karlin, K. D.; Nam, W. *J. Am. Chem. Soc.* **2012**, *134*, 15269. (b) Yokoyama, A.; Cho, K.-B.; Karlin, K. D.; Nam, W. *J. Am. Chem. Soc.* **2013**, *135*, 14900.

19) Saha, S.; Ghosh, S.; Gogoi, K.; Deka, H.; Mondal, B.; Mondal, B. *Inorg. Chem.* **2017**, *56*, 10932.

20) Kalita, A.; Kumar, P.; Mondal, B. *Chem. Commun.* **2012**, *48*, 4636.

21) Saha, S.; Gogoi, K.; Mondal, B.; Ghosh, S.; Deka, H.; Mondal, B. *Inorg. Chem.* **2017**, *56,* 7781.

22) Kadish, K. M.; Araullo-McAdams, C.; Han, B. C.; Franzen, M. M. *J. Am. Chem. Soc.* **1990**, *112*, 8364.

23) Choi, In-K.; Liu, Y.; Wei, Z.; Ryan, M. D. *Inorg. Chem.* **1997**, *36,* 3113.

24) Mondal, B.; Saha, S.; Borah, D.; Mazumdar, R; Mondal, B. *Inorg. Chem*. **2019**, *58*, 1234.

25) (a) Saha, S.; Gogoi, K.; Mondal, B.; Ghosh, S.; Deka, H.; Mondal, B. *Inorg. Chem*. **2017**, *56*, 7781. (b) Addo, G. B. R.; Hodge, S. J.; Yi, G. B.; Khan, M. A.; Ma, T.; Caemelbecke, E. V.; Guo, N.; Kadish, K. M. *Inorg. Chem*. **1996**, *35*, 6530.

Chapter 1

Introduction

1.1 General aspect of peroxynitrite ion

Nitric oxide (NO) is a free radical species which is continuously synthesized by nitric oxide synthase (NOS) enzymes from L-arginine.[1] Being a signaling molecule in the mammal, NO plays major roles in controlling various physiological processes.[2,3] It is known to function as a neurotransmitter, constitutive mediator and cytoprotective molecule when produced in permissible limit.[3-5] However excessively produced NO reacts with oxygen (O_2) or superoxide (O_2^-) ion to yield cytotoxic peroxynitrite ion ($ONOO^-$) (PN).[6,7] Alternatively, PN can also be generated by the reaction of hydrogen peroxide (H_2O_2) and nitrite (NO_2^-) in the presence of the peroxidase enzymes.[8,9] This short lived molecule is a potent oxidant and indirect nitrating agent which can react with different biomolecules and modulates diverse chemical modifications of lipids, proteins and nucleic acids.[6,10-12] It can also react with electron-rich groups, such as sulfhydryls,[13] iron-sulfur centers,[14] zinc-thiolates[15] and the active site of sulfhydryl in tyrosine phosphatases.[16] At pH 7.4, anionic form of PN ($ONOO^-$) is favorable while at pH 6.2 the protonated form (ONOOH) dominates.[17] Protonated form is more toxic than the anionic form due to the weakening of the O-O bond present in ONOOH which favors the homolytic cleavage to strongly oxidizing / hydroxylating and nitrating species, hydroxyl radicals ($^{\bullet}OH$) and nitrogen dioxide (NO_2) (Equation 1.1).[17,18]

$$ONOO^- \rightleftharpoons ONOOH \longrightarrow {}^{\bullet}OH + NO_2 \quad \text{---------- (Eq. 1.1)}$$

But the anionic form of PN becomes pro-nitrating agent which reacts rapidly with carbon dioxide (CO_2) to form a nitrosoperoxocarboxylate adduct ($ONOOCO_2^-$) that undergoes a fast homolysis to NO_2 and carbonate radicals ($CO_3^{\bullet-}$) (Equation 1.2).[19]

$$ONOO^- + CO_2 \longrightarrow ONOOCO_2^- \longrightarrow {}^{\bullet}CO_3^- + NO_2 \quad \text{---------(Eq. 1.2)}$$

An important aspect of PN mediated toxicity is protein tyrosine nitration.[24] This can alter the protein function by inactivating it or increasing the efficiency.[20] Thus, nitration of proteins can prevent or modulate cellular signal transduction, which requires tyrosine phosphorylation.[21]

Protein tyrosine nitration involves two step mechanism, (i) tyrosine group gets oxidized to tyrosine radical by physiologically active oxidants ($CO_3^{\bullet-}$) or oxo-metal complexes and to a lesser extent, $^{\bullet}OH$ and NO_2, (ii) combination of tyrosine radical with NO_2 to form 3-nitrotyrosine. But the dimerization of tyrosyl radicals to 3,3′-dityrosine and formation of 3-hydroxytyrosine competes the nitration reaction.[17] PN can react with the transition metal ions to catalyse the reaction of either one or two electron redox processes.[22] Nitric oxide dioxygenases (NODs) enzymes are known to control the over production of NO in *vivo* by converting it to the biologically benign nitrate (NO_3^-). This reaction is believed to proceed through a PN intermediate.[23]

1.2 Literature survey

The chemistry of PN has attracted much attention recently. Although its lifetime is very short, (which isomerizes rapidly to NO_3^- anion in the presence of metal ion or acid) the potentiality of the oxidative damage of biomolecules has motivated extensive study of the chemistry of PN. The dioxygen iron complex of oxymyoglobin (oxyMb) react rapidly with NO to form their corresponding met forms and NO_3^- ion (Scheme 1.1).[24,25]

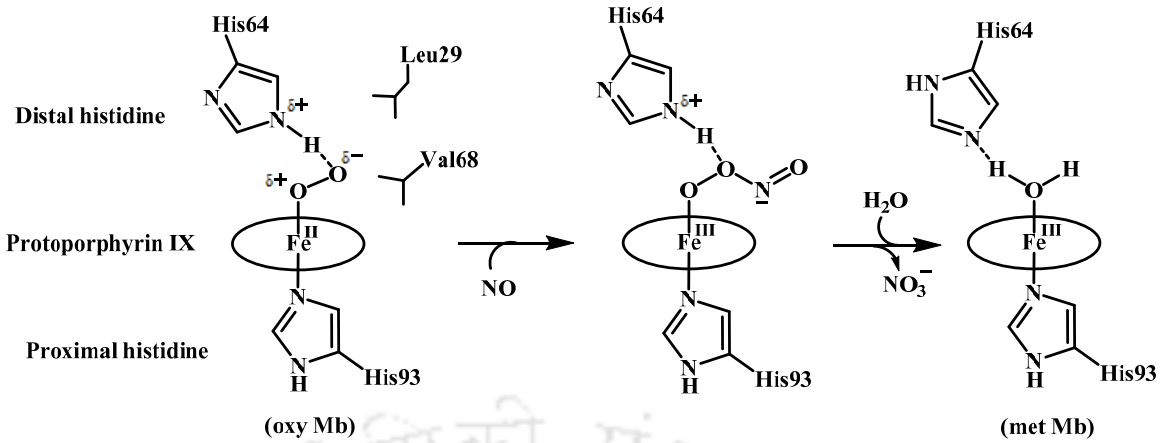

Scheme 1.1

Water-soluble iron porphyrin complexes such as 5,10,15,20-tetrakis(*N*-methyl-4-pyridyl)porphinatoiron(III), $[Fe^{III}(TMPyP)]^{5+}$, 5,10,15,20-tetrakis(2,4,6-trimethyl-3,5-disulfonatophenyl)porphinatoiron(III), $[Fe^{III}TMPS]^{7-}$, and 5,10,15,20-tetrakis(4-sulfonatophenyl)porphinatoiron(III), $[Fe^{III}TPPS]^{3-}$ (Figure 1.1) efficiently catalyze the isomerization of PN to NO_3^- or NO_2^-.[24,26-29]

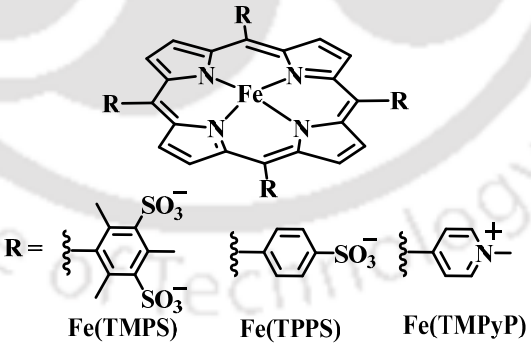

Figure 1.1: Iron TMPS/ TPPS/ TMPyP systems

The mechanism of these reactions involves two pathways, one involving Fe^{III}-PN complex and the other is high-valent Fe^{IV}-oxo complex (Scheme 1.2). When $[Fe^{III}(TMPyP)]^{5+}$ was

allowed to react with two equivalents of PN (at pH 7.4 and 25 °C) the trace collected at 427 nm indicated the formation of an intermediate, which was assigned as $[(O)Fe^{IV}(TMPyP)]^{4+}$. It was believed to be formed by the homolytic cleavage of the O-O bond of the very unstable PN complex, $[Fe^{III}(PN)(TMPyP)]^{4+}$.[26] NO_2 is also produced along with $[(O)Fe^{IV}(TMPyP)]^{4+}$ during the decomposition of Fe^{III}-PN.

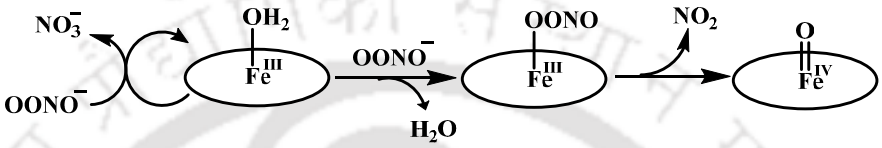

Scheme 1.2

Groves *et al.* reported that $[Mn^{III}(TMPyP)]^{5+}$ reacts rapidly with PN to form the corresponding Mn^{III}-PN complex. This PN complex decomposes to generate the oxo complex, $[(O)Mn^{IV}(TMPyP)]^{4+}$ and NO_2 (Scheme 1.3). But Mn^{IV}=O is quite stable so the conversion from Mn^{IV}=O to the Mn^{III} oxidation state is slow and the recombination of NO_2 doesn't take place. Thus $[Mn^{III}TMPyP]^{5+}$ is not catalytic in PN decomposition. But any reductants like ascorbate / glutamate, etc. can make $[Mn^{III}TMPyP]^{5+}$ complex as the PN

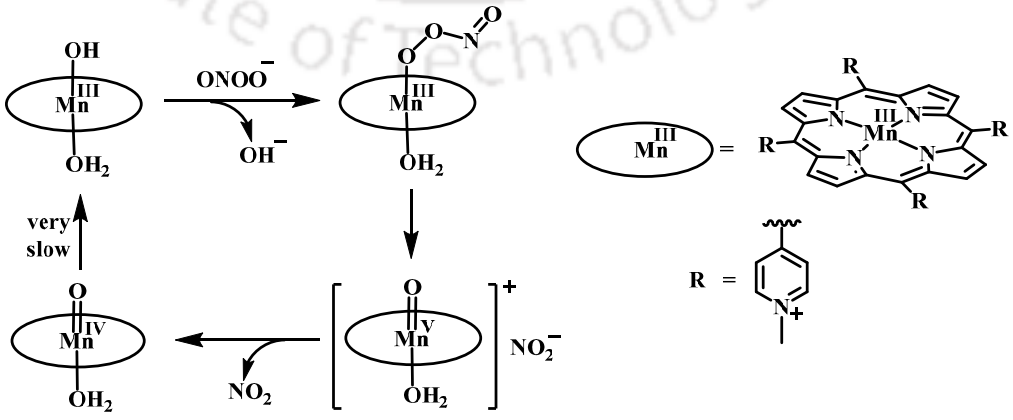

Scheme 1.3

decomposition catalyst.[30]

In the case of MnSOD enzyme it is proposed that PN is responsible for the nitration and the inactivation of the enzyme. In this reaction PN can both oxidize and reduce the active manganese site i.e. Mn^{II} or Mn^{III} ions (Scheme 1.4). The nitration of MnSOD mediated by PN resulted in selective reaction on the tyrosine residue close to the active site.[31]

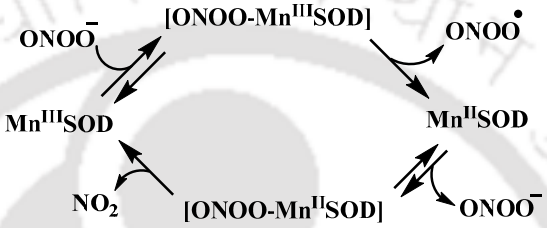

Scheme 1.4

NO reactivity of a stable chromium peroxo complex of 12-membered tetraazamacrocyclic N-tetramethylated cyclam (TMC) ligand was studied and was found to proceed through a Cr^{III}-PN intermediate (Scheme 1.5). This intermediate then isomerizes to Cr^{III}-(NO_3^-) complex. This isomerization occurred by the recombination of the Cr^{IV}-oxo species and NO_2, which formed during the subsequent homolytic O-O bond cleavage of the PN moiety.[32]

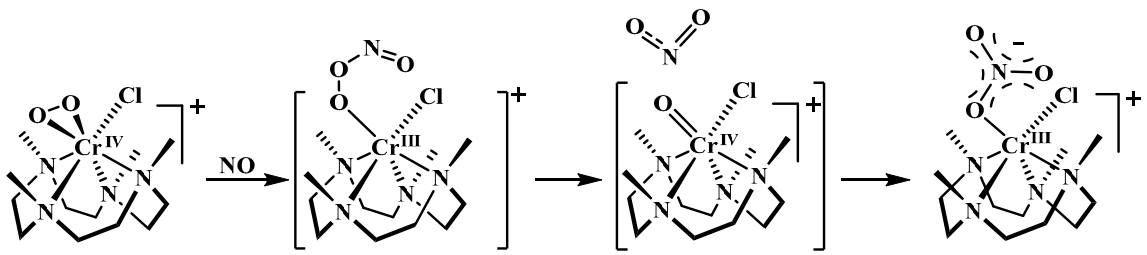

Scheme 1.5

Another classic example of formation of an oxo species *via* the formation of transient PN complex was reported by Nam and coworkers. When NO was allowed to react with an end-on Cr^{III}-superoxo complex bearing a 14-membered tetraazamacrocyclic TMC ligand, $[Cr^{III}(14\text{-TMC})(O_2)(Cl)]^+$, it gives a Cr^{III}-PN intermediate which undergoes homolysis of the O-O bond to result in a stable oxo, $[Cr^{IV}(14\text{-TMC})(O)(Cl)]^+$ (Scheme 1.6).[33]

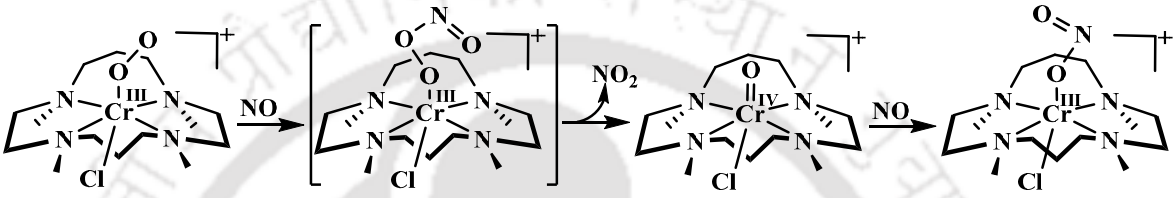

Scheme 1.6

The phenol ring nitration chemistry was employed to prove the formation of PN complexes. The formation of a Cr^{III}-hydroxo complex, $[(14\text{-TMC})Cr^{III}(OH)(Cl)]^+$ along with 46% of nitrated DTBP (2,4-di-*tert*-butyl-6-nitrophenol, nitro-DTBP) and 12% of dimerized DTBP (3,3',5,5'-tetra-*tert*-butyl-(1,1'-biphenyl)-2,2'-diol, DTBP dimer) product was observed *via* radical mechanism (Scheme 1.7). [33]

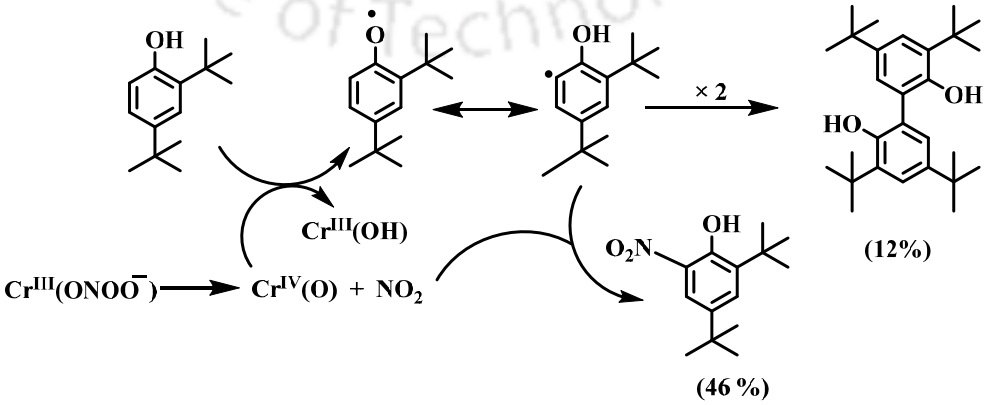

Scheme 1.7

Karlin group reported the reaction of NO with a superoxo of heme iron system, $[(THF)(F_8TPP)Fe^{III}(O_2^{-})]$ which leads to the corresponding NO_3^- complex *via* a PN intermediate formation (Scheme 1.8). Nitrophenol formation was observed when the DTBP was added before the addition of NO in the system which confirms the formation of the PN complex.[34]

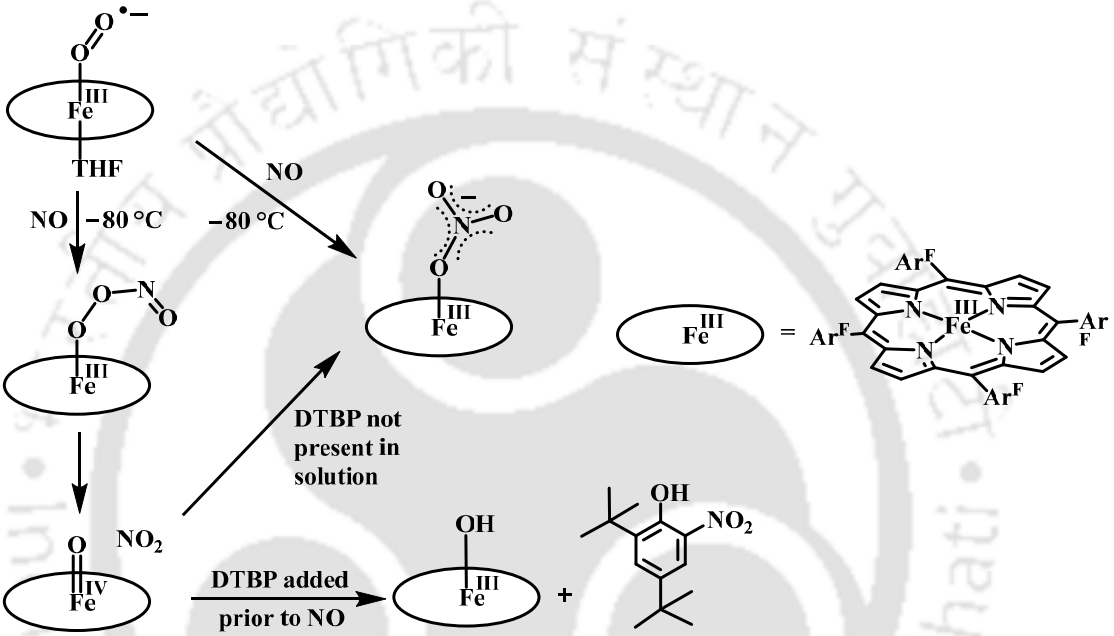

Scheme 1.8

The same group has reported a relatively stable PN complexes by the reaction of NO with the copper superoxide species $[(TMG_3tren)Cu^{II}(O_2^{-})]^+$ at −80 °C (Scheme 1.9). The PN formation was evidenced by ESI-Mass spectrometry and EPR spectroscopy techniques.[35]

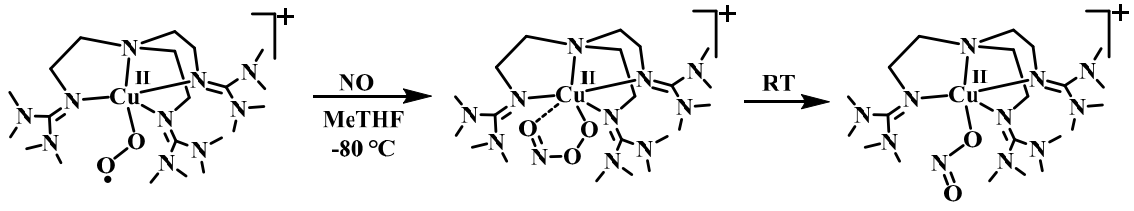

Scheme 1.9

Kurtikyan *et al.* reported the reaction of oxy-coboglobin models [(Py)Co(Por)(O_2) (Por = *meso*-tetraphenyl and *meso*-tetra-*p*-tolylporphyrinato dianions)] with NO at very low temperature gives NO_3^- complex (Scheme 1.10). The formation of PN complex was evidenced by FT-IR spectroscopy.[36]

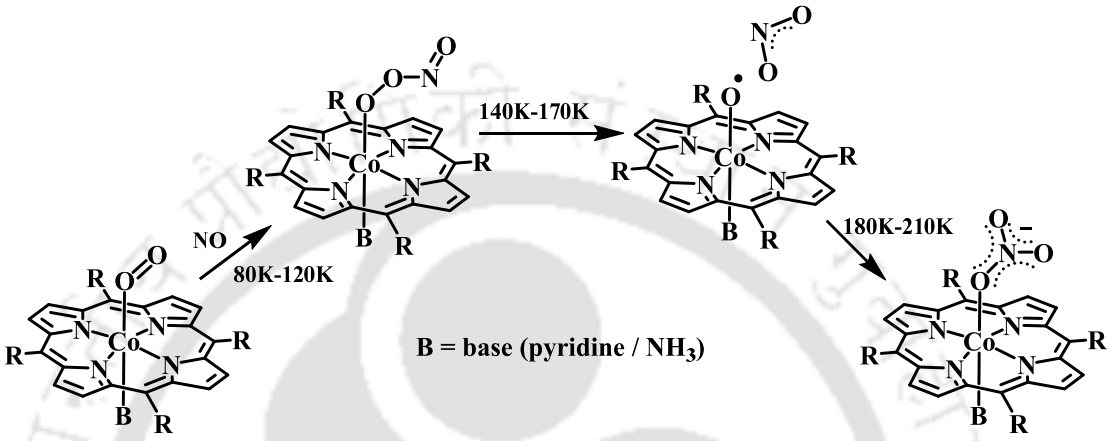

Scheme 1.10

Nam group reported two Co^{III}-nitrosyl complexes, [(12-TMC)Co(NO)]$^{2+}$ and [(13-TMC)Co(NO)]$^{2+}$, which are inert towards O_2, but reacts with O_2^- to form the corresponding Co^{II}-(NO_2^-) complex and with release of O_2. This reaction was proposed to go through unstable Co^{II}-PN intermediates (Scheme 1.11).[37]

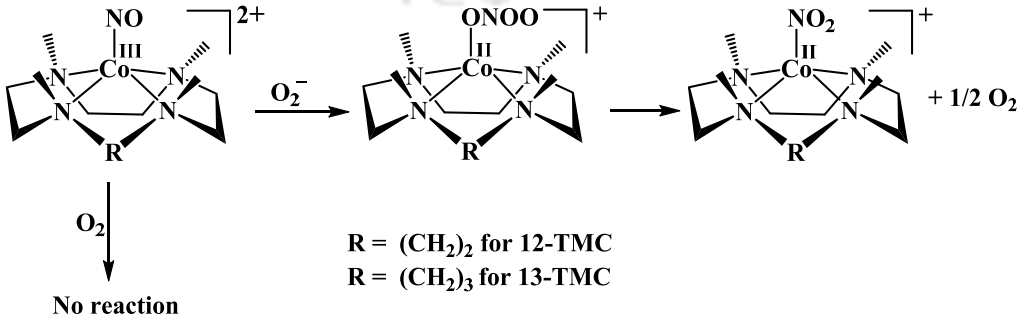

Scheme 1.11

Whereas in the case of 14-TMC ligand the Co^{III}-nitrosyl, $[(14\text{-TMC})Co(NO)]^{2+}$ reacts with O_2 to result in $[(14\text{-TMC})Co^{III}(NO_3)]^{+}$. The formation of a putative Co^{II}-PN intermediate is involved in this reaction (Scheme 1.12).[38]

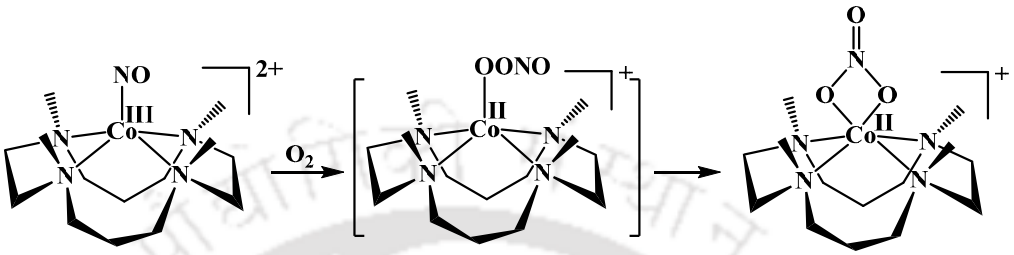

Scheme 1.12

It has been reported that a $\{CuNO\}^{10}$ complex of histidine-derived ligand, methyl 2-(2-hydroxybenzylamino)-3-(1*H*-imidazol-5-yl)propanoate in the presence of H_2O_2 resulted in Cu^{I}-PN intermediate complex (Scheme 1.13). This intermediate afforded the nitration of the ligand.[39]

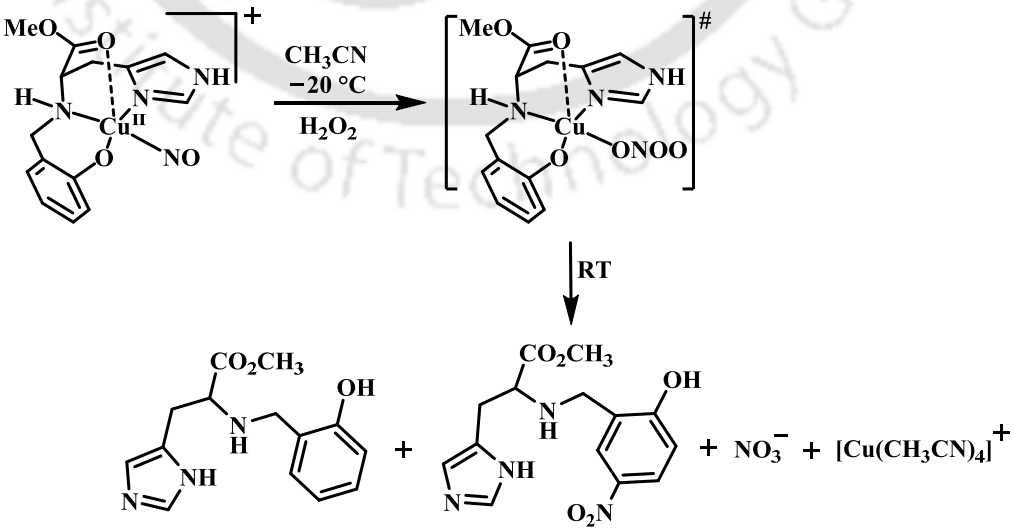

Scheme 1.13

Another {CuNO}^{10} complex, $[L_2Cu(NO)](ClO_4)_2$, [L = bis(2-ethyl-4-methyl-imidazol-5-yl)methane] when allowed to react with H_2O_2 at −20 °C to resulted in the corresponding Cu^I-(NO_3^-) complex. This reaction was proposed to proceed through a Cu^I-PN intermediate. The characteristic phenol ring nitration was employed to support the formation of the PN intermediate (Scheme 1.14).[40]

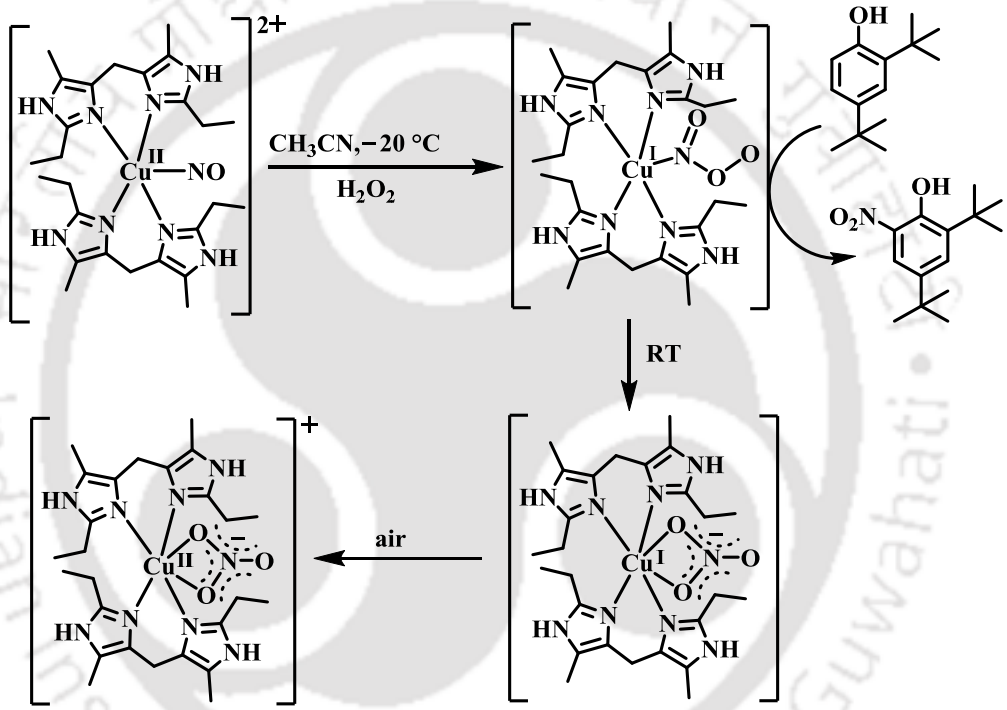

Scheme 1.14

Recently, the Co^{III}-peroxo complex of the aforementioned ligand was found to result in the corresponding NO_3^- complex in presence of NO environment (Scheme 1.15). The involvement of a PN intermediate was implicated from the isolation of corresponding NO_3^- product as well as nitration of externally added phenol.[41]

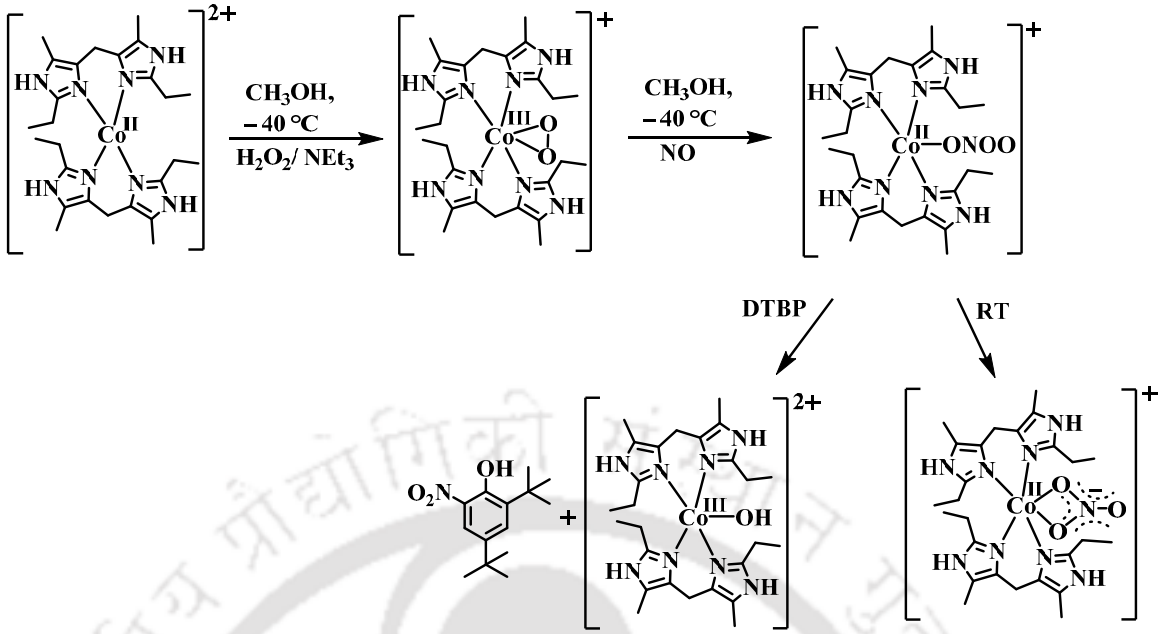

Scheme 1.15

Karlin group reported a binuclear mixed-valent copper nitrosyl complex, $[Cu^{I,II}_2(UN\text{-}O^-)(NO)]^{2+}$ reacts with O_2 and undergoes one electron oxidation. During this reaction a new intermediate designated as a superoxide and nitrosyl adduct, $[Cu^{II}_2(UN\text{-}O^-)(NO)(O_2^-)]^{2+}$ was observed (Scheme 1.16). This intermediate converts to PN complex, $[Cu^{II}_2(UN\text{-}O^-)(PN)]^{2+}$.[42]

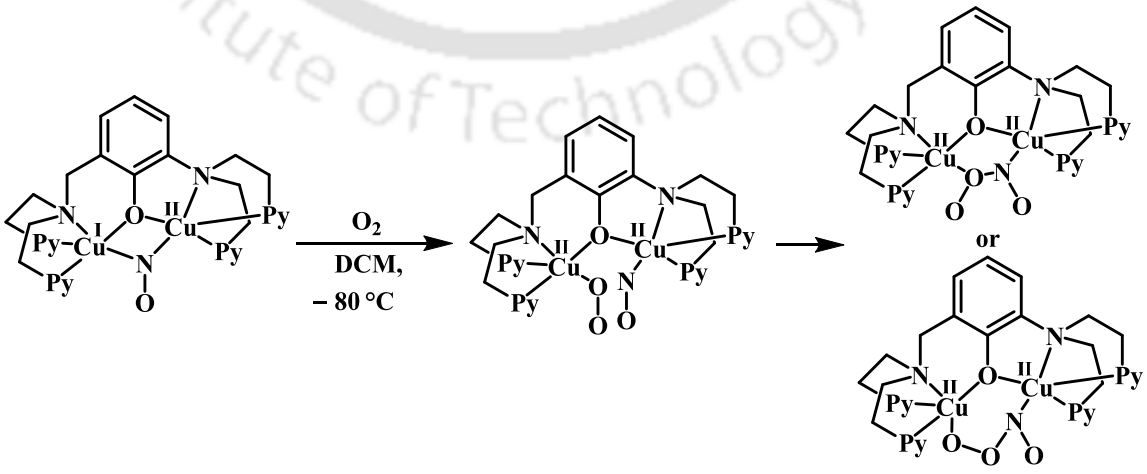

Scheme 1.16

Our group reported a cobalt-nitrosyl complex, [(BPI)Co(NO)(OAc)] (BPI = 1,3-bis(2′-pyridylimino)isoindol) reacts with O_2 to result in the NO_2^- complex. Involvement of the [(BPI)Co^{III}(NO)(O_2^-)(OAc)] intermediate was evidenced spectroscopically (Scheme 1.17).[43]

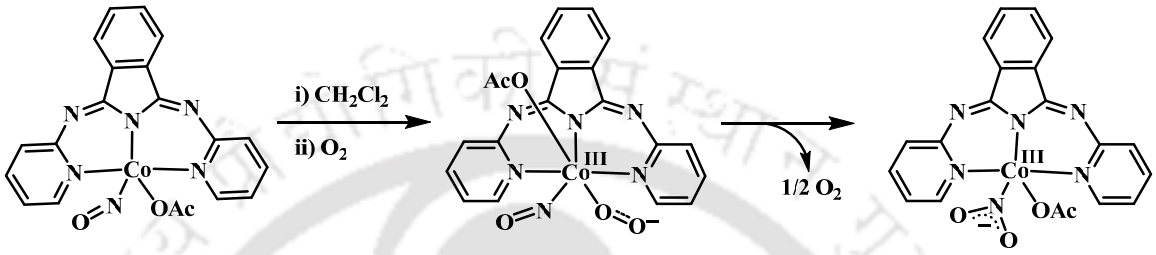

Scheme 1.17

In continuation to our study, nitrosyl complex of a cobalt porphyrinate [(Cl_4TPP)Co], [Cl_4TPPH_2 = 5,10,15,20-tetrakis(4-chlorophenyl)porphyrin] was prepared. The reaction of this cobalt nitrosyl with H_2O_2 was reported to yield the Co^{III}-(NO_2^-) complex with the simultaneous release of O_2 (Scheme 1.18). The involvement of a cobalt PN intermediate was presumed.[44]

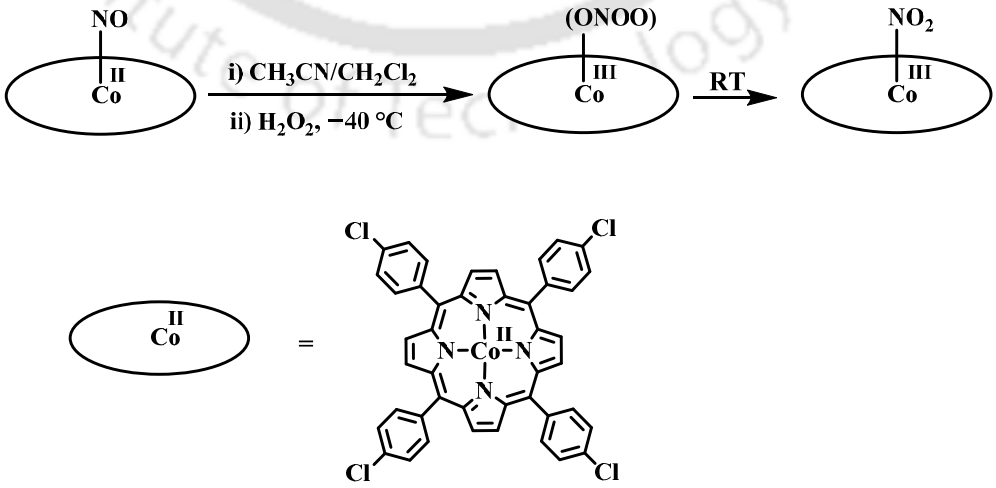

Scheme 1.18

1.3 Scope of the thesis

The present thesis work has been originated from our interest to identify the metal-PN as an intermediate in the reactions of metal nitrosyls with reactive oxygen species, which is still illusive in literature. Further, the examples of the decomposition of metal PNs to result in metal-oxo and NO_2 are in scarce. Attempts have been made to identify the involvement of high valent metal-oxo species in the decomposition or nitration reaction of metal-PNs. In short the objective of the thesis was:

i. Systematic synthesis and characterization of nitrosyl complexes of metal porphyrinates.

ii. Study of the reaction of these complexes with reactive oxygen species with an aim to identify PN intermediate.

iii. To understand the detailed mechanism of the decomposition of metal PNs.

iv. To identify the high valent metal oxo intermediates spectroscopically to prove their involvement in the said reaction.

1.4 References

1) (a) Ignarro, L. J. *FASEB J.* **1989**, *3*, 31. (b) Moncada, S.; Palmer, R. M.; Higgs, E. A. *Pharmacol. Rev.* **1991**, *43*, 109.

2) (a) Ignarro, L. J. *Nitric Oxide, Biology and Pathobiology* Ed. Academic Press, San Diego, CA, **2000**. (b) Richter-Addo, G. B.; Legzdins, P. *Metal Nitrosyls* Oxford University Press, New York, **1992**. (c) Feelisch, M.; Stamler, J. S. *Methods in Nitric Oxide Research* John Wiley and Sons, New York, **1996**.

3) (a) Furchgott, R. F. *Angew. Chem. Int. Ed.* **1999**, *38*, 1870. (b) Ignarro, L. J.; Buga, G. M.; Wood, K. S.; Byrns, R. E.; Chaudhuri, G. *Proc. Natl. Acad. Sci. U.S.A.* **1987**, *84*, 9265. (c) Murrad, F. *Angew. Chem. Int. Ed.* **1999**, *38*, 1856. (d) Ignaro, L. J. *Angew. Chem. Int. Ed.* **1999**, *38*, 1882.

4) Culotta, E.; Koshland, D. E. Jr. *Science* **1992**, *258*, 1862.

5) Palmer, R. M. J.; Ferrige, A. G.; Moncada, S. *Nature* **1987**, *327*, 524.

6) Pacher, P.; Beckman, J. S.; Liaudet, L. *Physiol. Rev.* **2007**, *87*, 315.

7) Beckman, J. S.; Koppenol, W. H. *Am. J. Physiol.***1996**, *271*, 1424.

8) Qiao, L.; Lu, Y.; Liu, B.; Girault, H. H. *J. Am. Chem. Soc*. **2011**, *133*, 19823.

9) Vliet, A.; Eiserich, J. P.; Halliwell, B.; Cross. C. E. *J. Biol. Chem.* **1997**, *272*, 7617.

10) Radi, R. *Chem. Res. Toxicol.* **1998**, *11*, 720.

11) Szabó, C.; Ischiropoulos, H.; Radi, R. *Nat. Rev. Drug. Discov.* **2007**, *6*, 662.

12) (a) Beal, M. F. *Free Radical Biol. Med.* **2002**, *32*, 797. (b) Radi, R.; Cassina, A.; Hodara, R.; Quijano, C.; Castro, L. *Free Radical Biol. Med.* **2002**, 33, 1451.

13) Radi, R.; Beckman, J. S.; Bush, K. M.; Freeman, B. A. *J. Biol. Chem.* **1991**, *266*, 4244.

14) Castro, L.; Rodriguez, M.; Radi, R. *J. Biol. Chem.* **1994**, *269*, 29409.

15) Crow, J. P.; Sampson, J. B.; Zhuang, Y.; Thompson, J. A.; Beckman, J. S. *J. Neurochem.* **1997**, *69*, 1936.

16) (a) Takakura, K.; Beckman, J. S.; MacMillan-Crow, L. A.; Crow, J. P. *Arch. Biochem. Biophys.* **1999**, *369*, 197. (b) Marla, S. S.; Lee, J.; Groves, J. T. *Proc. Natl. Acad. Sci. U. S. A.* **1997**, *94*, 14243. (c) Minetti, M.; Mallozzi, C.; Stasi, A. M. M. D. *Free Radical Biol. Med.* **2002**, *33*, 744.

17) Radi, R. *J. Biol. Chem.* **2013**, *288*, 26464.

18) Beckman, J. S.; Beckman, T. W; Chen, J.; Marshall, P. A.; Freeman, B. A. *Proc. Natl. Acad. Sci. USA* **1990**, *87*, 1620.

19) (a) Goldstein, S.; Merényi, G. *Methods Enzymol.* **2008**, *436*, 49. (b) Lymar, S. V.; Hurst, J. K. *J. Am. Chem. Soc.* **1995**, *117*, 8867. (c) Denicola, A.; Freeman, B. A.; Trujillo, M.; Radi, R. *Arch. Biochem. Biophys.* **1996**, *333*, 49.

20) Souza, J. M.; Peluffo, G.; Radi, R. *Free Radical Biol. Med.* **2008**, *45*, 357.

21) (a) Mondoro, T. H.; Shafer, B. C.; Vostal, J. G. *Free Radical Biol. Med.* **1997**, *22*, 1055. (b) Kong, S. K.; Yim, M. B.; Stadtman, E. R.; Chock, P. B. *Proc. Natl. Acad. Sci. U. S. A.* **1996**, *93*, 3377.

22) Ferrer-Sueta, G.; Quijano, C.; Alvarez, B.; Radi, R. *Methods Enzymol.* **2002**, *349*, 23.

23) (a) Cooper, C. E.; Torres, J.; Sharpe, M. A.; Wilson, M. T. *FEBS Lett.* **1997**, *414*, 281. (b) Tocheva, E. I.; Rosell, F. I.; Mauk, A. G.; Murphy, M. E. *Science* **2004**, *304*, 867. (c) Gardner, P. R.; Gardner, A. M.; Martin, L. A.; Salzman, A. L. *Proc. Natl. Acad. Sci. U.S.A.* **1998**, *95*, 10378.

24) Herold, S.; Koppenol, W. H. *Coord. Chem. Rev.* **2005**, *249*, 499.

25) (a) Doyle, M. P.; Hoekstra, J. W. *J. Inorg. Biochem.* **1981**, *14*, 351. (b) Herold, S.; Exner, M.; Nauser, T. *Biochemistry*, **2001**, *40*, 3385.

26) Stern, M. K.; Jensen M. P.; Kramer K. *J. Am. Chem. Soc.* **1996**, *118*, 8735.

27) Lee, J.; Hunt, J. A.; Groves, J. T. *J. Am. Chem. Soc.*, **1998**, *120*, 7493.

28) Shimanovich, R.; Groves, J. T. *Arch. Biochem. Biophys.* **2001**, *387*, 307.

29) Jensen, M. P.; Riley, D. P. *Inorg. Chem.*, **2002,** *41*, 4788.

30) Lee, J.; Hunt, J. A.; Groves, J. T. *J. Am. Chem. Soc.* **1998**, *120*, 6053.

31) Surmeli, N. B.; Litterman, N. K.; Miller, A-F.; Groves J. T. *J. Am. Chem. Soc.* **2010**, *132*, 17174.

32) Yokoyama, A.; Han, J. E.; Cho, J.; Kubo, M.; Ogura, T.; Siegler, M. A.; Karlin, K. D.; Nam, W. *J. Am. Chem. Soc.* **2012**, *134*, 15269.

33) Yokoyama, A.; Cho, K.-B.; Karlin, K. D.; Nam, W. *J. Am. Chem. Soc.* **2013**, *135*, 14900.

34) Schopfer, M. P.; Mondal, B.; Lee, D. H.; Sarjeant, A. A. N.; Karlin, K. D. *J. Am. Chem. Soc.*, **2009**, *131*, 11304.

35) Maiti, D.; Lee, D.-H.; Sarjeant, A. A. N.; Pau, M. Y. M.; Solomon, E. I.; Gaoutchenova, K.; Sundermeyer, J.; Karlin, K. D. *J. Am. Chem. Soc.* **2008**, *130*, 6700.

36) (a) Kurtikyan, T. S.; Eksuzyan, Sh. R.; Hayrapetyan, V. A.; Martirosyan, G. G.; Hovhannisyan, G. S.; Goodwin, J. A. *J. Am. Chem. Soc.* **2012**, *134*, 13861. (b) Kurtikyan, T. S.; Eksuzyan, Sh. R.; Goodwin, J. A.; Hovhannisyan, G. S.; *Inorg. Chem.* **2013**, *52*, 12046.

37) Kumar, P.; Lee, Y.-M.; Park, Y. J.; Siegler, M. A.; Karlin, K. D.; Nam, W. *J. Am. Chem. Soc.* **2015**, *137*, 4284

38) Kumar, P.; Lee, Y.-M.; Hu, L.; Chen, J.; Park, Y. J.; Yao, J.; Chen, H.; Karlin, K. D.; Nam, W. *J. Am. Chem. Soc.* **2016**, *138*, 7753.

39) Kalita, A.; Deka, R. C.; Mondal, B. *Inorg. Chem.* **2013**, *52*, 10897.

40) Kalita, A.; Kumar, P.; Mondal, B. *Chem. Commun.* **2012**, *48*, 4636.

41) Saha, S.; Ghosh, S.; Gogoi, K.; Deka, H.; Mondal, B.; Mondal, B. *Inorg. Chem.* **2017**, *56*, 10932.

42) Cao, R.; Elrod, L. T.; Lehane, R. L.; Kim, E.; Karlin, K. D. *J. Am. Chem. Soc.* **2016**, *138*, 16148.

43) Gogoi, K.; Saha, S.; Mondal, B.; Deka, H.; Ghosh, S.; Mondal, B. *Inorg. Chem.* **2017**, *56*, 14438.

44) Saha, S.; Gogoi, K.; Mondal, B.; Ghosh, S.; Deka, H.; Mondal, B. *Inorg. Chem.* **2017**, *56,* 7781.

Chapter 2

Nitric Oxide Dioxygenase Activity of a Nitrosyl Complex of Co^{II}-Porphyrinate in the Presence of Hydrogen Peroxide *via* Putative Peroxynitrite Intermediate

Abstract

The reaction of a cobalt porphyrin complex, [(L1)Co], **2.1** (**L1H$_2$** = 5,10,15,20-tetrakis(2,6-difluorophenyl)porphyrin) in dichloromethane with nitric oxide (NO) gas led to the formation of the corresponding nitrosyl complex, [(L1)Co(NO)], **2.2**. Spectroscopic studies and structural characterization revealed it as a bent nitrosyl having $\{CoNO\}^8$ description. It is stable in the presence of dioxygen (O_2). However, it reacts with H_2O_2 in acetonitrile (or THF) solution at −40 °C (or −80 °C) to result in the corresponding Co^{III}-nitrate (NO_3^-) complex, [(L1)Co(NO_3)], **2.3**. The reaction presumably proceeds *via* the formation of a Co^{III}-PN intermediate. X-Band EPR and ESI-mass spectroscopic studies suggest the intermediate formation of the [(L1)Co^{III}-O$^\bullet$] radical, which in turn supports the generation of the corresponding Co^{IV}-oxo species during the reaction. This is in accord with the homolytic cleavage of the O-O bond in heme-PN proposed in the nitric oxide dioxygenases (NODs) activity. In addition, the characteristic PN-induced phenol ring nitration was also observed.

2.1 Introduction

Nitric oxide (NO) plays important roles in mammalian biology including neurotransmission and in immune response.[1,2] It is believed that only a submicromolar concentration of NO is required for its functions. However, when produced at high concentrations, it induces cytotoxicity *via* the formation of reactive nitrogen species (RNS) such as peroxynitrite ($ONOO^-$) (PN) or nitrogen dioxide (NO_2).[3,4] These RNS are proposed to form in the reaction of NO with superoxide (O_2^-), hydrogen peroxide (H_2O_2) and/or in the presence of transition metal ions.[3] The NODs control the level of NO by converting it into the biologically benign NO_3^-.[5,6] The oxy-heme species of the NODs upon reaction with NO results in NO_3^- through the intermediate formation of a PN ion. A number of examples are reported where the involvement of a metal-PN intermediate is proposed in the reaction of NO with metal-oxygen species. The superoxo complexes of heme and non-heme iron, cobalt and copper are exemplified to result in the metal-PN intermediates in the presence of NO.[7-9] Recently, a non-heme Cr^{IV}-peroxo complex was reported to react with NO to result in Cr^{III}-(NO_3^-); whereas the Cr^{III}-superoxo analogue resulted in the corresponding Cr^{IV}-oxo and NO_2 presumably *via* a Cr^{III}-PN intermediate.[10]

The examples related to the formation of a presumed metal-PN in the reaction of a metal-nitrosyl and O_2 are known in literature. The formation of the nitrite (NO_2^-) product in the reaction of cobalt-nitrosyl with O_2 was reported long back.[11] In recent time, the reaction of a non-heme dinitrosyl iron complex with O_2 was found to afford the corresponding NO_3^- complex.[12] However, Cu^I-nitrosyl complex was exemplified to result in NO_2^- product in the presence of O_2 through a presumed PN intermediate.[13] In addition, $\{CuNO\}^{10}$ complex in the presence of H_2O_2 was also found to result in the copper-nitrato complex through a presumed Cu^I-PN intermediate formation.[14]

Hence, the reaction of the nitrosyl complexes of transition metal ions with O_2 and the reduced O_2 species is of great interest. In this direction, the examples involving the reaction of metal-nitrosyls with H_2O_2 are limited in literature.

This chapter describes the NOD activity of a cobalt-nitrosyl porphyrin, [(L1)Co(NO)] (**2.2**) in the presence of hydrogen peroxide (H_2O_2), where the intermediate formation of PN is implicated. Spectroscopic evidence suggests the formation of the corresponding [(L1)Co^{III}-$O^{\bullet}$] radical and NO_2 in the reaction.

2.2 Results and Discussion

The ligand, **L1H$_2$** and its Co^{II} complex (**2.1**) were prepared by following the literature methods.[18] The single crystal structure of ligand was reported earlier.[18] Complex **2.1** was characterized spectroscopically as well as by X-ray single crystal structure determination (Experimental Section and Appendix I, Figures A1.5-A1.8). The nitrosyl complex **2.2** was prepared by bubbling NO gas into the degassed dichloromethane solution of complex **2.1**. Complex **2.2** was characterized by UV-visible, FT-IR spectroscopy, mass spectrometry and X-ray structure determination (Experimental Section and Appendix I, Figures A1.9-A1.11). The crystallographic data and the metric parameters are listed in the Appendix I (Tables A1.1-A1.3). The ORTEP views of complexes **2.1** and **2.2** are shown in figure 2.1(i, ii). In complex **2.1**, the central metal ion is coordinated by four N atoms from the porphyrinate dianion in a square planar geometry. The Co-N_P distances are in the limit of reported distances in analogous complexes.[19] In complex **2.2**, the Co^{II} centre is coordinated by four N atoms from the porphyrinate moiety. The NO group is coordinated to the metal ion from the axial position resulting in a square pyramidal geometry around the Co^{II} center. The Co-N_{NO} and N-O distances are 1.894(10) and 1.158(13) Å, respectively, which are within the range in other reported analogues.[20] The observed Co-N-O angle is 127.4(14)°.

The metric parameters of the nitrosyl complex are in accord with the bent nitrosyls having $\{CoNO\}^8$ configuration.[20] It would be worth mentioning here that the Spiro's group reported the same compound *in situ* generated for ^{1}H NMR and FT-IR studies; however, it was not isolated in solid state and structurally characterized.[21] The Co-N_{NO} and N-O bond lengths were calculated to 1.810 and 1.186 Å, respectively.[21] The calculated Co-N-O bond angle is 121°.[21] These are also in good agreement with the structurally characterized parameters.

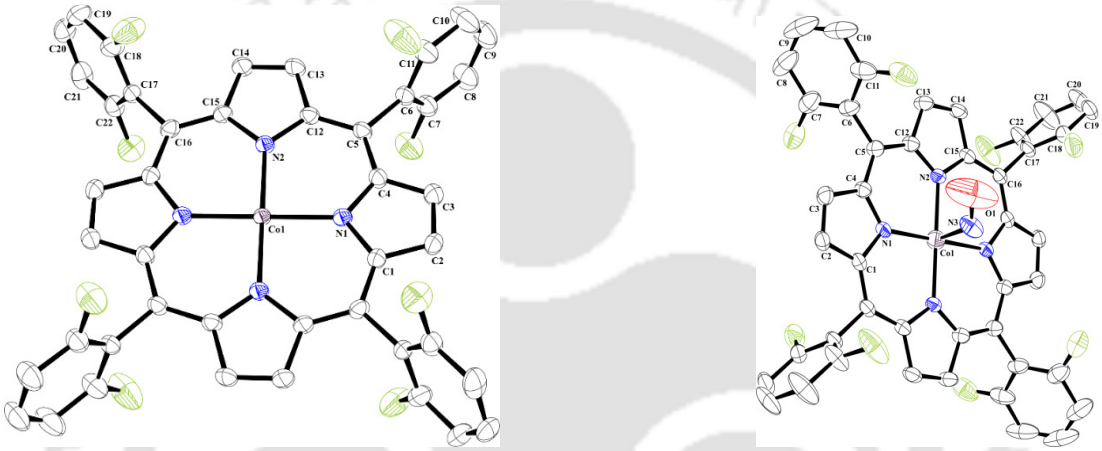

(i) (ii)

Figure 2.1. ORTEP diagrams of complexes **2.1** (i) and **2.2** (ii) (50% thermal ellipsoid plot, H-atoms and solvent molecules are omitted for clarity).

In the FT-IR spectrum, the strong stretching frequency at 1692 cm^{-1} in KBr is assignable to the coordinated NO moiety (Figure 2.2). Spiro and co-workers reported the ν_{NO} stretching to appear at 1699 cm^{-1} in dichloromethane.[21] In earlier reported examples like [(TPP)Co(NO)] and [(OEP)Co(NO)], the NO stretching was observed at 1689 cm^{-1} (in KBr) and 1675 cm^{-1} (in dichloromethane), respectively.[22] In the cases of cobalt porphyrin nitrosyls having general formula [{T(p/m-X)PP}Co(NO)] [*p*/*m*-X = *p*-OCH3, *p*-CH3, *m*-CH3, *p*-H, *m*-OCH3, *p*-OCF3, *p*-CF3, *p*-CN etc.] in dichloromethane, the NO stretching frequency appeared in the range of 1681-1695 cm^{-1}.[22] It was appeared at 1701 cm^{-1} in KBr

disc for complex [(Cl_4TPP)Co(NO)].[23] In the ESI-mass spectrum, complex **2.2** displayed a peak at m/Z 815.27 assignable to the [(L1)Co] (Calcd. m/Z = 815.08). This is attributed to the facile loss of the axial NO group, which has been observed earlier in other nitrosyl complexes of Co^{II}-porphyrinates.[23,24]

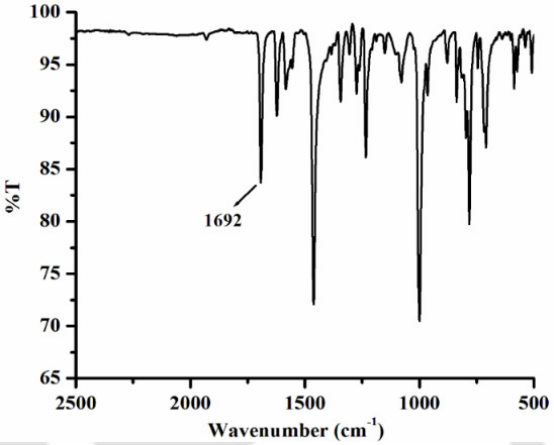

Figure 2.2. FT-IR spectrum of complex **2.2** in KBr.

Complex **2.2** in dichloromethane or acetonitrile did not react with O_2; however, it reacts with H_2O_2. Upon addition of 2.2 equivalents of H_2O_2, complex **2.2** in acetonitrile solution at −40 °C resulted in the formation of corresponding NO_3^- complex, **2.3** (Scheme 2.1).

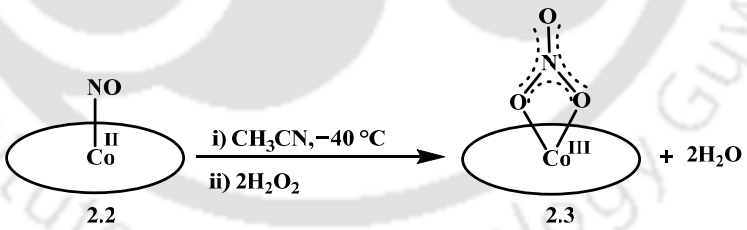

Scheme 2.1

The complex **2.2** in acetonitrile solution at −40 °C shows absorption at 531 and 404 nm, respectively. Addition of 2.2 equivalents of precooled H_2O_2 resulted in the gradual decay of these absorption maxima along with a simultaneous formation of new absorption bands at 542 and 430 nm, respectively (Figure 2.3). These are assignable to the complex **2.3**. The reaction was also carried out in THF solution at −80 °C (Appendix I, Figure A1.12) and no

intermediate formation was observed. Isolation as solid and spectroscopic characterization revealed complex **2.3** as the NO_3^- complex of the corresponding Co^{III} porphyrinate, [(L1)Co(NO_3)] (Experimental Section). Even after several attempts we could not grow the X-ray quality crystals of complex **2.3**.

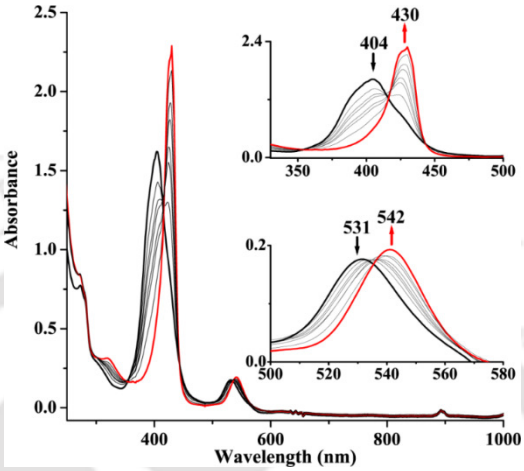

Figure 2.3. UV-visible spectral monitoring of complex **2.2** (black) and after addition of H_2O_2 to result in complex **2.3** (red) at –40 °C in acetonitrile.

In the FT-IR spectroscopy, the NO_3^- stretching frequency was observed at 1385 cm^{-1} (Appendix I, Figure A1.13). The assignment has been done based on the observed stretching frequencies for the NO_3^- groups in the earlier reported metal porphyrin complexes.[25] In ^1H NMR spectrum, complex **2.3** displays well-resolved signals in $CDCl_3$ suggesting the presence of a low spin Co^{III} ion in the complex (Appendix I, Figure A1.15). The signal at 9.10 ppm corresponding to altogether eight protons is assignable to the protons from pyrrole moiety. The signals appeared 7.79 and 7.39 ppm, respectively, are assigned to the protons from the phenyl group (Experimental Section and Appendix I).

Complex **2.3** shows the molecular ion peak at m/Z, 877.05 (calcd. 877.07) corresponding to [(L1)Co(NO_3)] in ESI-mass spectrum (Figure 2.4). The isotopic distribution pattern was found to be in accord with the simulated spectrum (Figure 2.4).

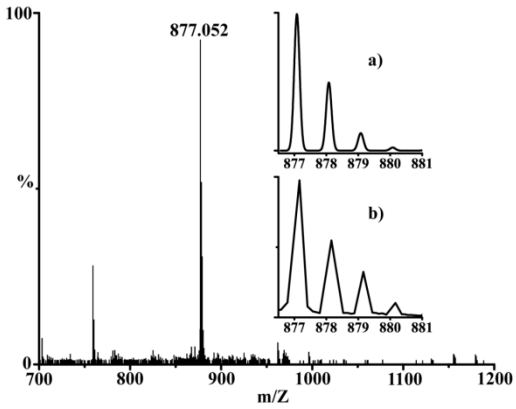

Figure 2.4. ESI-mass spectrum of complex **2.3** in acetonitrile. [Inset: (a) simulated and (b) experimental isotopic distribution pattern].

It is proposed that the reaction of complex **2.2** with H_2O_2 leading to the formation of the complex **2.3** proceeds through the formation of a Co^{III}-PN intermediate; however, no intermediate was observed in UV-visible spectroscopy even when the reaction was carried out in THF at −80 °C. It is to be noted here that thermo-kinetic and theoretical studies suggested that PN intermediates should be too short-lived to detect.[26] Interestingly, when the reaction was carried out in THF solution at −80 °C and followed by freezing at 77 K, the frozen (at 77 K) reaction mixture displayed a signal at g = 2.002 in the X-band EPR spectrum (Figure 2.5(i)). The sharp and isotropic nature of the signal suggested the presence of a radical in the mixture. The spectrum was contaminated with a small fraction of Co^{II} species. Even after several attempts we could not remove this. Similar signal was reported earlier for the Co^{III} porphyrin radical cations generated by electro-oxidation of the Co^{II} porphyrinates.[27] It is to be noted that the Co^{III} porphyrin radical cations show characteristic bleaching of their Soret bands due to loss of π-conjugation.[27] However, in the present case no indication of such feature was observed even at −80 °C temperature. The intensity of the signal decreases gradually with warming it up and finally disappeared suggesting the formation of final product, complex **2.3**. It is proposed that in case of NODs, the reaction of the Fe^{III}-oxy complex with NO resulted in the formation of the PN

intermediate. In subsequent step, the O-O bond cleaved homolytically to produce an oxo-ferryl (Fe^{IV}=O) species and NO_2 (Scheme 2.2).[7–9] In the present case, the appearance of the isotropic signal at g = 2.002 is actually suggestive to the formation of a Co^{IV}-oxo species and NO_2 (Scheme 2.2). It has been reported by Winkler and Gray that for oxo-metal complexes having d^5 configuration, the [M^{III}-O$^\bullet$] is more likely than [M^{IV}=O] configuration.[28] In the present case, the Co^{IV}-oxo species owing to its d^5 configuration would convert into [(L1)Co^{III}-O$^\bullet$]. This accounts for the appearance of sharp EPR signal at g = 2.002 and non-observance of the quenching of Soret band in UV-visible spectroscopy. NO_2 at 77 K dimerizes to form diamagnetic N_2O_4. The [(L1)Co^{III}-O$^\bullet$] in the presence of NO_2 undergoes fast decomposition to the final product, complex **2.3**. In the ESI-mass spectrum of this reaction mixture, a molecular ion peak (m/Z) was observed at 831.09 (calculated: 831.08) which is assignable to the [(L1)Co^{III}-O$^\bullet$] (Figure 2.5(ii)).

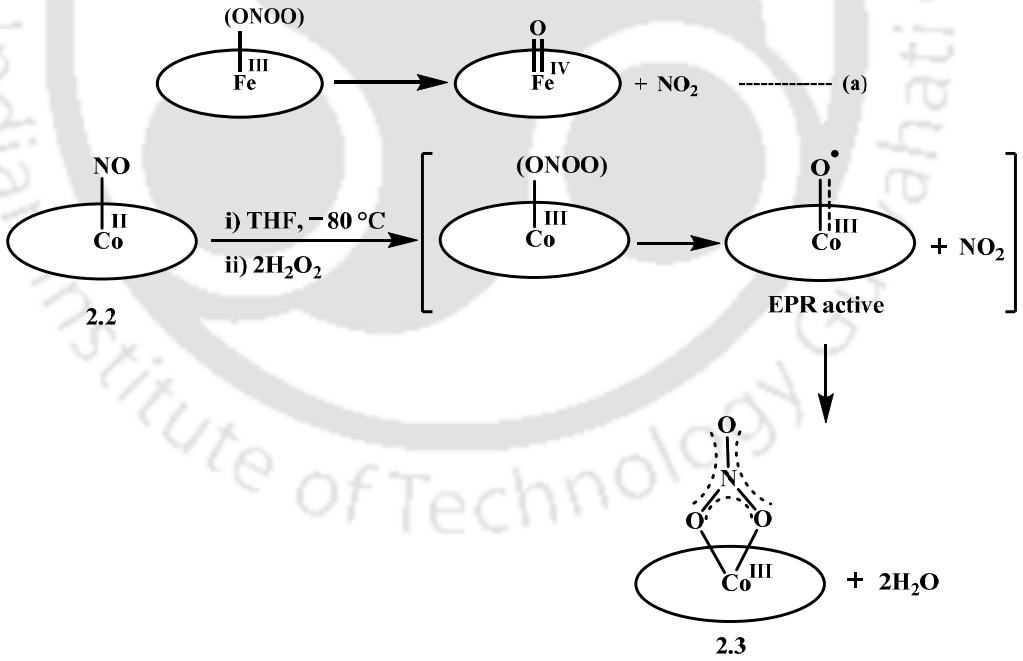

Scheme 2.2

Comparison of the spectral characteristics with an authentic sample generated in a separate reaction of [Co^{II}-L1] complex, **2.1** and *m*CPBA also support the proposition (Appendix I,

Figures A1.18-A1.20). Highly unstable nature of the species precluded its further characterization.

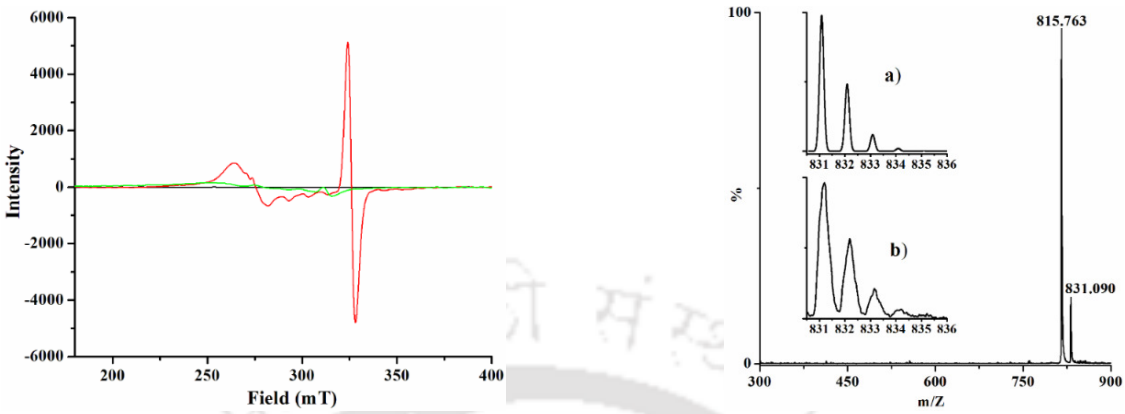

(i) (ii)

Figure 2.5. (i) X-band EPR spectra of complex **2.2** (black), the intermediate (red) formed in the reaction of complex **2.2** and H_2O_2 and complex **2.3** (green) in THF at 77K. (ii) ESI-mass spectrum of the reaction mixture obtained from the reaction of complex **2.2** and H_2O_2 (in acetonitrile) in THF at −80 °C. [Inset: (a) simulated and (b) experimental isotopic distribution pattern].

Because of very short lifetime of the proposed Co^{III}-PN, no direct spectroscopic evidence has been observed, and indirect chemical evidence for the postulated species has been sought. It is to be noted that commonly a phenol nitration reaction is used to provide evidence in support of the presence of metal-PN. It has been observed that when the reaction of complex **2.2** with H_2O_2 was done in the presence of 2,4-di-*tert*-butylphenol, it resulted in an effective phenol ring nitration (~50%). Isolation and characterization of the products from the mixture revealed the formation of the corresponding Co^{III}-hydroxo product, [(L1)Co(OH)], **2.4** (~67%) and 2,4-di-*tert*-butyl-6-nitrophenol (~50%) (Scheme 2.3; Experimental Section and Appendix I, Figures A1.16-A1.17 and A1.21-A1.23). No product corresponding to the oxidative coupled phenol is observed in isolable scale. However, when reaction is followed by the addition of 2,4-di-*tert*-butylphenol, exclusive formation of complex **2.3** was observed along with unreacted 2,4-di-*tert*-butylphenol.

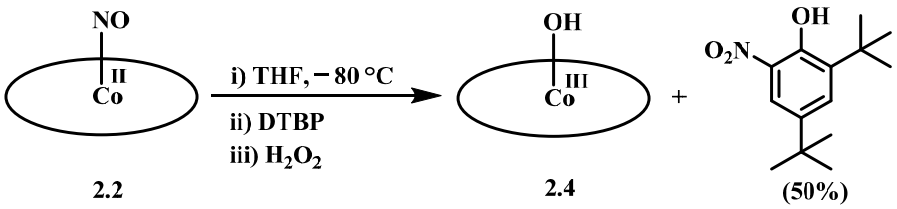

Scheme 2.3

An appreciable amount of phenol ring nitration was observed in those cases. Recently, [(Cl_4TPP)Co(NO)] complex in the presence of H_2O_2 in acetonitrile at −40 °C was exemplified to result in the corresponding NO_2^- complex, [(Cl_4TPP)Co(NO_2)], and the formation of a PN intermediate was implicated.[25] However, in that case no indication of the formation of Co^{IV}-oxo ↔ [(L1)Co^{III}-$O^{\bullet}$] was evidenced.

2.3 Experimental Section

2.3.1 Materials and methods

All the reagents and solvents were purchased from commercial sources and used as received unless specified. All the reactions were carried out under Ar or N_2 atmosphere. Repeated vacuum / purge cycles or bubbling with Ar was used to remove the O_2 from the solvents and solutions. Acetonitrile was distilled from calcium hydride. UV-visible spectra were recorded on Agilent Cary 8454 UV-visible spectrophotometer using Chemstation software. FT-IR spectra were taken on a Perkin Elmer spectrophotometer with samples prepared as KBr pellets or in solutions using KBr cell having 1 cm path length. ^{1}H NMR spectra were obtained with 600 MHz and 400 MHz Varian FT spectrometer. Chemical shifts (ppm) were referenced with respect to Me_4Si as internal standard for organic compounds or to the residual solvent peaks. Elemental analyses were obtained from a Perkin Elmer Series II Analyzer. Mass spectra were recorded on a Waters, Model Q-Tof Premier instrument with ESI mode of ionization. The X-band electron paramagnetic resonance (EPR) spectra were recorded on a JES-FA200 ESR spectrometer, at room

temperature or at 77 K with microwave power, 0.998 mW; microwave frequency, 9.14 GHz; and modulation amplitude, 2.

Single crystals were grown from the respective dichloromethane and chloroform solutions using slow evaporation technique. The intensity data were collected using a Bruker SMART APEX-II CCD diffractometer, equipped with a fine focus 1.75 kW sealed tube MoK_α radiation (λ = 0.71073 Å) at 293(3) K, with increasing ω (width of 0.3° per frame) at a scan speed of 3 s/frame. The SMART software was used for data acquisition. Data integration and reduction were undertaken with SAINT and XPREP software.[15] Multiscan empirical absorption corrections were applied to the data using the program SADABS.[16] Structures were solved by direct methods using SHELXS-2016 and refined with full-matrix least squares on F^2 using SHELXL-2016/6.[17a] Structural illustrations have been drawn with ORTEP-3 for Windows.[17b]

2.3.2 Syntheses

2.3.2.1 Synthesis of ligand $L1H_2$, [5,10,15,20-tetrakis(2, 6-difluorophenyl)porphyrin)]

The ligand **$L1H_2$** was prepared by general procedure of porphyrin synthesis with some modification.[18] 2,6-difluorobenzaldehyde (2.84 g, 20 mmol) and freshly distilled pyrrole (1.34 g, 20 mmol) were added to 37 mL of propionic acid. The solution was refluxed for 2 h and then brought to room temperature. The reaction mixture was then neutralized using aqueous Na_2CO_3. The precipitated mass was filtered off, washed with water and dried under vacuum. The crude mass was subjected to column chromatography to result in the pure ligand as a purple crystalline solid (0.61 g, ~16% yield). Elemental analyses for $C_{44}H_{22}N_4F_8$. Calcd. (%): C, 69.66; H, 2.92; N, 7.38, found (%): C, 69.80; H, 2.90; N, 7.46. FT-IR (in KBr): 3334, 2925, 2853, 2852, 1621, 1588, 1462, 1273, 1234, 1001, 962, 780, 573 cm^{-1}. ^1H NMR (600 MHz, $CDCl_3$): δ_{ppm}, 8.88 (s, 8H), 7.82-7.77 (m, 4H), 7.40-7.37 (m, 8H). ESI-mass (m/Z): Calcd: 758.17, found: 758.51 (Molecular ion peak).

2.3.2.2 Syntheses of the complexes

(a) [(L1)Co], 2.1

The ligand **L1H$_2$** (0.15 g, 0.20 mmol) and $Co(OAc)_2.4H_2O$ (0.50 g, 2.00 mmol) was taken in 200 mL of acetonitrile and refluxed for 12 h. The solid mass was filtered off and the filtrate was collected. After removal of the solvent, the crude product was subjected to column chromatography using neutral alumina column and complex **2.1** was isolated as red solid (0.11 g, ~66 % yield). Elemental analyses for $C_{44}H_{20}N_4F_8Co$, Calcd. (%): C, 64.80; H, 2.47; N, 6.87, found (%): C, 64.90; H, 2.45; N, 6.99. FTIR (in KBr): 1626, 1585, 1463, 1234, 1003, 783, 708, 586 and 508 cm^{-1}. UV-visible (acetonitrile): 406 nm ($\varepsilon/M^{-1}cm^{-1}$, 1.79×10^5), 525 nm ($\varepsilon/M^{-1}cm^{-1}$, 1.75×10^4). EPR in acetonitrile at 77 K: g_{av}, 2.37. ESI-mass (m/Z): Calcd. 815.08, found: 815.09 (Molecular ion peak).

(b) [(L1)Co(NO)], 2.2

Complex **2.1** (0.81 g, 1 mmol) was dissolved in dry and degassed dichloromethane. NO gas was bubbled for ~10 minutes to this solution. The color of the solution changes to deep orange red. After removal of the excess NO, the product was isolated by continuous argon flash with ~85% yield (0.72 g). Elemental analyses for $C_{44}H_{20}N_5OF_8Co$, Calcd. (%): C, 62.50; H, 2.38; N, 8.28, found (%): C, 62.58; H, 2.35; N, 8.39. FT-IR (in KBr): 1692, 1461, 1000, 783, 710, 588, 509 cm^{-1}. UV-visible (acetonitrile): 404 nm ($\varepsilon/M^{-1}cm^{-1}$, 1.40×10^5), 531 nm (ε/M^{-1} cm^{-1}, 1.53×10^4). ^1H NMR (400 MHz, $CDCl_3$): δ_{ppm}, 8.95 (s, 8H), 7.80-7.75 (m, 4H), 7.39-7.36 (m, 8H). ESI-mass (m/Z): Calcd. 815.08; found 815.27 (molecular ion peak for [Co(L1)]).

(c) [(L1)Co(NO$_3$)], 2.3

Complex **2.2** (0.42 g, 0.5 mmol) was taken in 20 mL of dry and degassed acetonitrile and cooled at –40 ºC. Pre-cooled hydrogen peroxide (37% v/v, 2.2 mmol) in acetonitrile was

added to this cold solution and stirred for 2 h. The solution was warmed up to room temperature and dried under reduced pressure (0.26 g, ~60% yield). Elemental analyses for $C_{44}H_{20}N_5O_3F_8Co$, Calcd. (%): C, 60.22; H, 2.30; N, 7.98, found (%): C, 60.30; H, 2.31; N, 8.06. FT-IR (in KBr): 1622, 1466, 1385, 1238, 1024, 880, 805 and 791 cm^{-1}. UV-visible (acetonitrile): 430 nm ($\varepsilon/M^{-1}cm^{-1}$, 2.18×10^5), 542 nm ($\varepsilon/M^{-1}cm^{-1}$, 1.77×10^4). ^1H NMR (400 MHz, $CDCl_3$): δ_{ppm}, 9.10 (s, 8H), 7.83-7.76 (m, 4H), 7.43-7.35 (m, 8H). ESI-mass (m/Z): Calcd: 877.07, found: 877.05 (Molecular ion peak for [Co(L1)(NO_3)]).

(d) Complex 2.4 and 2,4-di-tert-butyl-6-nitrophenol

To a dry and degassed acetonitrile solution of complex **2.2** (0.84 g, 1 mmol), precooled 2,4-di-*tert*-butylphenol (1.03 g, 5 mmol) was added followed by pre-cooled H_2O_2 (37% v/v, 2.2 mmol) in acetonitrile at −40 °C and stirred for 1/2 h at the same temperature. The reaction mixture was then brought to room temperature and dried in a rotavapor. Purification of the crude mass through column chromatography resulted in pure 2,4-di-*tert*-butyl-6-nitrophenol. Yield: 0.125 g (~50%). Complex **2.4**. Yield: 0.558 g (~67%).

2,4-di-*tert*-butyl-6-nitrophenol

Elemental analyses for $C_{14}H_{21}NO_3$, Calcd. (%): C, 66.91; H, 8.42; N, 5.57, found (%):C, 67.07; H, 8.40; N, 5.68. ^1H NMR (600 MHz, $CDCl_3$): δ_{ppm}, 7.40 (s, 1H), 7.11 (s, 1H), 5.22 (s, 1H), 1.45 (s, 9H), 1.32 (s, 9H). ^{13}C NMR (150 MHz, $CDCl_3$): δ_{ppm}, 149.7, 142.9, 136.1, 125.2, 124.8, 122.3, 35.2, 34.4, 31.6, 29.6. ESI-mass (m/Z): Calcd: 251.15, found: 250.53 (M−1).

Complex 2.4: Yield: 0.558 g (~67%). Elemental analyses for $C_{44}H_{21}N_4OF_8Co$, Calcd. (%): C, 63.47; H, 2.54; N, 6.73, found (%): C, 63.56; H, 2.55; N, 6.88. FT-IR (in KBr): 3449, 2925, 2855, 1624, 1574, 1464, 1428, 1372, 1348, 1276, 1234, 1074, 999 and 761 cm^{-1}.

UV-visible (acetonitrile): 426 nm ($\varepsilon/M^{-1}cm^{-1}$, 1.91×10^5), 548 nm ($\varepsilon/M^{-1}cm^{-1}$, 1.96×10^4).

2.4 Conclusion

Thus, the nitrosyl complex of cobalt porphyrin, [(L1)Co(NO)] having $\{CoNO\}^8$ description in acetonitrile (or THF) solution at −40 °C (or −80 °C) was found to react with H_2O_2 to result in the corresponding NO_3^- complex, [(L1)Co(NO_3)]. The reaction proceeds *via* the formation of a presumed Co^{III}-PN intermediate. X-Band EPR and ESI-mass spectroscopic studies suggest the intermediate formation of the [(L1)Co^{III}-$O^{\bullet}$], which in turn supports the generation of the corresponding Co^{IV}-oxo species during the reaction. This is in accord with the homolytic cleavage of the O-O bond in heme-PN proposed in the NOD activity. In addition, the nitration of phenol ring induced by the above reaction also suggests the formation of a PN intermediate.

2.5 References

1) Ignarro L. J. *Nitric oxide: Biology and Pathobiology*; Ed.; Academic press; San Diego, **2000**.

2) (a) Moncada, S.; Palmer, R. M. J.; Higgs, E. A. *Pharmacol. Rev.* **1991**, *43*, 109. (b) Butler, A. R.; Williams, D. L. H. *Chem. Soc. Rev.* **1993**, *22*, 233. (c) Feelisch, M.; Stamler, J. S. *Methods in nitric oxide research*; Ed. John Wiley and Sons; Chichester, England, **1996**. (d) Jia, L.; Bonaventura C.; Bonaventura, J.; Stamler, J. S. *Nature*, **1996**, *380*, 221. (e) Galdwin, M. T.; Lancaster, J. R. Jr.; Freeman, B. A.; Schechter, A. N. *Nat. Med.* **2003**, *9*, 496.

3) (a) Radi, R. *Proc. Natl. Acad. Sci. U. S. A.* **2004**, *101*, 4003. (b) Qiao, L.; Lu, Y.; Liu, B.; Girault, H. H. *J. Am. Chem. Soc.* **2011**, *133*, 19823. (c) Ford, P. C.; Wink, D. A.; Stanbury, D. M. *FEBS Lett.* **1993**, *326*, 1. (d) Tran, N. G.; Kalyvas, H.;

Skodje, K. M.; Hayashi, T.; Moënne- Loccoz, P.; Callan, P. E.; Shearer, J.; Kirschenbaum, L. J.; Kim, E. *J. Am. Chem. Soc.* **2011**, *133*, 1184.

4) (a) Goldstein, S.; Lind, J.; Merenyi, G. *Chem. Rev.* **2005**, *105*, 2457. (b) Pacher, P.; Beckman, J. S.; Liaudet, L. *Physiol. Rev.* **2007**, *87*, 315. (c) Blough, N. V.; Zafiriou, O. C. *Inorg. Chem.* **1985**, *24*, 3502. (d) Nauser, T.; Koppenol, W. H. *J. Phys. Chem. A* **2002**, *106*, 4084. (e) Speelman, A. L.; Lehnert, N. *Acc. Chem. Res.* **2014**, *47*, 1106. (f) Fry, N. L. Mascharak, P. K. *Acc. Chem. Res.* **2011**, *44*, 289.

5) (a) Doyle, M. P.; Hoekstra, J. W *Inorg. Biochem.* **1981**, *14*, 351. (b) Cooper, C. E.; Torres, J.; Sharpe, M. A.; Wilson, M. T. *FEBS Lett.* **1997**, *414*, 281. (c) Tocheva, E. I.; Rosell, F. I.; Mauk, A. G.; Murphy, M. E. *Science* **2004**, *304*, 867.

6) (a) Gardner, P. R.; Gardner, A. M.; Martin, L. A.; Salzman, A. L. *Proc. Natl. Acad. Sci. U.S.A.* **1998**, *95*, 10378. (b) Ford,P. C.; Lorkovic, I. M. *Chem. Rev.* **2002**, *102*, 993. (c) Schopfer, M. P.; Mondal, B.; Lee, D.-H.; Sarjeant, A. A. N.; Karlin, K. D. *J. Am. Chem. Soc.* **2009**, *131*, 11304.

7) Wick, P. K.; Kissner, R.; Koppenol, W. H. *Helv. Chim. Acta* **2000**, *83*, 748.

8) (a) Roncaroli, F.; Videla, M.; Slep, L. D.; Olabe, J. A. *Coord. Chem. Rev.* **2007**, *251*, 1903. (b) Maiti, D.; Lee, D. -H.; Sarjeant, A. A. N.; Pau, M. Y. M.; Solomon, E. I.; Gaoutchenova, K.; Sundermeyer, J.; Karlin, K. D. *J. Am. Chem. Soc.* **2008**, *130*, 6700.

9) (a) Goodwin, J. A.; Coor, J. L.; Kavanagh, D. F.; Sabbagh, M.; Howard, J. W.; Adamec, J. R.; Parmley, D. J.; Tarsis, E. M.; Kurtikyan, T. S.; Hovhannisyan, A. A.; Desrochers, P. J.; Standard, J. M. *Inorg. Chem.* **2008**, *47*, 7852. (b) Kurtikyan, T. S.; Ford, P. C. *Chem. Commun.* **2010**, *46*, 8570. (c) Kurtikyan, T. S.; Eksuzyan, S. R.; Goodwin, J. A.; Hovhannisyan, G. S. *Inorg. Chem.* **2013**, *52*, 12046.

10) (a) Yokoyama, A.; Han, J. E.; Cho, J.; Kubo, M.; Ogura, T.; Siegler, M. A.; Karlin, K. D.; Nam, W. *J. Am. Chem. Soc.* **2012**, *134*, 15269. (b) Yokoyama, A.; Cho, K. -B.; Karlin, K. D.; Nam, W. *J. Am. Chem. Soc.* **2013**, *135*, 14900.

11) (a) Clarkson S. G., Basolo F. *J. Chem. Soc. Chem. Commun.* **1972**, *119*, 670. (b) Clarkson S. G., Basolo F. *Inorg. Chem.* **1973**, *12*, 1528.

12) Skodje, K. M.; Williard, P. G.; Kim, E. *Dalton Trans.* **2012**, *41*, 7849.

13) Park, G. Y.; Deepalatha, S.; Puiu, S. C.; Lee, D.-H.; Mondal, B.; Sarjeant, A. A. N.; del Rio, D.; Pau, M. Y. M.; Solomon, E. I.; Karlin, K. D. *J. Biol. Inorg. Chem.* **2009**, *14*, 1301.

14) Kalita, A.; Kumar, P.; Mondal, B. *Chem. Commun.* **2012**, *48*, 4636.

15) SMART, SAINT and XPREP, Siemens Analytical X-ray Instruments Inc., Madison, Wisconsin, USA, **1995**.

16) Sheldrick, G. M. SADABS: software for Empirical Absorption Correction, University of Gottingen, Institut fur Anorganische Chemieder Universitat, Tammanstrasse 4, D-3400 Gottingen, Germany, **1999**.

17) (a) Sheldrick, G. M. SHELXS-2014, University of Gottingen, Germany. (b) Farrugia, L. J. ORTEP-3 for Windows - a version of ORTEP-III with a Graphical User Interface (GUI) *J. Appl. Crystallogr.* **1997**, *30*, 565.

18) Soman, R.; Sujatha, S.; Arunkumar, C. *J. Fluorine Chem.* **2014**, *163*, 16.

19) (a) Dey, S.; Rath, S. P. *Dalton Trans.* **2014**, *43*, 2301. (b) Smirnov, V. V.; Woller, E. K.; DiMagno, S. G. *Inorg. Chem.* **1998**, *37*, 4971. (c) Cheng, R. J.; Chen, Y. H.; Chen, C. C.; Lee, G. H.; Peng, S. M.; Chen, P. P. Y. *Inorg. Chem.* **2008**, *53*, 8848. (d) Dey, S.; Sil, D.; Rath, S. P. *Angew. Chem. Int. Ed.* **2016**, *55*, 996.

20) (a) Addo, G. B. R.; Hodge, S. J.; Yi, G. B.; Khan, M. A.; Ma, T.; Caemelbecke, E. V.; Guo, N.; Kadish, K. M. *Inorg. Chem.* **1996**, *35*, 6530. (b) Enemark, J. H.;

Feltham, R. D. Coord. *Chem. Rev.* **1974**, *13*, 339. (c) Richter-Addo, G. B.; Legzdins, P. Metal Nitrosyls; Oxford University Press: New York, **1992**. (d) McCleverty, J. A. *Chem. Rev.* **2004**, *104*, 403.

21) Soldatova, A. V.; Ibrahim, M.; Spiro, T. G. *Inorg. Chem.* **2013**, *52*, 7478.

22) (a) Scheidt, W. R.; Hoard, J. L. *J. Am. Chem. Soc.* **1973**, *95*, 8281. (b) Wayland, B. B.; Minkiewicz, J. V.; Abd-Elmageed, M. E. *J. Am. Chem. Soc.* **1974**, *96*, 2795. (c) Fujita, E.; Chang, C. K.; Fazer, J. *J. Am. Chem. Soc.* **1985**, *107*, 7665. (d) Fujita, E.; Fazer, J. *J. Am. Chem. Soc.* **1983**, *105*, 6743.

23) Saha, S.; Gogoi, K.; Mondal, B.; Ghosh, S.; Deka, H.; Mondal, B. *Inorg. Chem.* **2017**, *56*, 7781.

24) Addo, G. B. R.; Hodge, S. J.; Yi, G. B.; Khan, M. A.; Ma, T.; Caemelbecke, E. V.; Guo, N.; Kadish, K. M. *Inorg. Chem.* **1996**, *35*, 6530.

25) (a) Kurtikyan, T. S.; Hayrpetyan, V. A.; Mehrabyan, M. M.; Ford, P. C. *Inorg. Chem.* **2014**, *53*, 11948. (b) Kurtikyan, T. S.; Ford. P. C. *Angew. Chem. Int. Ed.* **2006**, *45*, 492. (c) Kurtikyan, T. S., Hovhannisyan, A. A., Gulyan, G. M., Ford, P. C. *Inorg. Chem.* **2007**, *46*, 7024.

26) (a) Schopfer, M. P.; Mondal, B.; Lee, D.-H.; Sargeant, A. N. N.; Karlin, K. D. *J. Am. Chem. Soc.* **2009**, *131*, 11304. (b) Goldstein, S.; Merenyi, G.; Samuni, A. *J. Am. Chem. Soc.* **2004**, *126*, 15694. (c) Herold, S.; Koppenol, W. H. *Coord. Chem. Rev.* **2005**, 249, 499. (d) Ford, P. C.; Lorkovic, I. M. *Chem. Rev.* **2002**, *102*, 993.

27) (a) Hong, S.; Pfaff, F.F.; Kwon, E.; Wang, Y.; Seo, M.-S.; Bill, E.; Ray, K.; Nam, W. *Angew. Chem. Int. Ed.* **2014**, *53*, 10403. (b) Dey, S.; Sil, D.; Rath, S. P. *Angew. Chem.* **2016**, *128*, 1008. (c) Ikezaki, A.; Takahashi, Nakamura, M. *Chem. Commun.* **2013**, *49*, 3098. (d) Ichimori, K.; Ohya-Nishiguchi, H.; Hirota, N.; Yamamoto, K. *Bull. Chem. Soc. Jpn.* **1985**, *58*, 623.

28) Winkler, J. R.; Gray, H. B. *Struct. Bonding (Berlin, Ger.)* **2011**, *142*, 17.

29) Kalita, A.; Deka, R. C.; Mondal, B. *Inorg. Chem.* **2013**, *52*, 10897.

Chapter 3

Reaction of a Nitrosyl Complex of Mn^{II}-(Cl_4TPP) Complex with Superoxide: Putative Formation of Peroxynitrite Intermediate

Abstract

A nitrosyl complex of Mn^{II}-porphyrinate, [(L2)Mn^{II}(NO)], **3.2** (**L2H$_2$** = 5,10,15,20-tetrakis(4-chlorophenyl)porphyrin) reacts with superoxide (O_2^-) in dichloromethane at −80 °C to result in the corresponding nitrite (NO_2^-) complex, **3.3**. Spectroscopic and structural characterization confirms the square pyramidal geometry of the penta-coordinated Mn^{II}-nitrosyl complex, **3.2**. The reaction proceeds through the formation of a presumed Mn^{III}-PN intermediate. The formation of the PN intermediate was further supported by the phenol ring nitration which resembles to the biologically well-established tyrosine nitration.

3.1 Introduction

Nitric oxide (NO) is a ubiquitous signal transduction molecule found in various physiological processes, like cellular signaling, platelet disaggregation, neurotransmission and in the immune response to bacterial infection.[1,2] In spite of being very important molecule, it can also become cytotoxic when overproduced.[3] *In vivo* the excess NO can react with superoxide ion (O_2^-) and converts to a more toxic reactive nitrogen species like, peroxynitrite ($OONO^-$) (PN).[3-5] This can lead to DNA cleavage,[6] lipid peroxidation,[7] protein nitration,[8] enzyme inactivation,[9,10] and the release of free metal ions.[10] These changes may cause cell death and tissue injury through oxidative stress and enhances different disease states.[11] It is now well established that PN is responsible for the protein tyrosine nitration.[12]

Nitric oxide dioxygenase enzymes (NODs) regulate the level of NO in biological systems by converting it into biologically benign nitrate ion (NO_3^-).[13,14] In NOD activity, an iron(III)-superoxo species reacts with NO to result in NO_3^- ion. The formation of a PN ion has been proposed as the intermediate in this transformation. It is proposed that an oxo-ferryl, [Fe^{IV}(O)] species formed in the reaction *via* the homolytic cleavage of O-O bond of the Fe^{III}-PN intermediate. Such an oxo-ferryl species has been evidenced spectroscopically in the reaction of myoglobin with PN ion. Though, in literature, the involvement of a proposed metal-PN species was exemplified in the reactions of NO with metal-oxygen species, the direct evidence is still elusive. This is because of the very short life time of metal-PN. In addition, the evidence of formation of high valent metal-oxo species as from the homolytic O-O bond cleavage of metal-PN intermediate is also in scarce because of very fast recombination of the metal-oxo species with NO_2 in the reaction cage to result in NO_3^-. Hence the reactivity study of metal-superoxo species with NO or a metal-nitrosyl

with O_2^- is of immense importance to elucidate the undetected intermediate/s in the reaction.

In literature, the reaction of superoxo and peroxo complexes of heme and non-heme iron, cobalt and chromium with NO are reported where the formation of the metal-PN intermediates is implicated.

On the other hand, presumed metal-PNs are reported to form in the reaction of a metal-nitrosyl and O_2. For example, the reaction of cobalt-nitrosyl with O_2 to yield NO_2^- was reported long back.[15] The reaction of a non-heme dinitrosyliron complex with O_2 resulted in NO_3^- complex.[16] In the presence of O_2 a Cu^I-nitrosyl complex results in NO_2^- product through a presumed PN intermediate.[17] In addition, $\{CuNO\}^{10}$ complex reacts with H_2O_2 to result in the copper-nitrato complex through a presumed Cu^I-PN intermediate formation.[18] Recently, a non-heme Cr^{IV}-peroxo and Cr^{III}-superoxo complexes were reported to react with NO to result in Cr^{III}-nitrate / nitrite to result in the corresponding Cr^{IV}-oxo and NO_2 presumably *via* a Cr^{III}-PN intermediate formation.[19] Recently two cobalt nitrosyl complexes were found to react with H_2O_2 to give the cobalt NO_3^- and NO_2^- product.[20,24a]

Therefore, the reaction of the nitrosyl complexes of transition metal ions with different O_2 species has attracted a lot of research interest to understand the formation and decomposition pathway of PN in biological systems. In this direction, the examples involving the reaction of manganese-nitrosyls with different O_2 species is rare in literature.

This chapter describes the synthesis, structural characterization of a nitrosyl complex of manganese porphyrin, [(L2)Mn(NO)] (**3.2**). In the presence of superoxide (O_2^-) ion the manganese-nitrosyl complex exhibits NOD reactivity where the intermediate formation of PN is implicated.

3.2 Results and Discussion

The ligand and complex **3.1** were synthesized by following reported procedure with slight modification.[21] Complex **3.1** was characterized by various spectroscopic techniques as well as single crystal X-ray structure determination (Appendix II, Figures A2.4-A2.6). The ORTEP diagram is shown in figure 3.1(i) and the metric parameters are listed in Appendix II, Tables A2.1-A2.3. The crystal structure of complex **3.1** confirms that penta-coordinated manganese ion is surrounded by the four nitrogen atoms of the porphyrin ring forming a square plane and the axial position is fulfilled by chloride ion. The Mn-N_P and Mn-Cl bond lengths are 2.013(7) and 2.581(10) Å, respectively.[22] The reaction of complex **3.1** and hydroxylamine resulted in the corresponding nitrosyl complex, **3.2**.[21] The structural characterization of complex **3.2** reveals the presence of a five-coordinated Mn center with axially bonded NO group. The ORTEP diagram is shown in figure 3.1(ii). The metric parameters (Appendix II, Tables A2.1-A2.3) are within the range of reported analogous complexes. The N-O bond distance and Mn-N-O bond angles are 1.096(9) Å and 180.0°, respectively. These values are in accord with reported analogous complexes. For example, the Mn-N-O bond angle is reported as 177.8(3)° and the N-O distance is 1.160(3) Å for nitrosyl complex of (5,10,15,20-tetratolylporphinato)manganese(II).[23]

The absorption bands for complex **3.2** appeared at 426 and 545 nm (Figure 3.2(ii)) and Appendix II, Figure A2.7). Addition of a precooled dichloromethane solution of KO_2 in C.E. (18-crown-6 ether) to complex **3.2** in dichloromethane at −80 °C resulted in the appearance of new bands at 478, 582 and 618 nm (Figure 3.2(ii)). No further change was observed in the UV-visible spectrum suggesting the formation of a new complex as the final product. No intermediate formation was observed at any stage in the UV-visible spectral monitoring. The final compound was isolated as solid and characterized as NO_2^- complex (**3.3**) (Experimental Section and Appendix II, Figures A2.10-A2.11).

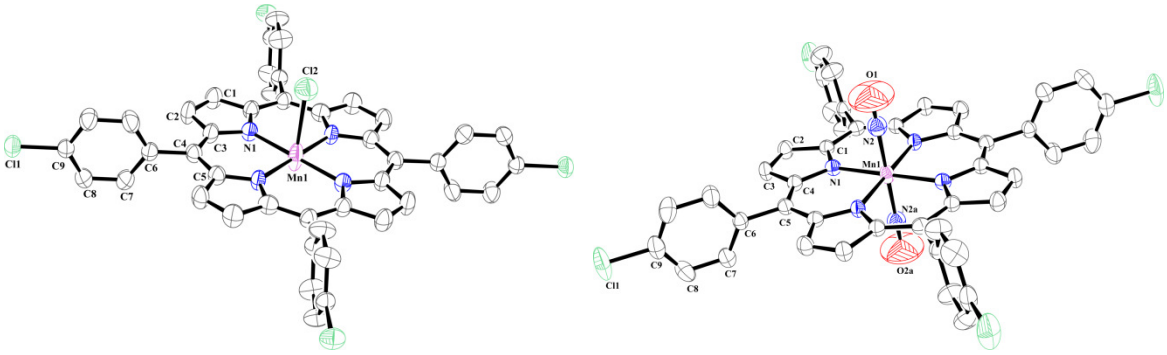

(i) (ii)

Figure 3.1. ORTEP diagrams of complexes **3.1** (i) and **3.2** (ii) (50% thermal ellipsoid plot, H-atoms and solvent molecules are omitted for clarity) (occupancy for both the NO is 50 %).

In FT-IR spectroscopy the characteristic nitrosyl stretching frequency was observed at 1770 cm^{-1} in the case of complex **3.2** (Figure 3.2(i)). Earlier reported analogous five-coordinated Mn-nitrosyl complex, $[(TPP)Mn^{II}(NO)]$ shows nitrosyl stretching at 1760 cm^{-1}.[24] Upon reaction of complex **3.2** with KO_2 in dichloromethane solution, the characteristic nitrosyl stretching at 1770 cm^{-1} disappeared with the appearance of a new stretching frequency at 1249 cm^{-1} (Appendix II, Figure A2.10). This is attributed to the NO_2^- group coordinated to Mn-center.

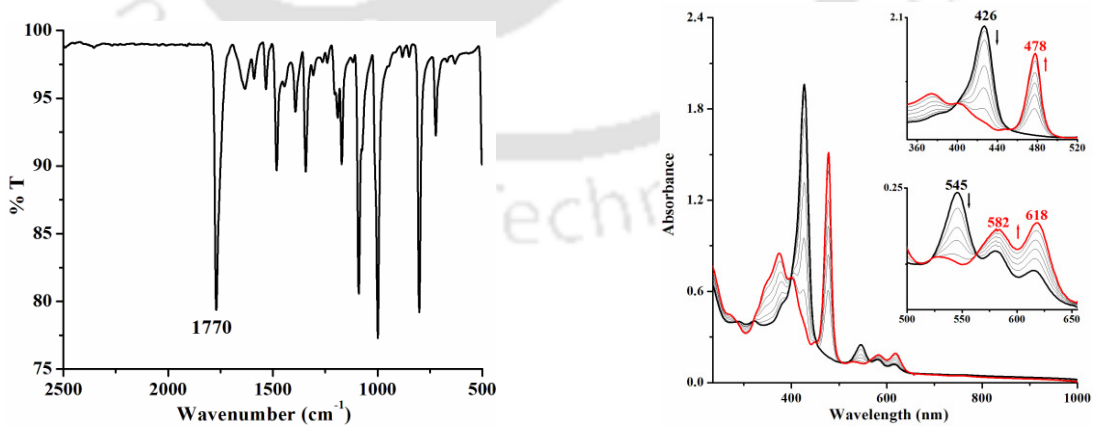

(i) (ii)

Figure 3.2. (i) FT-IR spectrum of complex **3.2** in KBr. (ii) UV-visible spectral monitoring of complex **3.2** (black) and after addition of KO_2 in C.E. to result in complex **3.3** (red) at −80 °C in dichloromethane.

The ESI-mass spectrum of complex **3.2** was populated by the molecular ion peak at m/Z 805.10, assignable to the [(L2)Mn] moiety (calcd. m/Z =805.01) (Appendix II, Figure A2.9). This is attributed to the facile loss of the axial nitrosyl group.[25]

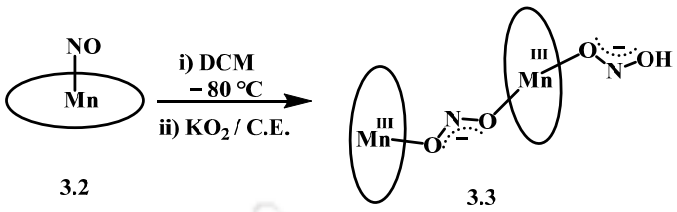

3.2 3.3

Scheme 3.1

Structural characterization of complex **3.3** further confirmed its formulation as a manganese NO_2^- complex. The ORTEP diagram suggests the presence of the bridging NO_2^- group in complex **3.3** (Figure 3.3). The Mn center is bonded to the four nitrogen atoms of the porphyrin ring and a NO_2^- group bridges between two Mn centers, fulfilling the axial coordination. The crystallographic data and metric parameters were listed in Appendix II, Tables A2.1-A2.3. The average Mn-N_P and Mn-O_{NO_2} bond distances are 2.003 and 2.183 Å, respectively. This type of *syn-anti* NO_2^- bridging mode though observed previously in non-heme manganese system with the average Mn-O_{NO_2} bond distance, 2.237 Å, are rare in literature.[26]

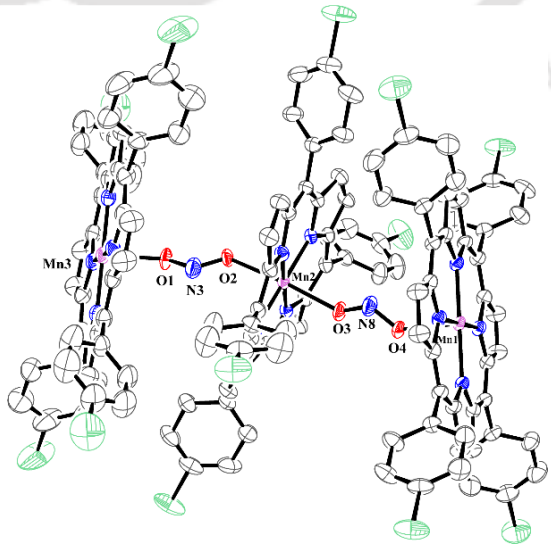

Figure 3.3. ORTEP diagram of complex **3.3** (35% thermal ellipsoid plot, H-atoms and solvent molecules are omitted for clarity).

The formation of complex **3.3** in the reaction of Mn-nitrosyl, **3.2** with superoxide can be envisaged to proceed through a Mn^{III}-PN intermediate step. It has been reported earlier that metal-PN complexes either isomerizes rapidly to the NO_3^- or can convert into the corresponding metal NO_2^- by the loss of ½ molecule of O_2 (Equation 3.1).[25a,27] The amount of released O_2, in the present study, has not been attempted to quantify.

$$\mathbf{M\text{-}PN \longrightarrow M\text{-}NO_2 + 1/2\ O_2} \quad \text{---------- (Eq. 3.1)}$$

Thus, the involvement of a Mn^{III}-PN complex is presumed in the present reaction. Since, no intermediate was evidenced in the spectroscopic monitoring of the reaction, we sought chemical evidence to confirm the formation of Mn^{III}-PN intermediate. As the PN ions are strong nitrating/oxidising agent, the phenol ring nitration / oxidation reaction has been used extensively in literature to establish the existence of a PN ion. In fact, this reaction resembles the tyrosine nitration in biological systems. It has been found that when the reaction of complex **3.2** in dichloromethane at −80 °C with KO_2 was carried out in the presence of externally added 2,4-di-*tert*-butylphenol, it resulted in ~40% of nitrophenol along with the dimerised product, bisphenol (~20 %) (Experimental Section and Appendix II, Figures A2.12-A2.19). On the other hand, when the phenol was added after the addition of KO_2 to the dichloromethane solution of complex **3.2** at −80 °C, resulted in the exclusive formation of complex **3.3** and the phenol was isolated in near quantitative amount.

3.3 Experimental Section

3.3.1 Materials and methods

All the reagents and solvents were purchased from commercial sources and used as received unless specified. All the reactions were carried out under Ar or N_2 atmosphere. Repeated vacuum / purge cycles or bubbling with Ar was used to remove the O_2 from the solvents and solutions. Acetonitrile, chloroform and dichloromethane were dried over

calcium hydride. UV-visible spectra were recorded on Agilent Cary 8454 UV-visible spectrophotometer using Chemstation software. FT-IR spectra were taken on a Perkin Elmer spectrophotometer with samples prepared as KBr pellets or in solutions using KBr cell having 1 cm path length. ^{1}H NMR spectra were obtained with 600 and 400 MHz Varian FT spectrometer. Chemical shifts (ppm) were referenced with respect to Me_4Si as internal standard for organic compounds or to the residual solvent peaks. Elemental analyses were obtained from a Perkin Elmer Series II Analyzer. Mass spectra were recorded on a Waters, Model Q-Tof Premier instrument with ESI mode of ionization. The X-band electron paramagnetic resonance (EPR) spectra were recorded on a JES-FA200 ESR spectrometer, at room temperature or at 77 K with microwave power, 0.998 mW; microwave frequency, 9.14 GHz; and modulation amplitude, 2.

Single crystals were grown from the respective dichloromethane and chloroform solutions using slow evaporation technique. The intensity data were collected using a Bruker SMART APEX-II CCD diffractometer, equipped with a fine focus 1.75 kW sealed tube MoK_α radiation (λ = 0.71073 Å) at 293(3) K, with increasing ω (width of 0.3° per frame) at a scan speed of 3 s/frame. The SMART software was used for data acquisition. Data integration and reduction were undertaken with SAINT and XPREP software.[28] Multiscan empirical absorption corrections were applied to the data using the program SADABS.[29] Structures were solved by direct methods using SHELXS-2016 and refined with full-matrix least squares on F^2 using SHELXL-2016/6.[30a] Structural illustrations have been drawn with ORTEP-3 for Windows.[30b]

3.3.2 Syntheses

3.3.2.1 Ligand L2H$_2$, [5,10,15,20-tetrakis(4-chlorophenyl)porphyrin]

The ligand **L2H$_2$** was prepared using regular TPP procedure using *p*-Chlorobenzaldehyde

(2.80 g, 20 mmol) and freshly distilled pyrrole (1.34 g, 20 mmol). The product was purified by column chromatography as purple crystal (0.75 g, ~20%).[21] Elemental analyses for $C_{44}H_{26}N_4Cl_4$. Calcd. (%): C, 70.23; H, 3.48; N, 7.45, found (%): C, 70.15; H, 3.47; N, 7.48. FT-IR (in KBr): 3444, 2922, 1487, 1469, 1090, 1015, 966, 797, 728, 491 cm^{-1}. ^1H NMR (600 MHz, $CDCl_3$): δ_{ppm}, 8.85 (s, 8H), 8.14-8.13 (d, 8H), 7.75-7.74 (d, 8H). ESI-mass (m/Z): Calcd: 752.52, found: 753.12 (M+1).

3.3.2.2 Syntheses of the complexes

(a) [(L2)MnCl], 3.1

To a mixture of ligand, **$L2H_2$** (0.19 g, 0.25 mmol) in $CHCl_3$ (12 mL) and AcOH (12 mL), $Mn(OAc)_2.4H_2O$ (0.61 g, 2.50 mmol) was added. After refluxing at 120 °C for 2 h, the solution was filtered. 50 mL of water was added to the mixture. The compound was then extracted with $CHCl_3$ (3 × 30 mL). The crude mass was subjected to column chromatography to result in complex **3.1** as green solid.[21] Yield: 0.19 g (~90%). Elemental analyses for $C_{44}H_{24}N_4Cl_5Mn$, Calcd. (%): C, 62.85; H, 2.88; N, 6.66, found (%): C, 62.80; H, 2.95; N, 6.60. UV-visible (dichloromethane): 470 nm ($\varepsilon/M^{-1}cm^{-1}$, 0.46 × 10^5), 577 nm ($\varepsilon/M^{-1}cm^{-1}$, 0.48 × 10^4), 612 nm ($\varepsilon/M^{-1}cm^{-1}$, 0.49 × 10^4). FT-IR (in KBr): 1606, 1484, 1316, 1092, 1008, 803, 743, 716 cm^{-1}. ESI-mass (m/Z): Calcd. 805.01, found: 805.12 (molecular ion peak for [Mn(L2)]).

(b) [(L2)Mn(NO)], 3.2

Triethylamine (0.76 g, 7.50 mmol) was added to a methanol (10 mL) solution of hydroxylamine hydrochloride (0.52 g, 7.50 mmol) at −20 °C. Triethylammonium chloride was precipitated and removed by filtration. Fresh solution of hydroxylamine was added to dichloromethane solution of complex **3.1** (1.26 g, 1.50 mmol) at −20 °C. Then complex **3.2** was precipitated out of solution as red crystals in a period of 3-4 days at −4 to −10 °C and

was isolated by filtration.[21] Yield 0.93 g, ~75%. Elemental analyses for $C_{44}H_{24}N_5OCl_4Mn$, Calcd. (%): C, 63.26; H, 2.90; N, 8.38, found (%): C, 63.30; H, 2.88; N, 8.40. UV-visible (dichloromethane): 426 nm ($\varepsilon/M^{-1}cm^{-1}$, 1.27×10^5), 545 nm ($\varepsilon/M^{-1}cm^{-1}$, 1.60×10^4), 582 nm ($\varepsilon/M^{-1}cm^{-1}$, 0.76×10^4) and 615 nm ($\varepsilon/M^{-1}cm^{-1}$, 0.55×10^4). FT-IR (in KBr): 1770, 1634, 1533, 1482, 1392, 1343, 1171, 1090, 999, 801, 722 cm^{-1}. ^1H NMR (400 MHz, DMSO-d_6): δ_{ppm}, 8.67 (s, 8H), 8.17-8.05 (m, 8H), 7.84-7.82 (d, 8H).

(c) [(L2)Mn(NO_2)], 3.3

Complex **3.2** (0.42 g, 0.5 mmol) was dissolved in 20 mL of dichloromethane and the solution was cooled at −80 °C. To this cold solution, 1 equivalent KO_2 in presence of C.E. (5 equivalent) in dichloromethane was added and stirred for 2 h. The red color solution changes to green. The solution was brought to room temperature and dried *in vacuo* (0.26 g, ~60% yield). Elemental analyses for $C_{44}H_{24}N_5O_2Cl_4Mn$, Calcd. (%): C, 62.07; H, 2.84; N, 8.23, found (%): C, 62.00; H, 2.80; N, 8.30. UV-visible (dichloromethane): 478 nm ($\varepsilon/M^{-1}cm^{-1}$, 1.62×10^5), 582 nm ($\varepsilon/M^{-1}cm^{-1}$, 1.96×10^4), 618 nm ($\varepsilon/M^{-1}cm^{-1}$, 2.07×10^4). FT-IR (in KBr): 1646, 1550, 1486, 1385, 1249, 1090, 1011, 805 cm^{-1}.

(d) Complex 3.4, 3,3',5,5'-tetra-*tert*-butyl-[1,1'-biphenyl]-2,2'-diol and 2,4-di-*tert*-butyl-6-nitrophenol

Complex **3.2** (0.83 g, 1 mmol) and 2,4-di-*tert*-butylphenol (1.03 g, 5 mmol) were dissolved in 20 mL dry and degassed dichloromethane. The mixture was cooled to −80 °C. To this degassed solution, 1 equivalent potassium superoxide in presence of C.E. (5 equivalent) in dichloromethane was added at −80 °C and stirred for 2 h. The reaction mixture was then brought to room temperature and dried under reduced pressure. The solid mass was then subjected to column chromatography using silica gel column to obtain pure 3,3',5,5'-tetra-*tert*-butyl-[1,1'-biphenyl]-2,2'-diol, 2,4-di-*tert*-buty-6-nitrophenol and complex **3.4**.

3,3',5,5'-tetra-*tert*-butyl-[1,1'-biphenyl]-2,2'-diol: yield: 0.08 g (~20%). Elemental analyses for $C_{28}H_{42}O_2$, Calcd. (%): C, 81.90; H, 10.31, found (%): C, 81.98; H, 10.33. ^{1}H NMR (400 MHz, $CDCl_3$) δ_{ppm}: 7.39 (s, 2 H), 7.12 (s, 2 H), 5.23 (s, 2 H), 1.45 (s, 18 H) and 1.32 (s, 18 H). ^{13}C NMR (100 MHz, $CDCl_3$) δ_{ppm}: 150.0, 143.2, 136.5, 125.5, 125.0, 122.6, 35.4, 34.7, 31.9 and 29.9. ESI-mass (m/Z): Calcd: 410.32, found: 409.27 (M-1).

2,4-di-tert-butyl-6-nitrophenol: yield: 0.10 g (~40%), Elemental analyses for $C_{14}H_{21}NO_3$, Calcd (%): C, 66.91; H, 8.42; N, 5.57. Found (%): C, 67.07; H, 8.40; N, 5.68.^{1}H NMR (600 MHz, $CDCl_3$): δ_{ppm}, 7.40 (s, 1H), 7.12 (s, 1H), 5.22 (s, 1H), 1.45 (s, 9H), 1.32 (s, 9H).^{13}C NMR (150 MHz, $CDCl_3$): δ_{ppm}, 149.8, 143.0, 136.2, 125.3, 124.8, 122.3, 35.2, 34.5, 31.6 and 29.7. ESI-mass (m/Z): Calcd: 251.15, found 250.13 (M-1).

Complex 3.4: yield: 0.53 g (~65%). Elemental analyses for $C_{44}H_{25}N_4OCl_4Mn$, Calcd. (%): C, 64.26; H, 3.06; N, 6.81, found (%): C, 64.23; H, 3.10; N, 6.78. FT-IR (in KBr): 3530, 1650, 1486, 1163, 1090, 1010, 804 cm^{-1}. UV-visible (dichloromethane): 476 nm ($\varepsilon/M^{-1}cm^{-1}$, 1.65×10^5), 582 nm ($\varepsilon/M^{-1}cm^{-1}$, 1.39×10^4), 617 nm ($\varepsilon/M^{-1}cm^{-1}$, 1.53×10^4).

3.4 Conclusion

A stable $\{MnNO\}^6$ complex (**3.2**) has been synthesized and characterized structurally. The reaction of the nitrosyl complex, **3.2** in dichloromethane at −80 °C with O_2^- afforded the corresponding NO_2^- complex (**3.3**). Complex **3.3** has been characterized structurally. Chemical evidence suggested the involvement of a transient Mn^{III}-PN intermediate in the reaction. Thus complex **3.2** in presence of O_2^- displays NOD activity.

3.5 References

1) (a) Ignarro L. J. *Nitric oxide: Biology and Pathobiology* Ed. Academic press; San Diego, **2000**.

2) (a) Moncada, S.; Palmer, R. M. J.; Higgs, E. A. *Pharmacol. Rev*. **1991**, *43*, 109. (b) Butler, A. R.; Williams, D. L. H. *Chem. Soc. Rev*. **1993**, *22*, 233. (c) Feelisch, M.; Stamler, J. S. *Methods in Nitric Oxide Research* Ed. John Wiley and Sons, New York **1996**. (d) Jia, L.; Bonaventura, C.; Bonaventura, J.; Stamler, J. S. *Nature* **1996**, *380*, 221. (e) Galdwin, M. T.; Lancaster, J. R. Jr.; Freeman, B. A.; Schechter, A. N. *Nat. Med*. **2003**, *9*, 496.

3) (a) Radi, R. *Proc. Natl. Acad. Sci. U. S. A.* **2004**, *101*, 4003. (b) Qiao, L.; Lu, Y.; Liu, B.; Girault, H. H. *J. Am. Chem. Soc.* **2011**, *133*, 19823. (c) Ford, P. C.; Wink, D. A.; Stanbury, D. M. *FEBS Lett*. **1993**, *326*, 1. (d) Tran, N. G.; Kalyvas, H.; Skodje, K. M.; Hayashi, T.; Moënne-Loccoz, P.; Callan, P. E.; Shearer, J.; Kirschenbaum, L. J.; Kim, E. *J. Am. Chem. Soc*. **2011**, *133*, 1184.

4) (a) Goldstein, S.; Lind, J.; Merenyi, G. *Chem. Rev*. **2005**, *105*, 2457. (b) Pacher, P.; Beckman, J. S.; Liaudet, L. *Physiol. Rev*. **2007**, *87*, 315. (c) Blough, N. V.; Zafiriou, O. C. *Inorg. Chem*. **1985**, *24*, 3502. (d) Nauser, T.; Koppenol, W. H. *J. Phys. Chem. A* **2002**, *106*, 4084.

5) Radi R. *J. Biol. Chem.* **2013**, *288*, 26464.

6) King, P. A.; Anderson, V. E.; Edwards, J. O.; Gustafson, G.; Plumb, R. C.; Suggs, J. W. *J. Am. Chem. Soc*. **1992**, *114*, 5430.

7) Radi, R.; Beckman, J. S.; Bush, K. M.; Freeman, B. A. *Arch. Biochem. Biophys*. **1991**, *288*, 481.

8) Vliet, A.; Eiserich, J. P.; Kaur, H.; Cross, C. E.; Halliwell, B. *Methods Enzymol*. **1996**, *269*, 175.

9) (a) Schmidt, K.; Klatt, P.; Mayer, B. *Biochem. J*. **1994**, *361*, 645. (b) Hausladen, A.; Fridovich, I. *J. Biol. Chem*. **1994**, *269*, 29405. (c) MacMillan-Crow, L. A.;

Crow, J. P.; Kerby, J. D.; Beckman, J. S.; Thompson, J. A. *Proc. Natl. Acad. Sci. U.S.A.* **1996**, *93*, 11853.

10) (a) Hausladen, A.; Fridovich, I. *J. Biol. Chem*. **1994**, *269*, 29405. (b) Castro, L.; Rodriguez, M.; Radi, R. *J. Biol. Chem*. **1994**, *269*, 29409.

11) Beckman, J. S.; Beckman, T. W.; Chen, J.; Marshall, P. A.; Freeman, B. A. *Proc. Natl. Acad. Sci. U.S.A.* **1990**, *87*, 1620.

12) Souza, J. M.; Peluffo, G.; Radi, R. *Free Radic. Biol. Med.* **2008**, *45*, 357.

13) (a) Doyle, M. P.; Hoekstra, J. W. *Inorg. Biochem.* **1981**, *14*, 351. (b) Cooper, C. E.; Torres, J.; Sharpe, M. A.; Wilson, M. T. *FEBS Lett.* **1997**, *414*, 281. (c) Tocheva, E. I.; Rosell, F. I.; Mauk, A. G.; Murphy, M. E. *Science* **2004**, *304*, 867.

14) (a) Gardner, P. R.; Gardner, A. M.; Martin, L. A.; Salzman, A. L. *Proc. Natl. Acad. Sci. U. S. A.* **1998**, *95*, 10378. (b) Ford, P. C.; Lorkovic, I. M. *Chem. Rev.* **2002**, *102*, 993. (c) Schopfer, M. P.; Mondal, B.; Lee, D.-H.; Sarjeant, A. A. N.; Karlin, K. D. *J. Am. Chem. Soc*. **2009**, *131*, 11304.

15) (a) Clarkson, S. G.; Basolo F. *J. Chem. Soc. Chem. Commun.* **1972**, *119*, 670. (b) Clarkson, S. G.; Basolo F. *Inorg. Chem.* **1973**, *12*, 1528.

16) Skodje, K. M.; Williard, P. G.; Kim, E. *Dalton Trans*. **2012**, *41*, 7849.

17) Park, G. Y.; Deepalatha, S.; Puiu, S. C.; Lee, D.-H.; Mondal, B.; Sarjeant, A. A. N.; del Rio, D.; Pau, M. Y. M.; Solomon, E. I.; Karlin, K. D. *J. Biol. Inorg. Chem.* **2009**, *14*, 1301.

18) Kalita, A.; Kumar, P.; Mondal, B. *Chem. Commun*. **2012**, *48*, 4636.

19) (a) Yokoyama, A.; Han, J. E.; Cho, J.; Kubo, M.; Ogura, T.; Siegler, M. A.; Karlin, K. D.; Nam, W. *J. Am. Chem. Soc.* **2012**, *134*, 15269. (b) Yokoyama, A.; Cho, K. – B.; Karlin, K. D.; Nam, W. *J. Am. Chem. Soc.* **2013**, *135*, 14900.

20) Mondal, B.; Saha, S.; Borah, D.; Mazumdar, R; Mondal, B. *Inorg. Chem*. **2019**, *58*, 1234.

21) (a) Adler, A. D.; Longo, F. R.; Finarelli.; Goldmacher, J.; Assour, J.; Korsakoff, L. *J. Org. Chem.* **1967**, *32*, 476. (b) Rothemund, P.; Menotti, A. R. *J. Am. Chem. Soc.* **1948**, *70*, 1808. (c) Choi, In-K.; Liu, Y.; Wei, Z.; Ryan, M. D. *Inorg. Chem.* **1997,** *36,* 3113.

22) (a) George, S.; Goldberg, I. *Cryst. Growth Des.* **2006**, *6*, 755. (b) Paulat, F.; Praneeth, V.; K. K. Nather, C.; Lehnert, N. *Inorg.Chem.* **2006**, *45*, 2835. (c) Jun-wei, Y.; Xiao-chun, H.; Jin-bin, L.; Tie, C.; Jing, X.; Shan-ling, T.; Ke-er, Y.; Yan, Y.; C*hem. Res. Chinese U.* **2007**, *23*, 384. (d) Milania, J. L. S.; Meireles, A. M.; Cabral, B. N.; Bezerra, W. d. A.; Martins, F. T.; Martins, D. C. d. S.; Chagas, R. P. d. *J. CO_2 Util.* **2019**, 30, 100.

23) Scheidt, W. R.; Hatano, K.; Rupprecht, G. A.; Piciulo, P. L. *Inorg. Chem.* **1979**, *18*, 292.

24) Wayland, B. B.; Olson, L. W.; Siddiqui, Z. U. *J. Am. Chem. Soc*. **1976**, *98*, 94.

25) (a) Saha, S.; Gogoi, K.; Mondal, B.; Ghosh, S.; Deka, H.; Mondal, B. *Inorg. Chem*. **2017**, *56*, 7781. (b) Addo, G. B. R.; Hodge, S. J.; Yi, G. B.; Khan, M. A.; Ma, T.; Caemelbecke, E. V.; Guo, N.; Kadish, K. M. *Inorg. Chem*. **1996**, *35*, 6530.

26) Kar, P.; Biswas, R.; Drew, M. G. B.; Ida, Y.; Ishida, T.; Ghosh, A. *Dalton Trans.* **2011**, *40*, 3295.

27) Maiti, D.; Lee, D.-H.; Sarjeant, A. A. N.; Pau, M. Y. M.; Solomon, E. I.; Gaoutchenova, K.; Sundermeyer, J.; Karlin, K. D. *J. Am. Chem. Soc.* **2008**, *130*, 6700.

28) SMART, SAINT and XPREP, Siemens Analytical X-ray Instruments Inc., Madison, Wisconsin, USA, **1995**.

29) Sheldrick, G. M. SADABS: software for Empirical Absorption Correction, University of Gottingen, Institut fur Anorganische Chemieder Universitat, Tammanstrasse 4, D-3400 Gottingen, Germany, **1999**.

30) (a) Sheldrick, G. M. SHELXS-2014, University of Gottingen, Germany. (b) Farrugia, L. J. ORTEP-3 for Windows - a version of ORTEP-III with a Graphical User Interface (GUI) *J. Appl. Crystallogr.* **1997**, *30*, 565.

Chapter 4

Reaction of a Nitrosyl Complex of Mn^{II}-(F_8TPP) with Superoxide: Putative Formation of Peroxynitrite Intermediate

Abstract

A nitrosyl complex of Mn^{II}-porphyrinate, [(L1)Mn^{II}(NO)], **4.2** (**L1H$_2$** = 5,10,15,20-tetrakis(2,6-difluorophenyl)porphyrin) can react with superoxide (O_2^-) in THF at −80 °C to result in the corresponding nitrate (NO_3^-) complex, **4.3**. The square pyramidal geometry of the penta-coordinated Mn^{II}-nitrosyl complex, **4.2** was confirmed by spectroscopic and structural characterization. The reaction proceeds through the formation of a presumed Mn^{III}-PN intermediate. The formation of PN intermediate was further supported by the phenol ring nitration which resembles to the biologically important tyrosine nitration.

4.1 Introduction

Nitric oxide (NO) is an important small molecule that is involved in various biochemical pathways such as neurotransmission, dilation of blood vessels, immune response etc.[1-3] Under normal conditions, NO is produced by nitric oxide synthase (NOS) at low concentrations. However, the production of excess amount of NO can have detrimental effects *via* the formation of reactive nitrogen species (RNS) such as nitrogen dioxide (NO_2), dinitrogen trioxide (N_2O_3) and peroxynitrite ($ONOO^-$) (PN).[4,5,7] RNS have been of great interest due to their important role in bio-molecule oxidation such as in ageing and disease development.[6] The formation of PN is particularly important because it can cause both oxidative and nitrosative stress under physiological conditions. The formation of these secondary intermediates from NO requires the presence of oxidants like hydrogen peroxide (H_2O_2), superoxide (O_2^-) radicals and transition metal centers.[7,8] PN is presumed to be generated *in vivo* by the diffusion-controlled combination of NO and O_2^- and also from nitrite (NO_2^-) oxidation by peroxidase enzymes.[9] NO_2 forms from the homolytic O–O cleavage of PN, however most aqueous PN isomerizes to NO_3^-. Recent reports describe PN intermediates forming from NO reaction of oxy-globin models [Fe(Por)(NH_3)(O_2)] and [Co(Por)(NH_3)(O_2)] prepared by sequential reactions of O_2 and NH_3 with thin porous layers of respective metal porphyrin complexes. These oxy-globin models react with NO to give NO_3^- complex as final product.[10] Another example was given by Karlin *et al.* where they showed that a (F_8TPP)Fe(III)superoxo complex reacts with NO to give the corresponding NO_3^- complex through a PN intermediate.[11] Cobalt-nitrosyls were reported to react with O_2 and O_2^- to afford cobalt-NO_3^-/NO_2^- complexes.[12,13] In these reactions the formation of a PN intermediate was involved.

Our group is also involved in the study of PN species by the reaction of the metal nitrosyls with O_2^- anion and H_2O_2 and to understand the decomposition of this transient

intermediate. We reported the reaction of a $\{CuNO\}^{10}$ complex with H_2O_2 to form a Cu^{II}-NO_3^- complex *via* the thermal decomposition of a presumed Cu^{I}-PN intermediate.[14] Reactions of cobalt nitrosyls with H_2O_2 were reported recently which proceeds through a presumed PN intermediate.[15]

This chapter describes the reactivity of a nitrosyl complex of Mn(II)-porphyrinate, **4.2** of ligand **L1H$_2$** (**L1H$_2$** = 5,10,15,20-tetrakis(2,6-difluorophenyl)porphyrin) with KO_2 in presence of C.E. (18-crown-6 ether). Addition of KO_2 leads to the formation of a Mn^{III}-NO_3^- complex, **4.3** presumably through the formation of a PN intermediate.

4.2 Results and Discussion

The manganese complex, [(L1)MnCl], **4.1** were prepared following the reported procedure.[16] The formation of the complex **4.1** was confirmed by various spectroscopic techniques (Experimental Section and Appendix III, Figure A3.1-A3.3). It was further characterized by X-ray single crystal structure determination. The ORTEP diagram of complex **4.1** is shown in figure 4.1(i). The crystallographic data and other metric parameters were listed in Appendix III, Tables A3.1-A3.3. The synthesis of the corresponding nitrosyl complex, **4.2** was done by previously reported reductive nitrosylation process with slight modification.[16] Complex **4.2** was characterized by various spectroscopic tools (Experimental Section and Appendix III, Figure A3.4-A3.5) and single crystal X-ray structure determination. The perspective ORTEP view of complex **4.2** is shown in figure 4.1(ii). The crystallographic data and metric parameters were listed in Appendix III, Tables A3.1-A3.3. It is to be noted that the structure of complex **4.2** shows some intrinsic disorder which could not be solved even after several attempts.

The structural characterization of complex **4.1** suggests that the manganese atom is coordinated by the four N atoms from the porphyrin ring to form a square plane and one

chloride atom from the axial position to offer a square pyramidal geometry around the central metal ion. In the case of complex **4.2**, the coordination geometry around the central metal ion is same but with the NO group as axial ligand. The bond distances for Mn-N_P for complex **4.1** ranges from 2.030(8) to 2.019(7) Å with an average value of 2.025 Å and the Mn-Cl bond length is 2.223(7) Å. These two bond lengths are comparable to the analogous compounds like, [Mn^{III}(THPP)Cl] (5,10,15,20-tetrakis(4-hydroxyphenyl)porphyrinmanganese chloride), [Mn^{III}(T2,3-DCDPP)Cl] or [Mn^{III}(TPP)Cl].[17] The N-O bond distance and Mn-N-O bond angles in complex **4.2** are 1.149(6) Å and 171.0(5)°, respectively. These values are in the range of reported nitrosyl complexes of Mn(II)-porphyrinates.[18] For instance, in [(TTP)Mn(NO)] and [(L_3)Mn(NO)], these bond lengths were 1.160(3) and 1.132(10) Å, respectively.

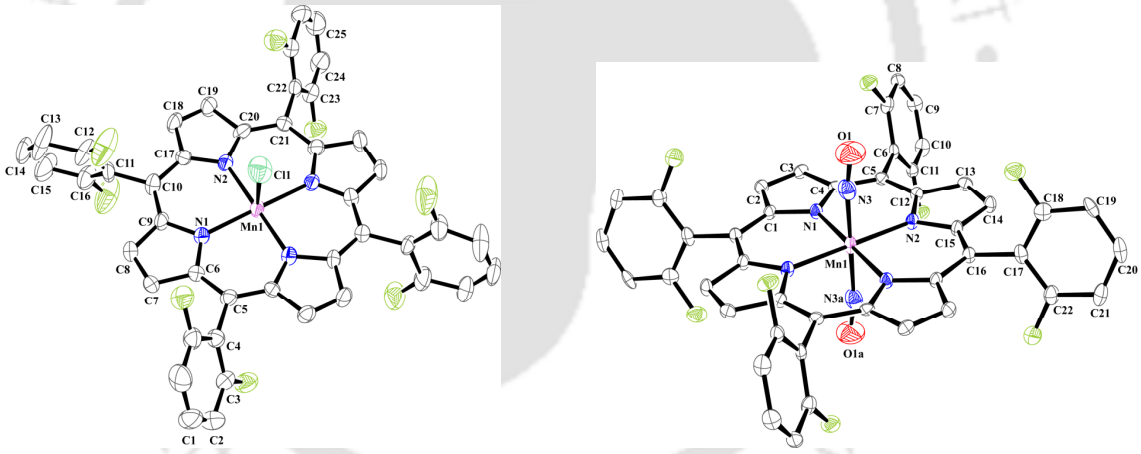

Figure 4.1. ORTEP diagrams of complexes **4.1** (i) and **4.2** (ii) (50% thermal ellipsoid plot, H-atoms are omitted for clarity) (occupancy for both the NO is 50 %).

In FT-IR spectroscopy, complex **4.2** in KBr pellet displays strong nitrosyl stretching at 1762 cm^{-1} (Figure 4.2). In the cases of other structurally characterized Mn-nitrosyl complexes of porphyrinate ligands, the nitrosyl stretching appeared in this range only. For example, in cases of [(TPP)Mn(NO)] and [(L3)Mn(NO)], the NO stretching appeared at 1760 and 1763 cm^{-1}, respectively.[19]

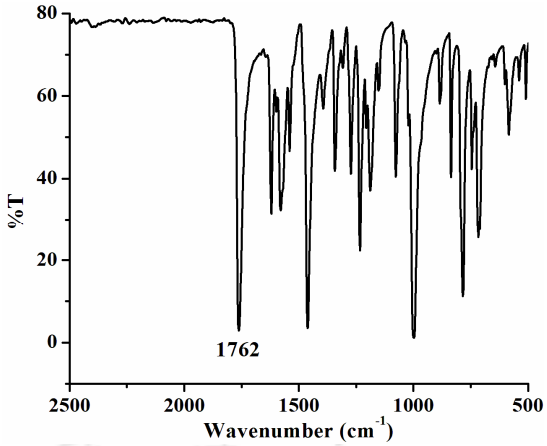

Figure 4.2. FT-IR spectrum of complex **4.2** in KBr.

EPR silent nature of complex **4.2** suggests diamagnetism due to the antiferromagnetic coupling of Mn^{II} and the unpaired electron from the NO moiety. As a result, well resolved signals were observed in ^{1}H NMR spectrum of complex **4.2** (Figure 4.3). The sharp singlet signal at 8.72 ppm appeared for the pyrrole protons. The multiplets at 8.01-7.94 ppm and 7.68-7.58 ppm are assigned to the protons present in the phenyl groups of the porphyrin ring.

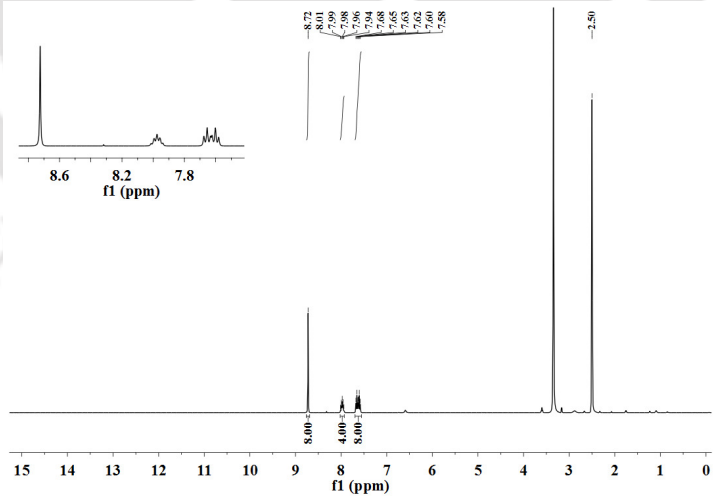

Figure 4.3. ^{1}H NMR spectrum of complex **4.2** in DMSO-d_6.

In the ESI-mass spectrum of complex **4.2**, a peak appears at m/Z, 811.28 assignable to $[(L1)Mn]^{+}$ [calcd. m/Z, 811.09] (Appendix III, Figure A3.5). The facile loss of the axial

NO group of the nitrosyl complexes during ionization is a well known fact and responsible for the m/Z value without the nitrosyl group.[15b,20]

Complex **4.2** in THF solution at −80 °C displays absorption at 418 ($\varepsilon/M^{-1}cm^{-1}$, 1.43×10^5) and 535 ($\varepsilon/M^{-1}cm^{-1}$, 1.97×10^4) nm in the UV-visible spectroscopy. Upon addition of KO_2, the intensity of these bands decreases gradually with the simultaneous formation of the absorption bands at 462 ($\varepsilon/M^{-1}cm^{-1}$, 1.25×10^5) and 553 ($\varepsilon/M^{-1}cm^{-1}$, 1.78×10^4) nm (Figure 4.4(i)). The occurrence of these absorption bands suggests the formation of the final product, [(L1)Mn(NO_3)], complex **4.3** in the reaction (Scheme 4.1). No intermediate was observed even at −80 °C. The final product complex **4.3** was isolated as solid and characterized by spectroscopic techniques.

In the FT-IR spectrum of complex **4.3**, the observed stretching at 1384 and 1295 cm^{-1} are assigned to the NO_3^- group (Figure 4.4(ii)). In [(TPP)Mn(NO_3)] complex, the NO_3^- stretching appeared at 1474, 1385 and 1286 cm^{-1}.[21] The $\nu_a(NO_2)$ and $\nu_s(NO_2)$ stretching frequencies are reported to appear at ~1474 and ~1286 cm^{-1} in the cases of O-coordinated NO_3^- group. The appearance of the 1384 cm^{-1} band in KBr pellets was attributed to the free KNO_3 formed in the reaction of [(TPP)Mn(NO_3)] and KBr.[21]

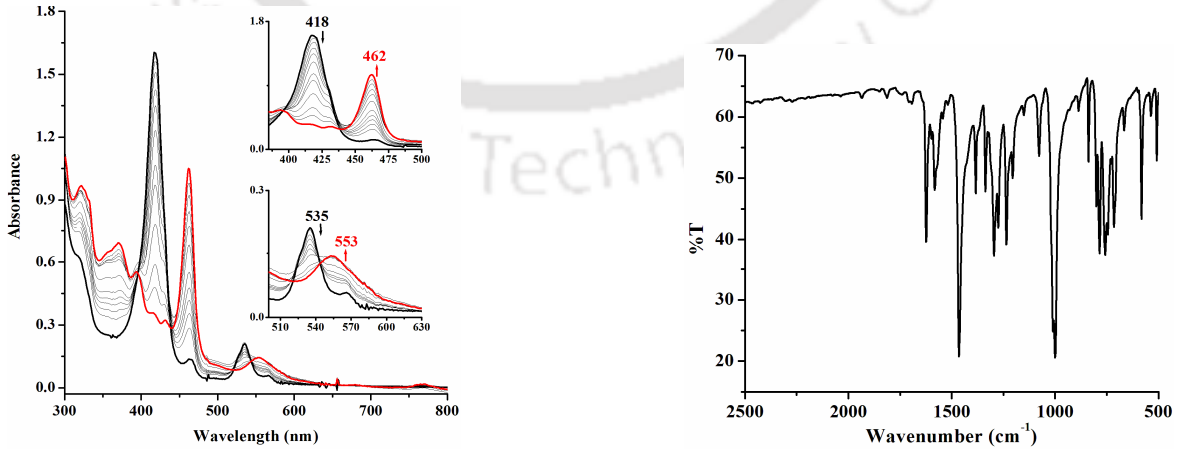

(i) (ii)

Figure 4.4. (i) UV-visible spectral monitoring of complex **4.2** (black) and after addition of KO_2 in C.E. to result in complex **4.3** (red) in THF at −80 °C. (ii) FT-IR spectrum of complex **4.3** in KBr.

The ESI-mass spectrum displays peak at m/Z value 873.03 [calcd. m/Z, 873.08] corresponds to the complex **4.3**. The isotopic distribution pattern is in good agreement with the simulated one (Figure 4.5(i)).

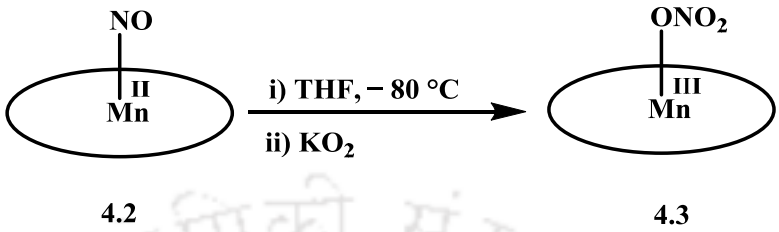

Scheme 4.1

The formation of complex **4.3** was further authenticated by structural characterization. The ORTEP diagram of complex **4.3** is shown in figure 4.5(ii). The crystallographic data and metric parameters were listed in the Appendix III, Tables A3.1-A3.3. The metal ion is in square pyramidal geometry bearing four nitrogen atoms from the porphyrin ring and one axially bonded NO_3^- in O-coordinated monodentate fashion. The average Mn-N_P bond distance of 2.006 Å are in the range of previously reported bond length of 2.007 Å.[21]

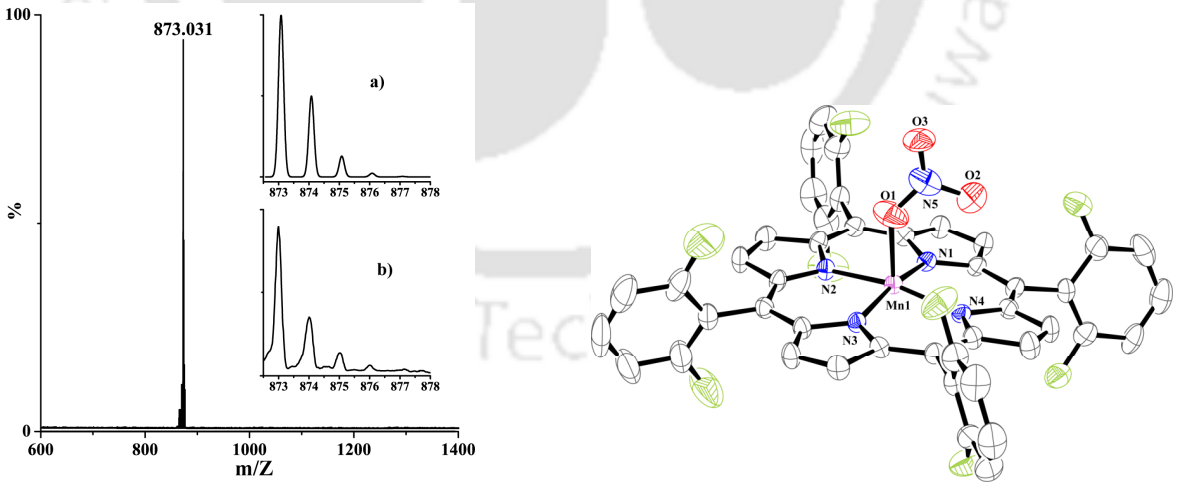

(i) (ii)

Figure 4.5. (i) ESI-mass spectrum of complex **4.3** in acetonitrile. [Inset: (a) simulated and (b) experimental isotopic distribution pattern.] (ii) ORTEP diagram of complex **4.3** (50% thermal ellipsoid plot, H-atoms are omitted for clarity).

It has been observed that the reaction of metal-nitrosyl with H_2O_2 or O_2^- lead to the corresponding metal-NO_3^- or NO_2^- complexes and the involvement of a PN intermediate were presumed in these reactions. Though no direct spectroscopic evidence was observed, in these reactions, the involvement of a proposed PN intermediate was established by its characteristic phenol ring nitration/oxidation reaction.

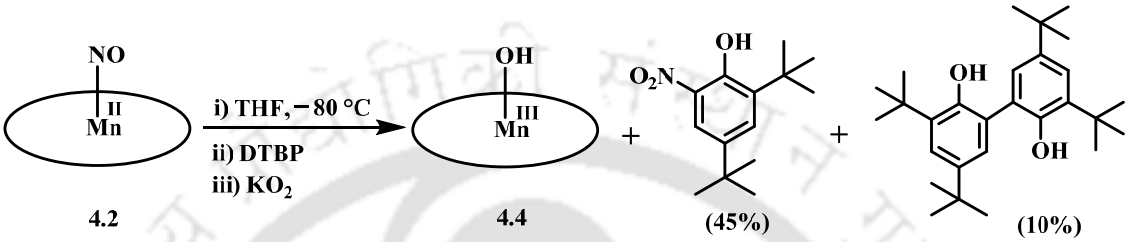

Scheme 4.2

In the present case, the formation of complex **4.3** from the reaction of complex **4.2** with KO_2 in THF suggests that the reaction might proceed through the formation of a PN intermediate. As no spectral evidence was observed, we sought chemical evidence to establish this. When the reaction of complex **4.2** with KO_2 is followed by the addition of 2,4-di-*tert*-butylphenol (DTBP), complex **4.3** is formed and unreacted DTBP is recovered. However, corresponding nitrophenol (~45%) bisphenol (~10%) and complex **4.4** (~70%) formations are observed when DTBP is added before the addition of one equivalent KO_2 (Scheme 4.2; Experimental Section and Appendix III, Figures A3.7-A3.14). This suggests the involvement of a PN intermediate in the reaction.

4.3 Experimental Section

4.3.1 Materials and methods

All the reagents and solvents were purchased from commercial sources in its best available purity and used as received or following the provided instructions. All the reactions were

performed under argon atmosphere unless specified. Repeated vacuum / purge cycles or bubbling with argon was used to remove the oxygen from the solvents and solutions. THF was distilled and dried from sodium / benzophenone mixture. Chloroform and dichloromethane were dried over calcium hydride. UV-visible spectral monitoring was studied on Agilent Cary 8454 UV-visible spectrophotometer using Chemstation software. FT-IR spectra were monitored on a Perkin Elmer spectrophotometer. The samples for FT-IR spectral monitoring were prepared as KBr pellets or in solution in KBr cell. ^{1}H NMR spectra were obtained from 600 MHz and 400 MHz Varian FT spectrometers. Chemical shifts (ppm) were referenced either with an internal standard (Me_4Si) for organic compounds or to the residual solvent peaks. Elemental analyses were obtained from a Perkin Elmer Series II Analyzer. Mass spectra were recorded on a Waters, Model: Q-Tof Premier instrument with ESI mode of ionization. The X-band Electron Paramagnetic Resonance (EPR) spectra were recorded on a JES-FA200 ESR spectrometer, at room temperature with microwave power, 0.998 mW; microwave frequency, 9.14 GHz and modulation amplitude, 2.

Single crystals were grown from the respective dichloromethane and chloroform solutions. The intensity data were collected using a Bruker SMART APEX-II CCD diffractometer, equipped with a fine focus 1.75 kW sealed tube MoK_α radiation (λ = 0.71073 Å) at 293(3) K, with increasing ω (width of 0.3° per frame) at a scan speed of 3 s/frame. The SMART software was used for data acquisition. Data integration and reduction were undertaken with SAINT and XPREP software.[22] Multi-scan empirical absorption corrections were applied to the data using the program SADABS.[23] Structures were solved by direct methods using SHELXS-2016 and refined with full-matrix least squares on F^2 using SHELXL-2016/7.[24] Structural illustrations have been drawn with ORTEP-3 for Windows.[24]

4.3.2 Syntheses

4.3.2.2 Synthesis of complexes

(a) [(L1)MnCl], 4.1

The ligand, **L1H$_2$** (0.19 g, 0.25 mmol) and Mn(OAc)$_2$.4H$_2$O (0.61 g, 2.50 mmol) was taken in a 50 mL round bottom flask. After that sodium chloride (0.09 g, 1.5 mmol) and 3 mL dimethylformamide were added to the mixture and refluxed for 3 h. 100 mL of brine solution was added to the reaction mixture. The compound was then extracted with $CHCl_3$ (3 × 30 mL). The organic solvent was evaporated under reduced pressure to get the crude product. The crude mass was purified by column chromatography using alumina column to result in complex **4.1** as red solid.[16] Yield: 0.12 g (~55%). Elemental analyses for $C_{44}H_{20}N_4F_8ClMn$, Calcd. (%): C, 62.39; H, 2.38; N, 6.61, found (%): C, 62.41; H, 2.35; N, 6.58. UV-visible (THF): 465 ($\varepsilon/M^{-1}cm^{-1}$, 0.90 × 10^5), 567 ($\varepsilon/M^{-1}cm^{-1}$, 1.47 × 10^4) nm. FT-IR (in KBr): 1623, 1583, 1464, 1337, 1275, 1235, 1078, 999, 782 and 582 cm^{-1}. ESI-mass (m/Z): Calcd. 811.09, found: 811.10 (Molecular ion peak for [Mn(L1)]).

(b) [(L1)Mn(NO)], 4.2

Complex **3.2** was synthesized following the previous report with slight modification. Hydroxylamine hydrochloride (0.52 g, 7.50 mmol) was dissolved in 10 mL methanol and cooled to −20 °C. Then triethylamine (0.76 g, 7.50 mmol) was added to it to make hydroxylamine solution which is stable below 0 °C. Freshly prepared solution of hydroxylamine was added to dichloromethane solution of complex **4.1** (1.27 g, 1.50 mmol) at −20 °C. Then red crystals of complex **4.2** was grown in a period of 3-4 days at low temperature and was isolated by filtration to get the pure product.[16] Yield 0.89 g, ~70%. Elemental analyses for $C_{44}H_{20}N_5OF_8Mn$, Calcd. (%): C, 62.79; H, 2.40; N, 8.32, found

(%): C, 62.81; H, 2.37; N, 8.33. UV-visible (THF): 418 ($\varepsilon/M^{-1}cm^{-1}$, 1.43×10^5) and 535 ($\varepsilon/M^{-1}cm^{-1}$, 1.97×10^4) nm. FT-IR (in KBr): 1762, 1620, 1579, 1540, 1461, 1342, 1272, 1233, 1188, 1076, 999, 885, 784, 745, 710 and 584 cm^{-1}. ^1H NMR (600 MHz, DMSO-d_6): δ_{ppm}, 8.72 (s, 8H), 8.01-7.94 (m, 4H), 7.68-7.58 (m, 8H).

(c) [(L1)Mn(NO_3)], 4.3

Complex **4.2** (0.42 g, 0.5 mmol) was dissolved in 20 mL of THF and the solution was cooled at −80 °C. To this cold solution, 1 equivalent potassium superoxide in presence of C.E. (5 equivalent) in THF was added at −80 °C and stirred for 2 h. The solution was slowly warmed to room temperature. The red solution changes to dark red. Then the solution was vacuum dried (0.33 g, ~75% yield). Elemental analyses for $C_{44}H_{20}N_5O_3F_8Mn$, Calcd. C, 65.12; H, 2.48; N, 6.90, found (%): C, 65.15; H, 2.50; N, 6.87. FT-IR (in KBr): 1623, 1582, 1464, 1384, 1337, 1295, 1235, 1077, 1010, 999, 838, 784, 758, 715 and 582 cm^{-1}. UV-visible (THF): 462 ($\varepsilon/M^{-1}cm^{-1}$, 1.25×10^5) and 553 ($\varepsilon/M^{-1}cm^{-1}$, 1.78×10^4) nm. ESI-mass (m/Z): Calcd: 873.08, found: 873.03 (Molecular ion peak for [Mn(L1)(NO_3)]).

(d) Complex 4.4, 3,3',5,5'-tetra-*tert*-butyl-[1,1'-biphenyl]-2,2'-diol and 2,4-ditertiarybutyl-6-nitrophenol

20 mL dry and degassed THF was added to a mixture of complex **4.2** (0.84 g, 1 mmol) and 2,4-di-*tert*-butyl phenol (1.03 g, 5 mmol). The mixture was cooled to −80 ℃. To this degassed solution, 1 equivalent potassium superoxide in presence of C.E. (5 equivalent) in THF was added at −80 °C and stirred for 2 h. After achieving room temperature, the reaction mixture was dried under reduced pressure. The solid mass was then subjected to column to obtain pure 3,3',5,5'-tetra-*tert*-butyl-[1,1'-biphenyl]-2,2'-diol, 2,4-di-*tert*-butyl-6-nitrophenol and complex **4.4**.

3,3',5,5'-tetra-*tert*-butyl-[1,1'-biphenyl]-2,2'-diol: Yield: 0.04 g (~10%). Elemental analyses for $C_{28}H_{42}O_2$, Calcd. (%): C, 81.90; H, 10.31; found (%): C, 81.88; H, 10.28. ^{1}H NMR (400 MHz, $CDCl_3$) δ_{ppm}: 7.39 (s, 2 H), 7.12 (s, 2 H), 5.23 (s, 2 H), 1.45 (s, 18 H) and 1.32 (s, 18 H). ^{13}C NMR (100 MHz, $CDCl_3$) δ_{ppm}: 150.0, 143.2, 136.5, 125.5, 125.0, 122.6, 35.4, 34.7, 31.9 and 29.9. ESI-mass (m/Z): Calcd: 410.32, found: 409.30 (M−1)

2,4-di-*tert*-butyl-6-nitrophenol: Yield: 0.11 g (~45%). Elemental analyses for $C_{14}H_{21}NO_3$, calcd (%): C, 66.91; H, 8.42; N, 5.57. Found (%): C, 66.89; H, 8.38; N, 5.64. ^{1}H NMR (600 MHz, $CDCl_3$): δ_{ppm}, 7.40 (s, 1H), 7.12 (s, 1H), 5.22 (s, 1H), 1.45 (s, 9H), 1.32 (s, 9H).^{13}C NMR (150 MHz, $CDCl_3$): δ_{ppm}, 149.8, 143.0, 136.2, 125.3, 124.8, 122.3, 35.2, 34.5, 31.6, 29.7. ESI-mass (m/Z): calcd 251.15, found 250.23 (M−1).

Complex 4.4: Yield: 0.58 g (~70%). Elemental analyses for $C_{44}H_{21}N_4OF_8Mn$, Calcd. (%): C, 63.78; H, 2.55; N, 6.76, found (%): C, 63.80; H, 2.54; N, 6.78. FT-IR (in KBr): 3433, 1625, 1507, 1483, 1466, 1407, 1362, 1280, 1252, 1085, 1004, 816, 784, 644 cm^{-1}. UV-visible (THF): 472 nm ($\varepsilon/M^{-1}cm^{-1}$, 0.74×10^5), 578 nm ($\varepsilon/M^{-1}cm^{-1}$, 1.25×10^4) and 613 nm ($\varepsilon/M^{-1}cm^{-1}$, 0.62×10^3)

4.4 Conclusion

In conclusion, a nitrosyl complex of manganese porphyrin, [(L1)Mn(NO)] having $\{MnNO\}^6$ description was synthesized and characterized. It reacts with KO_2 in THF solution result in the corresponding NO_3^- complex. Oxidation of externally added phenol suggests that the reaction presumably proceeds through the formation of a PN intermediate. Thus, the present study demonstrates an example of the reaction of a nitrosyl complex of Mn-porphyrinate with KO_2 which led to the formation of the corresponding NO_3^- complex *via* a presumed metal-PN intermediate.

4.5 References

1) Ignarro L. J. Nitric oxide: Biology and Pathobiology; Ed.; Academic press; San Diego, **2000**.

2) (a) Moncada, S.; Palmer, R. M. J.; Higgs, E. A. *Pharmacol. Rev*. **1991**, *43*, 109. (b) Butler, A. R.; Williams, D. L. H. *Chem. Soc. Rev*. **1993**, *22*, 233. (c) Feelisch, M.; Stamler, J. S. Methods in nitric oxide research; Ed. John Wiley and Sons; Chichester, England, **1996**. (d) Jia, L.; Bonaventura C.; Bonaventura, J.; Stamler, J. S. *Nature* **1996**, *380*, 221. (e) Galdwin, M. T.; Lancaster, J. R. Jr.; Freeman, B. A.; Schechter, A. N. *Nat. Med*. **2003**, *9*, 496.

3) (a) Goyal, R. K.; Hirano, I. *N. Engl. J. Med.* **1996**, *334***,** 1106. (b) Stark, M. E.; Szurszewski, J. H. *Gastroenterology* **1992**, *103*, 1928. (c) Jaffrey, S. R.; Snyder, S. H. *Annu. Rev. Cell Dev. Biol.* **1995**, *11***,** 417. (d) Bogdan, C. *Nature Immunology* **2001**, *2*, 907.

4) (a) Ford, P. C.; Wink, D. A.; Stanbury, D. M. *FEBS Lett*. **1993**, 326, 1. (b) Tran, N. G.; Kalyvas, H.; Skodje, K. M.; Hayashi, T.; Moënne-Loccoz, P.; Callan, P. E.; Shearer, J.; Kirschenbaum, L. J.; Kim, E. *J. Am. Chem. Soc*. **2011**, *133*, 1184.

5) (a) Goldstein, S.; Lind, J.; Merenyi, G. *Chem. Rev*. **2005**, *105*, 2457. (b) Pacher, P.; Beckman, J. S.; Liaudet, L. *Physiol. Rev*. **2007**, *87*, 315. (c) Blough, N. V.; Zafiriou, O. C. *Inorg. Chem*. **1985**, *24*, 3502. (d) Nauser, T.; Koppenol, W. H. *J. Phys. Chem. A* **2002**, *106*, 4084.

6) Beckman J. S.; Koppenol, W. H. *Am. J. Physiol*. **1996**, *271*, 1424.

7) Radi, R. *Proc. Natl. Acad. Sci. U.S.A.* **2004**, *101*, 4003.

8) Qiao, L; Lu, Y. ; Liu, B.; Girault, H. H. *J. Am. Chem. Soc*. **2011**, *133*, 19823.

9) Vliet, A.; Eiserich, J. P.; Halliwell, B.; Cross. C. E. *J. Biol. Chem.* **1997**, *272*, 7617.

10) (a) Kurtikyan, T. S.; Eksuzyan, Sh. R.; Hayrapetyan, V. A.; Martirosyan, G. G.; Hovhannisyan, G. S.; Goodwin, J. A. *J. Am. Chem. Soc.* **2012**, 134, 13861. b) Kurtikyan,T. S.; Ford, P. C. *Chem. Commun.* **2010**, 46, 8570.

11) Schopfer, M. P.; Mondal, B.; Lee, D. H.; Sarjeant, A. A. N.; Karlin, K. D. *J. Am. Chem. Soc.* **2009**, *131*, 11304.

12) (a) Clarkson, S. G.; Basolo, F. *J. Chem. Soc. Chem. Commun.* **1972**, *119*, 670. (b) Clarkson, S. G.; Basolo, F. *Inorg. Chem.* **1973**, *12*, 1528.

13) (a) Goodwin, J. A.; Coor, J. L.; Kavanagh, D. F.; Sabbagh, M.; Howard, J. W.; Adamec, J. R.; Parmley, D. J.; Tarsis, E. M.; Kurtikyan, T. S.; Hovhannisyan, A. A.; Desrochers, P. J.; Standard, J. M. *Inorg. Chem.* **2008**, *47*, 7852. (b) Kurtikyan, T. S.; Eksuzyan, S. R.; Goodwin, J. A.; Hovhannisyan, G. S. *Inorg. Chem.* **2013**, *52*, 12046.

14) Kalita, A.; Kumar, P.; Mondal, B. *Chem. Commun.* **2012**, *48*, 4636.

15) (a) Saha, S.; Ghosh, S.; Gogoi, K.; Deka, H.; Mondal, B.; Mondal, B. *Inorg. Chem.* **2017**, *56*, 10932. (b) Saha, S.; Gogoi, K.; Mondal, B.; Ghosh, S.; Deka, H.; Mondal, B. *Inorg. Chem.* **2017**, *56,* 7781.

16) (a) Rothemund, P.; Menotti, A. R. *J. Am. Chem. Soc.* **1948**, *70*, 1808. (b) Choi, In-K.; Liu, Y.; Wei, Z.; Ryan, M. D. *Inorg. Chem.* **1997,** *36,* 3113.

17) (a) George, S.; Goldberg, I. *Cryst. Growth Des.* **2006**, *6*, 755. (b) Paulat, F.; Praneeth, V. K. K.; Näther, C.; Lehnert, N. *Inorg.Chem.* **2006**, *45*, 2835. (c) Jun-wei, Y.; Xiao-chun, H.; Jin-bin, L.; Tie, C.; Jing, X.; Shan-ling, T.; Ke-er, Y.; Yan, Y. C*hem. Res. Chinese U.* **2007**, *23*, 384. (d) Milani, J. L. S.; Meireles, A. M.; Cabral, B. N.; Bezerra, W. d. A.; Martins, F. T.; Martins, D. C. d. S.; Chagas, R. P. d. *J. CO_2 Util.* **2019**, *30*, 100.

18) Scheidt, W. R.; Hatano, K.; Rupprecht, G. A.; Piciulo, P. L. *Inorg. Chem.* **1979**, *18*, 292.

19) Wayland, B. B.; Olson, L. W.; Siddiqui, Z. U. *J. Am. Chem. Soc*. **1976**, *98*, 94.

20) Addo, G. B. R.; Hodge, S. J.; Yi, G. B.; Khan, M. A.; Ma, T.; Caemelbecke, E. V.; Guo, N.; Kadish, K. M. *Inorg. Chem*. **1996**, *35*, 6530.

21) (a) Mondal, B.; Saha, S.; Borah, D.; Mazumdar, R; Mondal, B. *Inorg. Chem*. **2019**, *58*, 1234. (b) Kurtikyan, T. S.; Hayrapetyan, V. A.; Mehrabyan, M. M.; Ford, P. C. *Inorg. Chem*. **2014**, *53*, 11948. (c) Suslick, K. S.; Watson, R. A. *Inorg. Chem*. **1991**, *30*, 912

22) SMART, SAINT and XPREP, Siemens Analytical X-ray Instruments Inc., Madison, Wisconsin, USA, **1995**.

23) Sheldrick, G. M. SADABS: software for Empirical Absorption Correction, University of Gottingen, Institut fur Anorganische Chemieder Universitat, Tammanstrasse 4, D-3400 Gottingen, Germany, **1999**.

24) (a) Sheldrick, G. M. SHELXS-2014, University of Gottingen, Germany. (b) Farrugia, L. J. ORTEP-3 for Windows - a version of ORTEP-III with a Graphical User Interface (GUI) *J. Appl. Crystallogr.* **1997**, *30*, 565.

Chapter 5

Nitric Oxide Dioxygenase Activity of a Nitrosyl Complex of Mn^{II}-($F_{20}TPP$) in the Presence of Superoxide: Formation of a Mn^{IV}-oxo Species through a Putative Peroxynitrite Intermediate

Abstract

A nitrosyl complex of Mn^{II}-porphyrinate, [(L3)Mn^{II}(NO)], **5.2** (**L3H$_2$** = 5,10,15,20-tetrakis(pentafluorophenyl)porphyrin) was synthesized and characterized. Spectroscopic and structural characterization revealed complex **5.2** as a penta-coordinated Mn^{II}-nitrosyl with a linear Mn-N-O (180.0°) moiety. Complex **5.2** does not react with O_2. However, it reacts with superoxide (O_2^-) in THF at −80 °C to result in the corresponding nitrate (NO_3^-) complex, **5.3** *via* the formation of a presumed Mn^{III}-PN intermediate. ESI-mass spectrometry, UV-visible and X-band EPR spectroscopic studies suggest the generation of Mn^{IV}-oxo species in the reaction through homolytic cleavage of O-O bond of the PN ligand as proposed in NOD activity. The intermediate formation of the Mn^{III}-PN was further supported by the well accepted phenol ring nitration which resembles to the biologically important tyrosine nitration.

5.1 Introduction

Nitric oxide (NO) is known to play important roles in mammalian biology including neurotransmission, immune response etc.[1,2] However, over production of NO has detrimental effects *via* the formation of secondary reactive nitrogen species (RNS), for example, nitrogen dioxide (NO_2) or peroxynitrite (PN) ($ONOO^-$).[3,4] The reaction of NO with superoxide (O_2^-), hydrogen peroxide (H_2O_2) and / or in the presence of transition metal ions are known to be responsible for the formation of these RNS.[3] Nitric oxide dioxygenases (NODs) control the level of NO by converting it into NO_3^-.[5,6] In NOD reactions, a Fe^{III}-superoxo species reacts with NO to result in biologically benign NO_3^- ion. The formation of a PN ion has been proposed as the intermediate in this transformation. It is proposed that an oxo-ferryl, [Fe^{IV}(O)] species formed in the reaction *via* the homolytic cleavage of O-O bond of the Fe^{III}-PN intermediate. Such an oxo-ferryl species has been evidenced spectroscopically in the reaction of myoglobin with PN ion.[7] Though, in literature, the involvement of a proposed metal-PN species was exemplified in the reactions of NO with metal-oxygen species, the direct evidence is still elusive. This is because of the very short life time of metal-PN. In addition, the evidence of formation of high valent metal-oxo species from the homolytic O-O bond cleavage of metal-PN intermediate is also in scarce because of very fast recombination of the metal-oxo species with NO_2 in the reaction cage to result in NO_3^-. Hence the reactivity study of metal-superoxo species with NO or a metal-nitrosyl with O_2^- is of immense importance to elucidate the undetected intermediate/s in the reaction.

In literature, the reaction of superoxo and peroxo complexes of heme and non-heme iron, cobalt and chromium with NO are reported where the formation of the metal-PN intermediates is implicated.[8-10] For instance, in addition to the examples of formation of PNs in the reaction of oxy-heme (formally, Fe^{III}-O_2^-) proteins with NO, it has been

reported recently that a Cr^{IV}-peroxo complex, $[Cr^{IV}$-(12-TMC)$(O_2)(Cl)]^+$ {12-TMC = 1,4,8,11-tetramethyl-1,4,8,11-tetraazacyclotetradecane} reacts with NO to lead to a Cr^{III}-NO_3^- complex, $[Cr^{III}(12\text{-TMC})(NO_3)(Cl)]^+$. On the other hand, the Cr^{III}-superoxo analogue, $[Cr^{III}(14\text{-TMC})(O_2)(Cl)]^+$ upon reaction with NO yielded the corresponding Cr^{IV}-oxo complex, $[Cr^{IV}$-(14-TMC)(O)$(Cl)]^+$ and NO_2. In both the reactions, the involvement of a Cr^{III}-PN intermediate, $[Cr^{III}(14\text{-TMC})(OON{=}O)(Cl)]^+$ was presumed.[11,12,9d,e] The reaction of an Fe^{III}-peroxo complex of the same ligand, $[Fe^{III}(14\text{-TMC})(O_2)]^+$ with NO^+ was also reported to proceed through the PN intermediate.[13] The example of the formation of a presumed PN intermediate in the reaction of the cobalt-peroxo complex of non-porphyrinate ligand with NO is reported recently from our laboratory.[14]

On the other hand, presumed metal-PNs are reported to form in the reaction of a metal-nitrosyl and dioxygen (O_2). For example, the reaction of cobalt-nitrosyl with O_2 to yield NO_2^- was reported long back.[15] The reaction of a non-heme dinitrosyl iron complex with O_2 resulted in NO_3^- complex.[16] A Cu^I-nitrosyl complex afforded NO_2^- product in the presence of O_2 *via* a presumed PN intermediate.[17] In addition, $\{CuNO\}^{10}$ complex in the presence of H_2O_2 was also found to result in the copper-nitrato complex through a presumed Cu^I-PN intermediate formation.[18]

This chapter describes the synthesis and characterization of a five coordinated manganese-nitrosyl, [(L3)Mn(NO)] (**5.2**) and its reactivity with O_2^- where the formation of PN intermediate is implicated. Spectroscopic evidence suggest the formation of the $[(L3)Mn^{IV}(O)]$ species in the reaction. Finally, this species resulted in the corresponding NO_3^- product upon recombination with NO_2.

5.2 Results and Discussion

The ligand was prepared following typical reported methods of porphyrin synthesis and

characterized using spectroscopic techniques (Experimental Section and Appendix IV, Figures A4.1-A4.4).[23a] The Mn^{II}-nitrosyl complex, [(L3)Mn(NO)] (**5.2**) has been prepared from the reaction of [(L3)Mn^{III}(Cl)] (**5.1**) with hydroxylamine using the reported literature procedure with a little modification (Experimental Section).[23c] It was characterized by various spectroscopic techniques as well as by single crystal structure determination (Appendix IV, Figures A4.9-A4.12). The ORTEP diagram of complex **5.2** is given in figure 5.1. It revealed complex **5.2** as five coordinated nitrosyl complex of Mn^{II}-porphyrinate. It is to be noted that though there are many examples of structurally characterized six coordinated nitrosyl complexes of Mn^{II}-porphyrinates, the number for five coordinated ones are much less. The metric parameters (Appendix IV, Tables A4.1-A4.3) are within the range of reported analogous complexes. The N-O bond distance and Mn-N-O bond angles are 1.132(10) Å and 180.0°, respectively. These values appear in the reported range for analogous complexes. For instance, in case of nitrosyl complex of (5,10,15,20-tetratolylporphinato)manganese(II), the Mn-N-O bond angle is reported as 177.8(3)° and the N-O distance is 1.160(3) Å.[24]

The complex **5.2** in THF solution at −80 °C shows absorption bands at 415, 532 and 564 nm (Figure 5.2 and Appendix IV, Figure A4.10). Addition of a precooled THF solution of

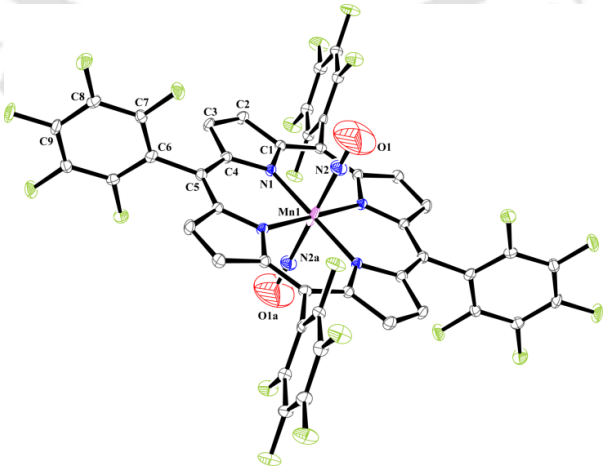

Figure 5.1. ORTEP diagram of complex **5.2** (50 % thermal ellipsoid plot) (H-atoms and solvent molecules are removed for clarity) (occupancy for both the NO is 50 %).

KO_2 in C.E. (18-crown-6 ether) resulted in the decrease of 415 nm band along with a concomitant formation of new absorption bands at 426 and 458 nm (Figure 5.2) (Scheme 5.1).

The 426 nm band was transient and disappeared with time whereas the intensity of the absorption at 458 nm increases. The final decomposition product was isolated and characterized as the corresponding NO_3^- complex of Mn^{III}-porphyrinate, **5.3**. It shows absorption band at 458 nm. The transient 426 nm band is attributed to the absorption of the corresponding Mn^{IV}-oxo species which is formed *via* the homolytic O-O bond cleavage of a presumed Mn^{III}-PN intermediate (Scheme 5.1). In literature, it has been reported that Mn^{IV}-oxo complexes absorbs in the range of 420-430 nm and owing to their very unstable nature, convert rapidly to the corresponding Mn^{III}-porphyrinate. Newcomb *et al.* reported the formation of the same [(L3)Mn^{IV}O] species in acetonitrile solution through Laser Flash Photolysis of [(L3)$Mn^{III}(ClO_3)$] and that shows absorption at 422 nm.[25]

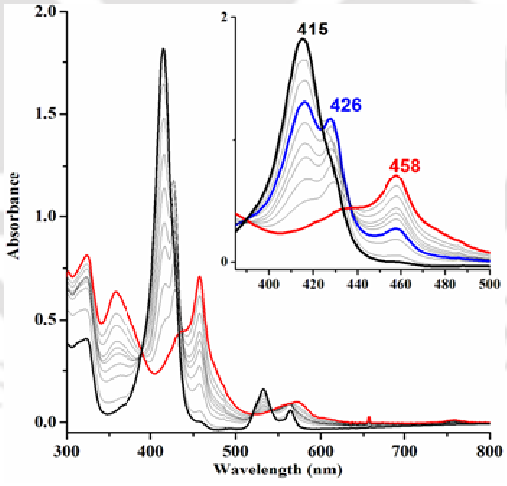

Figure 5.2. UV-visible spectral monitoring of complex **5.2** (black) and after addition of KO_2 in C.E. to result in complex **5.3** (red) in THF at −80 °C.

The minor shift in absorption wavelength is perhaps because of the change of solvent and temperature.

It is to be noted that when [(L3)Mn^{II}] was made to react with KO_2 in THF at −80 °C, the absorption bands in the UV-visible spectrum appeared at 451 and 569 nm, respectively (Appendix IV, Figure A4.30) and these bands are stable at that temperature for hours. In the reaction of the complex **5.2** and KO_2 in THF at −80 °C, we have not observed any such bands in the UV-visible monitoring. Hence, the possibility of the replacement of NO group by superoxide could be ruled out in the reaction of complex **5.2** and KO_2.

In FT-IR spectroscopy, the complex **5.2** in KBr pellet displays nitrosyl stretching at 1763 cm^{-1} (Figure 5.3(i)). This is in well agreement with the reported nitrosyl stretching in analogous complexes. For example, [(TPP)Mn^{II}(NO)] shows nitrosyl stretching at 1760 cm^{-1}.[26] We attempted to monitor the FT-IR spectral change during the reaction; however, ended up to a spectrum where the 1763 cm^{-1} band disappeared with the appearance of new stretching at ~1430 and 1261 cm^{-1}. This is assignable to the corresponding NO_3^- stretching of complex **5.3** (Appendix IV, Figure A4.13b).[27] When the FT-IR spectrum of the isolated complex **5.3** was recorded in KBr pellets, a stretching at 1384 cm^{-1} was observed (Appendix IV, Figure A4.13a). It is to be noted that is case of [(TPP)Mn(ONO_2)], the NO_3^- stretching appeared at ~1470 and 1284 cm^{-1}. However, when the spectrum was recorded in KBr pellets, three bands were observed at 1474, 1385 and 1286 cm^{-1}. The appearance of 1384 cm^{-1} band was attributed to the stretching of free NO_3^- which is formed in the reaction of [(TPP)Mn(ONO_2)] with KBr.[27] In comparison with the other reported analogous complexes, the bands at 1430 and 1261 cm^{-1} are assigned to the $\nu_a(NO_2)$ and $\nu_s(NO_2)$, respectively, of the uncoordinated NO_2 group in [Mn(η^1-ONO_2)] moiety suggesting the presence of a NO_3^- ion in O-coordinated monodentate fashion.[27] The stretching corresponding to the coordinated O-N fragment appears in the range of ~1000 cm^{-1}. However, we have not observed that in the present case perhaps because of masking by the presence of strong porphyrin stretching bands.[27]

The ESI-mass spectrum of complex **5.2** was populated by the molecular ion peak at m/Z, 1027.15 assignable to the [(L3)Mn] moiety (calcd. m/Z = 1026.98) (Appendix IV, Figure A4.11). This is attributed to the loss of axial nitrosyl group in the experimental condition.[28] However, the ESI-mass spectrum of the reaction mixture obtained from the reaction of complex **5.2** with KO_2 in THF at −80 °C shows the molecular ion peak at 1043.07 which is assignable to the [(L3)Mn^{IV}(O)] moiety (calcd.1042.98) (Figure 5.3(ii)).

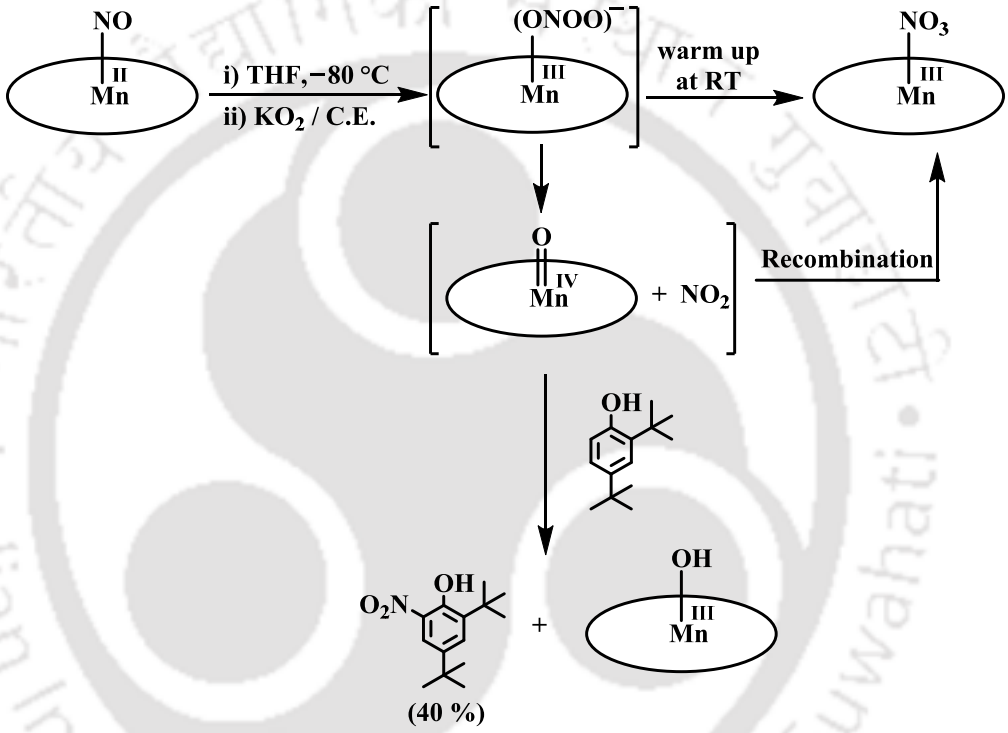

Scheme 5.1

Isotopic distribution pattern in the observed spectrum matches well with the simulated one (Figure 5.3 (ii)). Thus, the ESI-mass spectrometry suggests the formation of [(L3)Mn^{IV}(O)] intermediate. In the mass spectrum of the decomposition product, the molecular ion peak appeared at m/Z 1088.88 corresponding to [(L3)Mn(NO_3)] unit (calcd m/Z, 1088.97) (complex **5.3**) (Appendix IV, Figure A4.14).

In X-band EPR spectroscopy, complex **5.2** appeared silent as expected for a low spin Mn^{II} center with anti-ferromagnetically coupled nitrosyl group. However, the frozen (at 77K)

reaction mixture obtained from the reaction of complex **5.2** in THF at −80 °C with KO_2 displayed strong broad EPR signal with g ~ 5.26 and a weak one at 2.27, respectively. This

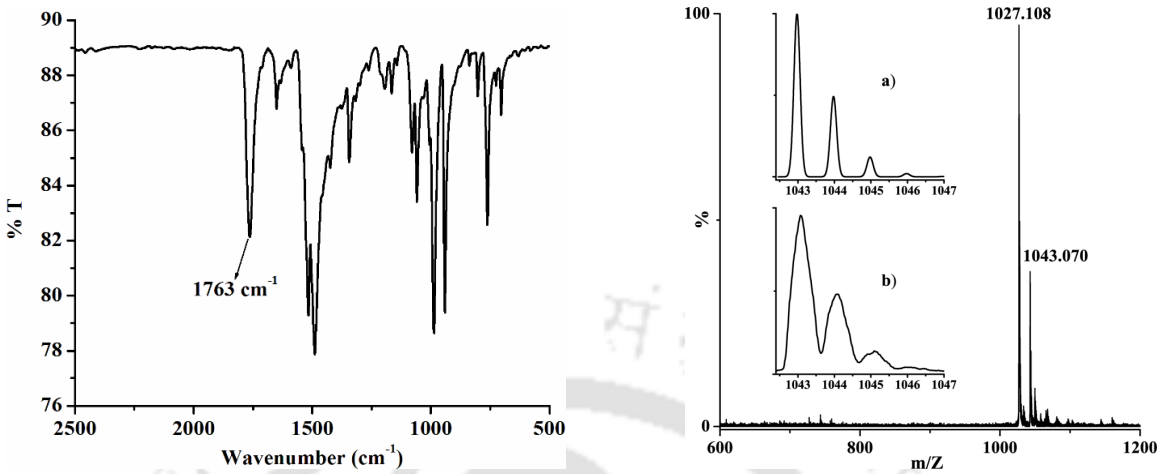

(i) (ii)

Figure 5.3. (i) FT-IR spectrum of complex **5.2** in KBr. (ii) ESI-mass spectrum of the reaction mixture obtained from the reaction of complex **5.2** and KO_2 in THF at −80 °C. [Inset: (a) simulated and (b) experimental isotopic distribution pattern].

is attributed to the presence of high spin Mn^{IV} center (S = 3/2) in a square pyramidal geometry (Figure 5.4).[29] Spin quantification experiment with respect to the authentic [Mn^{IV}=O] sample generated in the reaction of [(L3)MnCl] complex, **5.1** and *m*CPBA suggests the presence of ~60% of the same species in the frozen (at 77K) sample obtained from the reaction of complex **5.2** and KO_2 in THF at −80 °C (Appendix IV, Figure A4.32). [(TMP)Mn^{IV}(O)] was reported to display strong and broad signal at g ~ 4 and a weak one at g ~ 2.[29] These g values, however, are in the range of the reported Mn^{IV}=O complexes. For instance, g_{eff} ~ 5.76 signal in the case of $[Mn^{IV}(O)(N_4py)]^{2+}$ [N_4py = (N, N-bis(2-pyridylmethyl)-N-bis(2-pyridyl)methylamine)].[30]

In case of [Mn^{IV}(H_3buea)(O)] species, [H_3buea^{3-} = tris[(N′-*tert*-butylureaylato)-N-ethylene]aminato)], the g values appeared at 5.15, 2.44 and 1.63.[31] To confirm the presence of Mn^{IV} center, an authentic sample was prepared from the reaction of [(L3)Mn^{III}Cl] with

*m*CPBA in acetonitrile at −40 °C and the EPR spectrum was recorded at 77K and compared with the observed one. It was found that both the spectra are in well agreement.

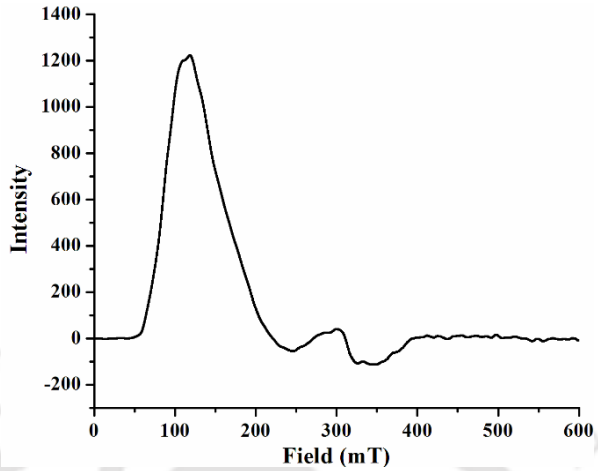

Figure 5.4. X-band EPR spectrum of the intermediate formed during the reaction between complex **5.2** and KO_2 in THF at 77K.

It should be worth mentioning that Mn(II) high spin (S =3/2) complexes show signals at g ~5.95 and ~2.10 in X-band EPR spectrum.[32] To confirm our assignment of the observed signals, the EPR of the authentic [(L3)Mn^{II}] was recorded in THF at 77K (Appendix IV, Figure A4.25-A4.26). The respective signals appeared at g ~6.10 and ~2.15.

Thus, UV-visible, ESI-mass, X-band EPR spectral studies suggest the formation of a Mn^{IV}-oxo intermediate in the reaction of complex **5.2** with KO_2. We have tried to record the resonance Raman spectrum of the intermediate, but could not succeed. This is perhaps because of thermal instability of the intermediate along with its photodecomposition under laser light. A probable mechanism of formation of the Mn^{IV}-oxo species in the reaction of Mn^{II}-nitrosyl complex, **5.2** with O_2^- is depicted in Scheme 5.1. According to the widely accepted mechanism of NOD activity, the Fe^{III}-(O_2^-) species reacts with NO to result in Fe^{III}-PN intermediate. In the subsequent step, the PN ligand undergoes homolytic O-O bond cleavage to generate Fe^{IV}-oxo species and NO_2.[7] In the present study, thus, the

reaction of Mn^{II}-nitrosyl with O_2^- is presumably resulting in the corresponding Mn^{III}-PN intermediate which gives rise to the Mn^{IV}-oxo and NO_2 following the NOD pathway.

The isolation and characterization of complex **5.3** as the decomposition product from the reaction of complex **5.2** and KO_2 also supports the formation of a Mn^{III}-PN intermediate.[27,28a] It is well established that very short life time of the metal-PN complexes precluded their spectral analyses. Therefore, the chemical evidence was sought to establish the intermediate formation of PN in the said reaction. When the reaction was carried out in presence of 2,4-di-*tert*-butylphenol, nitration was observed leading to 2,4-di-*tert*-butyl-6-nitrophenol formation in ~40% yield with a fraction of oxidative product, bis-phenol (~20%). It is to be noted that phenol nitration / oxidative coupling has been used extensively as an evidence to establish the presence of metal-PN species. This reaction has considerable importance as this resembles to the biologically well-known tyrosine nitration.[3a,b,4e,33] In addition, the complex **5.2** itself does not react with 2,4-di-*tert*-butylphenol under reaction condition.

In NOD reactivity of heme-iron complexes, it is proposed that metal-PN ion mediated nitration or oxidation proceeds through the formation of Fe^{IV}-oxo intermediate along with NO_2. The phenolic substrates reduce the Fe^{IV}-oxo species rapidly to the Fe^{III} state to result phenoxyl radical. This radical then either combines with NO_2 to result nitro-phenol or two phenoxyl radicals couple to yield corresponding bis-phenol product. In the present case, the spectral evidence suggests the formation of Mn^{IV}-oxo species in the reaction of complex **5.2** with KO_2. Recently, it has been reported that Cr^{III}-superoxo complex of tetramethylated cyclam ligand reacts with NO in acetonitrile at −40 °C to result in the formation of Cr^{IV}-oxo species *via* homolytic O-O bond cleavage of the presumed Cr-PN intermediate.[9d] Earlier, cobalt nitrosyl, [(L1)Co(NO)] was found to show NOD reactivity in presence of H_2O_2 through the formation of a transient [(L1)Co^{III}-O•] radical.[27a] Complexes

of Cu, Cr were also reported in the literature to display NOD activity. This result demonstrates the example of a nitrosyl complex of Mn-porphyrin which displays NOD reactivity in the presence of KO_2. The spectral evidence clearly suggests the involvement of a Mn^{IV}-oxo intermediate in the NOD reactivity of complex **5.2**.

5.3 Experimental Section

5.3.1 Materials and methods

All reagents and solvents of reagent grade were purchased from commercial sources and used as received except specified. All the reactions were performed under inert conditions unless specified. Deoxygenation of the distilled solvents and solutions was effected by repeated vacuum/purge cycles or bubbling with argon. UV-visible spectra were monitored on an Agilent Technologies Cary 8454 UV-visible spectrophotometer. FT-IR spectra of the samples were taken on a Perkin Elmer spectrophotometer and the samples were prepared either as KBr pellets or in solution in KBr cell. 600 MHz Varian FT spectrometer was used for ^1H NMR spectra recording. Chemical shifts (ppm) were referenced either with an internal standard (Me_4Si) or to the residual solvent peaks. The X-band Electron Paramagnetic Resonance (EPR) spectra were recorded on a JES-FA200 ESR spectrometer, at room temperature as well as liquid nitrogen temperature with microwave power, 0.998 mW; microwave frequency, 9.14 GHz and modulation amplitude, 2. Elemental analyses were obtained from a Perkin Elmer Series II Analyzer.

Single crystals were grown by slow evaporation of chloroform and dichloromethane solution of ligand and complexes respectively. The intensity data were collected using a Bruker SMART APEX-II CCD diffractometer, equipped with a fine focus 1.75 kW sealed tube MoK_α radiation (λ = 0.71073 Å) at 293(3) K, with increasing ω (width of 0.3° per frame) at a scan speed of 3 s/frame. The SMART software was used for data acquisition.

Data integration and reduction were undertaken with SAINT and XPREP software.[19] Multi-scan empirical absorption corrections were employed to the data using the program SADABS.[20] Structures were solved by direct methods using SHELXS-2016 and refined with full-matrix least squares on F^2 using SHELXL-2016/6.[21] Structural illustrations have been drawn with ORTEP-3 for Windows.[22]

5.3.2 Syntheses

5.3.2.1 Synthesis of ligand $L3H_2$ [(5,10,15,20-tetrakis(pentafluorophenyl)porphyrin)]

The ligand **$L3H_2$** was prepared by mixing 2,3,4,5,6-pentafluorobenzaldehyde (3.92 g, 20 mmol) and freshly distilled pyrrole (1.34 g, 20 mmol) in 37 mL propionic acid following reported procedure of porphyrin synthesis.[19] The solution was refluxed for 3 h and cooled at room temperature. Neutralization of the reaction mixture was done by aqueous Na_2CO_3 to precipitate out the crude product. This crude product was purified by column chromatography as purple crystals (0.49 g, ~10% yield). Elemental analyses for $C_{44}H_{10}F_{20}N_4$, Calcd. (%): C, 54.23; H, 1.03; N, 5.75, found (%): C, 54.33; H, 1.07; N, 5.84. FT-IR (in KBr): 3318, 2923, 1648, 1514, 1500, 1435, 1078, 989, 919, 807, 772, 757 and 724 cm^{-1}. ^1H NMR (600 MHz, $CDCl_3$): δ_{ppm}, 8.93 (s, 8H). ESI-mass (m/Z): Calcd: 974.06, found: 975.03 (M+1).

5.3.2.2 Syntheses of complexes

(a) [(L3)MnCl], 5.1

The ligand **$L3H_2$** (0.24 g, 0.25 mmol), $Mn(OAc)_2.4H_2O$ (0.61 g, 2.50 mmol) and sodium chloride (0.09 g, 1.5 mmol) in $CHCl_3$ (12 mL) and acetic acid (12 mL) was taken in a 100 mL round bottom flask. The mixture was refluxed at 120 °C for 6 h. The solution was cooled and filtered. 60 mL of water was poured to the filtrate. The solution was then

extracted with $CHCl_3$ (3 × 30 mL). The crude mass was column chromatographed to result in complex **5.1** as red solid.[20] Yield: 0.11 g (~40%). Elemental analyses for $C_{44}H_8N_4F_{20}ClMn$, Calcd. (%): C, 49.72; H, 0.76; N, 5.27 found (%): C, 49.80; H, 0.81; N, 5.39. UV-visible (THF): 429 nm ($\varepsilon/M^{-1}cm^{-1}$, 1.11×10^5) and 561 nm ($\varepsilon/M^{-1}cm^{-1}$, 1.34×10^4). FT-IR (in KBr): 1651, 1516, 1492, 1426, 1340, 1165, 1085, 1059, 1011, 989, 943 and 761 cm^{-1}. ESI-mass (m/Z): Calcd. 1026.98, found: 1027.00 (molecular ion peak for [Mn(L3)]).

(b) [(L3)Mn(NO)], 5.2

Complex **5.2** was prepared following the reported procedure with minor modification.[21] Triethylamine (0.76 g, 7.50 mmol) was added to a methanolic (10 mL) solution of hydroxylamine hydrochloride (0.52 g, 7.50 mmol) at 0 °C. Fresh solution of hydroxylamine was added to CH_2Cl_2 solution of complex **5.1** (1.59 g, 1.50 mmol) at −20 °C. Then complex **5.2** precipitated out of solution as red crystals in a period of 3-4 days at low temperature and was isolated by filtration. Yield 1.11 g, ~70%. Elemental analyses for $C_{44}H_8N_5OF_{20}Mn$, Calcd. (%): C, 49.98; H, 0.76; N, 6.62 found (%): C, 50.06; H, 0.73; N, 6.70. UV-visible (THF): 415 nm ($\varepsilon/M^{-1}cm^{-1}$, 1.04×10^5), 532 nm ($\varepsilon/M^{-1}cm^{-1}$, 1.02×10^4) and 564 nm ($\varepsilon/M^{-1}cm^{-1}$, 3.95×10^3). FT-IR (in KBr): 1763, 1650, 1516, 1489, 1344, 1195, 1165, 1079, 1059, 987, 941 and 762 cm^{-1}. ^1H NMR (400 MHz, DMSO- d_6): δ_{ppm}, 9.09 (s, 8H). ESI-mass (m/Z): Calcd. 1026.98, found: 1027.15 (molecular ion peak for [Mn(L3)]).

(c) [(L3)Mn(NO_3)], 5.3

Complex **5.2** (0.53 g, 0.5 mmol) was dissolved in 20 mL of dry THF and the solution was cooled at −80 °C. To this cold solution, 1 equivalent potassium superoxide in presence of 18-crown-6 (5 equivalent) in THF was added at −80 °C and stirred for 2 h. The solution was slowly warmed to room temperature. The red solution changes to dark red. Then the

solution was vacuum dried (0.41 g, ~75% yield). Elemental analyses for $C_{44}H_8N_5O_3F_{20}Mn$, Calcd. (%): C, 48.51; H, 0.74; N, 6.43, found (%): C, 48.59; H, 0.70; N, 6.56. UV-visible (THF): 458 nm ($\varepsilon/M^{-1}cm^{-1}$, 0.54× 10^5), 572 nm ($\varepsilon/M^{-1}cm^{-1}$, 0.77 × 10^4). FT-IR (in KBr): 1650, 1525, 1492, 1384, 1335, 1162, 1073, 1052, 988, 937, 800 and 759 cm^{-1}. ESI-mass (m/Z): Calcd: 1088.97, found: 1088.88 (Molecular ion peak for [Mn(L3)(NO_3)]).

(d) Complex 5.4, 3,3',5,5'-tetra-*tert*-butyl-[1,1'-biphenyl]-2,2'-diol and 2,4-ditertiarybutyl-6-nitrophenol

Complex **5.2** (1.06 g, 1 mmol) and 2,4-di-*tert*-butylphenol (1.03 g, 5 mmol) were dissolved in 20 mL dry and degassed THF. The mixture was cooled to −80 ºC. To this degassed solution, 1 equivalent potassium superoxide in presence of 18-crown-6 (5 equivalent) in THF was added at −80 °C and stirred for 2 h. The reaction mixture was then brought to room temperature and dried under reduced pressure. The solid mass was then subjected to column chromatography using silica gel column to obtain pure 3,3',5,5'-tetra-*tert*-butyl-[1,1'-biphenyl]-2,2'-diol, 2,4-ditertiarybutyl-6-nitrophenol and complex **5.4**.

3,3',5,5'-tetra-*tert*-butyl-[1,1'-biphenyl]-2,2'-diol: yield: 0.08 g (~20%). Elemental analyses for $C_{28}H_{42}O_2$, Calcd. (%): C, 81.90; H, 10.31, found (%): C, 81.98; H, 10.33. ^{1}H NMR (400 MHz, $CDCl_3$) δ_{ppm}: 7.39 (s, 2 H), 7.12 (s, 2 H), 5.23 (s, 2 H), 1.45 (s, 18 H) and 1.32 (s, 18 H). ^{13}C NMR (100 MHz, $CDCl_3$) δ_{ppm}: 150.0, 143.2, 136.5, 125.5, 125.0, 122.6, 35.4, 34.7, 31.9 and 29.9. ESI-mass (m/Z): Calcd: 410.32, found: 409.31 (M−1).

2,4-di-*tert*-butyl-6-nitrophenol: yield: 0.10 g (~40%), Elemental analyses for $C_{14}H_{21}NO_3$, calcd (%): C, 66.91; H, 8.42; N, 5.57. Found (%): C, 66.86; H, 8.45; N, 5.66. ^{1}H NMR (600 MHz, $CDCl_3$): δ_{ppm}, 7.40 (s, 1H), 7.12 (s, 1H), 5.22 (s, 1H), 1.45 (s, 9H), 1.32 (s, 9H).

^{13}C NMR (150 MHz, $CDCl_3$): δ_{ppm}, 149.8, 143.0, 136.2, 125.3, 124.8, 122.3, 35.2, 34.5, 31.6, 29.7. ESI-mass (m/Z): calcd 251.15, found 250.41 (M−1).

Complex 5.4: yield: 0.68 g (~65%). Elemental analyses for $C_{44}H_9N_4OF_{20}Mn$, Calcd. (%): C, 50.60; H, 0.87; N, 5.36, found (%): C, 50.63; H, 0.89; N, 5.34. FT-IR (in KBr): 3530, 1650, 1490, 1423, 1163, 1087, 990, 761 cm^{-1}. UV-visible (THF): 430 nm ($\varepsilon/M^{-1}cm^{-1}$, 0.35×10^5), 569 nm ($\varepsilon/M^{-1}cm^{-1}$, 0.49×10^4)

5.4 Conclusion

Thus, the nitrosyl complex of Mn^{II}-porphyrinate, $[(F_{20}TPP)Mn^{II}(NO)]$, **5.2** upon reaction with superoxide (O_2^-) in THF at −80 °C resulted in the corresponding NO_3^- complex, **5.3** *via* the formation of a presumed Mn^{III}-PN intermediate. ESI-mass spectrometry, UV-visible and X-band EPR spectroscopic studies suggest the generation of Mn^{IV}-oxo species in the reaction through homolytic cleavage of O-O bond of the PN ligand as proposed in NOD activity. The intermediate formation of the Mn^{III}-PN was further supported by the well accepted phenol ring nitration which resembles to the biologically well-established tyrosine nitration.

5.5 References

1) Ignarro L. J. Nitric oxide: Biology and Pathobiology; Ed.; Academic press; San Diego, **2000**.

2) (a) Moncada, S.; Palmer, R. M. J.; Higgs, E. A. *Pharmacol. Rev*. **1991**, *43*, 109. (b) Butler, A. R.; Williams, D. L. H. *Chem. Soc. Rev*. **1993**, *22*, 233. (c) Feelisch, M.; Stamler, J. S. Methods in nitric oxide research; Ed. John Wiley and Sons; Chichester, England, **1996**. (d) Jia, L.; Bonaventura C.; Bonaventura, J.; Stamler, J.

S. *Nature* **1996**, *380*, 221. (e) Galdwin, M. T.; Lancaster, J. R. Jr.; Freeman, B. A.; Schechter, A. N. *Nat. Med*. **2003**, *9*, 496.

3) (a) Radi, R. *Proc. Natl. Acad. Sci. U. S. A*. **2004**, *101*, 4003. (b) Ford, P. C.; Wink, D. A.; Stanbury, D. M. *FEBS Lett*. **1993**, 326, 1. (c) Tran, N. G.; Kalyvas, H.; Skodje, K. M.; Hayashi, T.; Moënne-Loccoz, P.; Callan, P. E.; Shearer, J.; Kirschenbaum, L. J.; Kim, E. *J. Am. Chem. Soc*. **2011**, *133*, 1184.

4) (a) Goldstein, S.; Lind, J.; Merényi, G. *Chem. Rev*. **2005**, *105*, 2457. (b) Pacher, P.; Beckman, J. S.; Liaudet, L. *Physiol. Rev*. **2007**, *87*, 315. (c) Blough, N. V.; Zafiriou, O. C. *Inorg. Chem*. **1985**, *24*, 3502. (d) Nauser, T.; Koppenol, W. H. *J. Phys. Chem. A* **2002**, *106*, 4084.

5) (a) Doyle, M. P.; Hoekstra, J. W. *Inorg. Biochem*. **1981**, *14*, 351. (b) Cooper, C. E.; Torres, J.; Sharpe, M. A.; Wilson, M. T. *FEBS Lett*. **1997**, *414*, 281. (c) Tocheva, E. I.; Rosell, F. I.; Mauk, A. G.; Murphy, M. E. *Science* **2004**, *304*, 867.

6) (a) Gardner, P. R.; Gardner, A. M.; Martin, L. A.; Salzman, A. L. *Proc. Natl. Acad. Sci. U.S.A*. **1998**, *95*, 10378. (b) Schopfer, M. P.; Mondal, B.; Lee, D.-H.; Sarjeant, A. A. N.; Karlin, K. D. *J. Am. Chem. Soc*. **2009**, *131*, 11304.

7) Su, J.; Groves, J. T. *Inorg. Chem.* **2010**, *49*, 6317.

8) (a) Wick, P. K.; Kissner, R.; Koppenol, W. H. *Helv. Chim. Acta*, **2000**, *83*, 748. (b) Maiti, D.; Lee, D.-H.; Sarjeant, A. A. N.; Pau, M. Y. M.; Solomon, E. I.; Gaoutchenova, K.; Sundermeyer, J.; Karlin, K. D. *J. Am. Chem. Soc*. **2008**, *130*, 6700.

9) (a) Goodwin, J. A.; Coor, J. L.; Kavanagh, D. F.; Sabbagh, M.; Howard, J. W.; Adamec, J. R.; Parmley, D. J.; Tarsis, E. M.; Kurtikyan, T. S.; Hovhannisyan, A. A.; Desrochers, P. J.; Standard, J. M. *Inorg. Chem*. **2008**, *47*, 7852. (b) Kurtikyan, T. S.; Ford, P. C. *Chem. Commun*. **2010**, *46*, 8570. (c) Kurtikyan, T. S.; Eksuzyan, S.

R.; Goodwin, J. A.; Hovhannisyan, G. S. *Inorg. Chem*. **2013**, *52*, 12046. (d) Yokoyama, A.; Cho, K.-B.; Karlin, K. D.; Nam, W. *J. Am. Chem. Soc*. **2013**, *135*, 14900. (e) Yokoyama, A.; Han, J. E.; Cho, J.; Kubo, M.; Ogura, T.; Siegler, M. A.; Karlin, K. D.; Nam, W. *J. Am. Chem. Soc*. **2012**, *134*, 15269.

10) Kumar, P.; Lee, Y.-M.; Park, Y. J.; Siegler, M. A. Karlin, K. D.; Nam, W. *J. Am. Chem. Soc.***2015**, *137*, 4284.

11) Hughes, M. N.; Nicklin, H. G.; Sackrule, W. A. C. *J. Chem. Soc.* **1971**, 3722.

12) (a) Herold, S.; Koppenol, W. H. *Coord. Chem. Rev.* **2005***, 249,* 499. (b) Roncaroli, F.; Videla, M.; Slep L. D.; Olabe, J. A. *Coord. Chem. Rev*. **2007**, *251*, 1903.

13) Yokoyama, A.; Han, J. E.; Karlin, K. D.; Nam, W. *Chem. Commun*. **2014**, *50*, 1742

14) Saha, S.; Ghosh, S.; Gogoi, K.; Deka, H.; Mondal, B.; Mondal, B. *Inorg. Chem.* **2017**, *56*, 10932

15) (a) Clarkson S. G., Basolo F. *J. Chem. Soc. Chem. Commun*. **1972**, *119*, 670. (b) Clarkson S. G., Basolo F. *Inorg. Chem*. **1973**, *12*, 1528.

16) Skodje, K. M.; Williard, P. G.; Kim, E. *Dalton Trans*. **2012**, *41*, 7849.

17) Park, G. Y.; Deepalatha, S.; Puiu, S. C.; Lee, D.-H.; Mondal, B.; Sarjeant, A. A. N.; del Rio, D.; Pau, M. Y. M.; Solomon, E. I.; Karlin, K. D. *J. Biol. Inorg. Chem.***2009**, *14*, 1301.

18) Kalita, A.; Kumar, P.; Mondal, B. *Chem. Commun*. **2012**, *48*, 4636.

19) *SMART*, *SAINT and XPREP*, Siemens Analytical X-ray Instruments Inc., Madison, Wisconsin, USA, **1995**.

20) Sheldrick, G. M. *SADABS*: *software for Empirical Absorption Correction* University of Gottingen, Institut fur Anorganische Chemieder Universitat, Tammanstrasse 4, D-3400 Gottingen, Germany, **1999**.

21) Sheldrick, G. M. *SHELXS-2014*, University of Gottingen, Germany.

22) Farrugia, L. J. *J. Appl. Crystallogr.* **1997**, *30*, 565.

23) (a) Adler, A. D.; Longo, F. R.; Finarelli.; Goldmacher, J.; Assour, J.; Korsakoff, L. *J. Org. Chem.* **1967**, *32*, 476. (b) Rothemund, P.; Menotti, A. R. *J. Am. Chem. Soc.* **1948**, *70*, 1808. (c) Choi, In-K.; Liu, Y.; Wei, Z.; Ryan, M. D. *Inorg. Chem.* **1997,** *36,* 3113.

24) Scheidt, W. R.; Hatano, K.; Rupprecht, G. A.; Piciulo, P. L. *Inorg. Chem*. **1979**, *18*, 292.

25) Zhang, R.; Horner, J. H.; Newcomb, M. *J. Am. Chem. Soc.* **2005**, *127*, 6573.

26) Wayland, B. B.; Olson, L. W.; Siddiqui, Z. U. *J. Am. Chem. Soc*. **1976**, *98*, 94.

27) (a) Mondal, B.; Saha, S.; Borah, D.; Mazumdar, R; Mondal, B. *Inorg. Chem*. **2019**, *58*, 1234. (b) Kurtikyan, T. S.; Hayrapetyan, V. A.; Mehrabyan, M. M.; Ford, P. C. *Inorg. Chem*. **2014**, *53*, 11948. (c) Suslick, K. S.; Watson, R. A. *Inorg. Chem*. **1991**, *30*, 912

28) (a) Saha, S.; Gogoi, K.; Mondal, B.; Ghosh, S.; Deka, H.; Mondal, B. *Inorg. Chem.* **2017**, *56*, 7781. (b) Addo, G. B. R.; Hodge, S. J.; Yi, G. B.; Khan, M. A.; Ma, T.; Caemelbecke, E. V.; Guo, N.; Kadish, K. M. *Inorg. Chem*. **1996**, *35*, 6530.

29) Groves, J. T.; Stern, M. K. *J. Am. Chem. Soc*. **1988**, *110*, 8628.

30) Leto, D. F.; Ingram, R.; Day, V.W.; Jackson, T. A. *Chem. Commun*. **2013**, *49*, 5378.

31) Parsell, T. H.; Behan, R. K.; Green, M. T.; Hendrich, M. P.; Borovik, A. S. *J. Am. Chem. Soc*. **2006**, *128*, 8728.

32) (a) Reed, C. A.; Kouba, J. K.; Grimes, C. J.; Cheung, S. K. *Inorg. Chem.* **1978**, *17*, 2666. (b) Boucher, L. *Coord. Chem. Rev*. **1972**, *7*, 289. (c) Hoffman, B. M.; Wescheler, C. J.; Basolo, F. *J. Am. Chem. Soc.* **1976**, *98*, 5473.

33) Kalyaraman, B. *Proc. Natl. Acad. Soc. U.S.A*. **2004**, *101*, 11527.

Appendix I

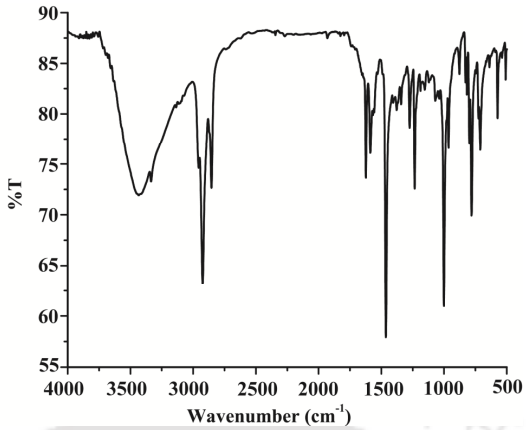

Figure A1.1. FT-IR spectrum of ligand **L1H$_2$** in KBr.

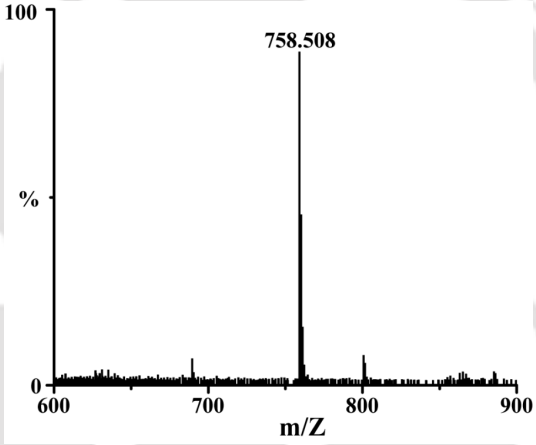

Figure A1.2. ESI-mass spectrum of ligand **L1H$_2$** in acetonitrile.

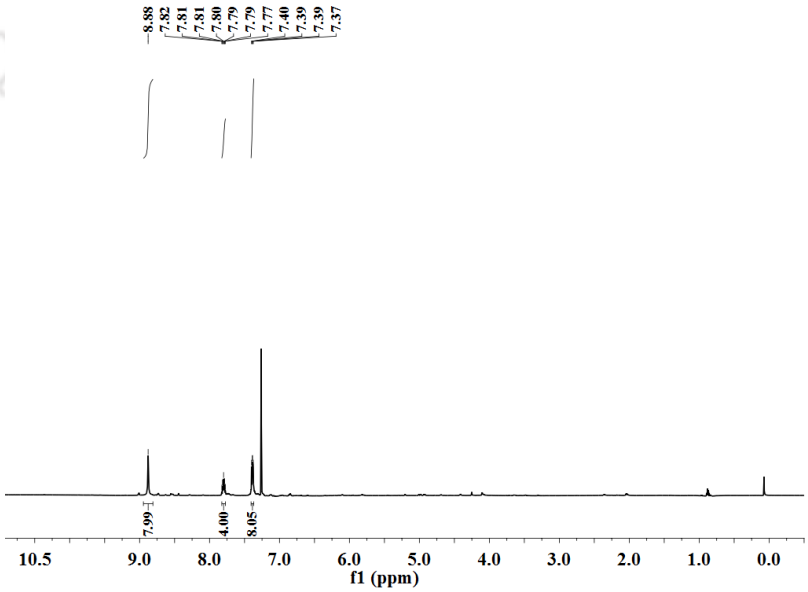

Figure A1.3. ^{1}H NMR spectrum of ligand **L1H$_2$** in $CDCl_3$.

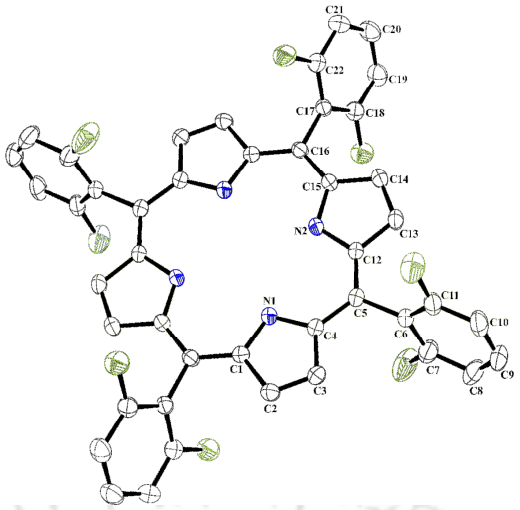

Figure A1.4. ORTEP diagram of ligand $\mathbf{L1H_2}$ (50% thermal ellipsoid plot, H-atoms are omitted for clarity).

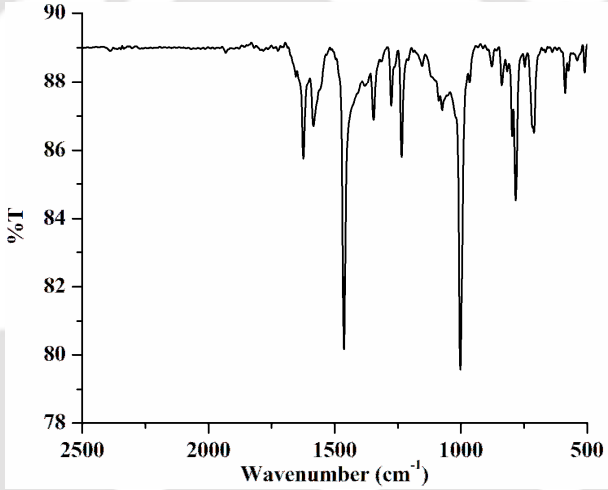

Figure A1.5. FT-IR spectrum of complex **2.1** in KBr.

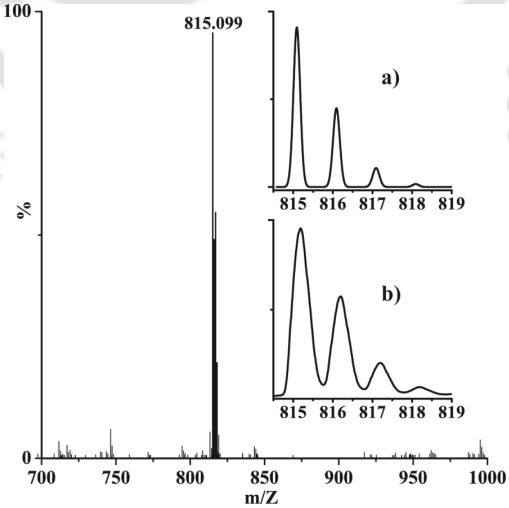

Figure A1.6. ESI-mass spectrum of complex **2.1** in acetonitrile. [Inset: (a) simulated and (b) experimental isotopic distribution pattern].

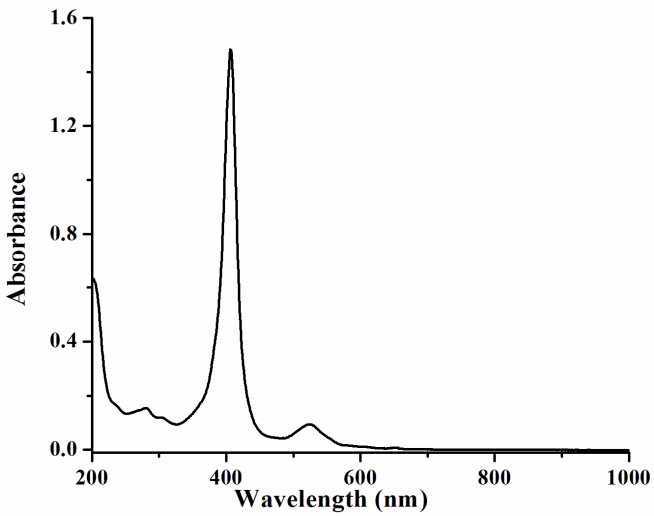

Figure A1.7. UV-visible spectrum of complex **2.1** in acetonitrile at room temperature (8.26 µM).

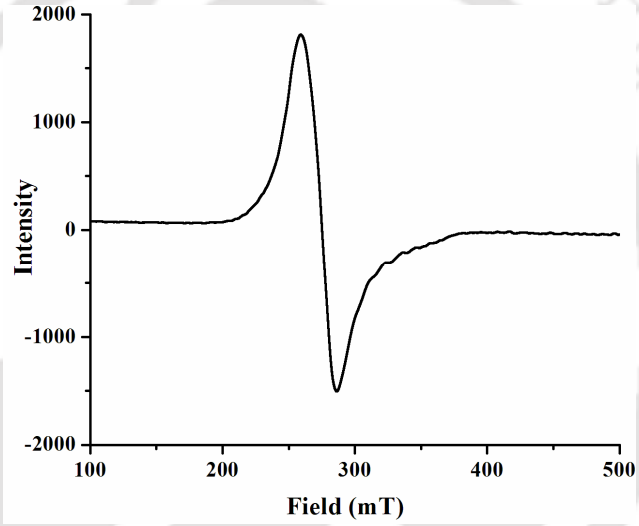

Figure A1.8. X-band EPR-spectrum of complex **2.1** in acetonitrile at 77K (6.14 mM).

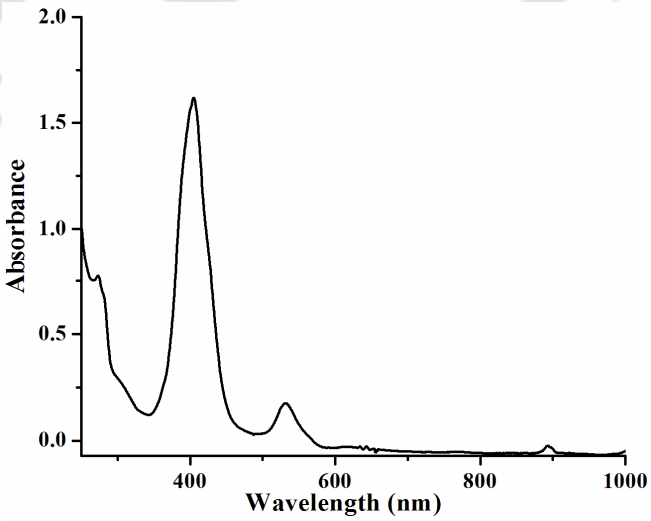

Figure A1.9. UV-visible spectrum of complex **2.2** in acetonitrile at –40 °C (11.5 µM).

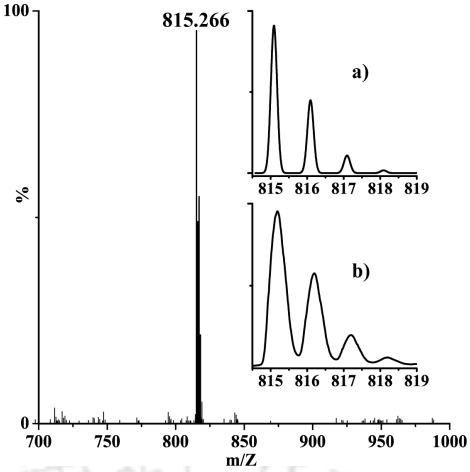

Figure A1.10. ESI-mass spectrum of complex **2.2** in acetonitrile. [Inset: (a) simulated and (b) experimental isotopic distribution pattern].

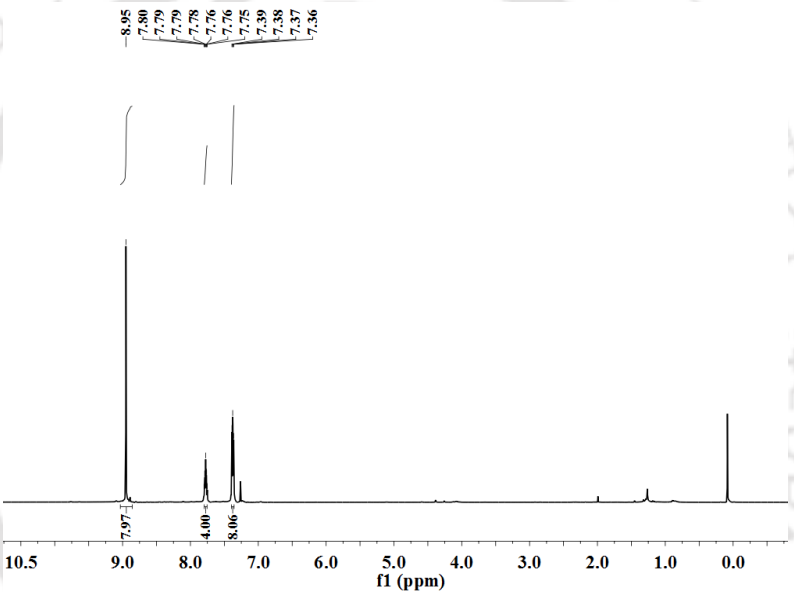

Figure A1.11. ^{1}H NMR spectrum of complex **2.2** in $CDCl_3$.

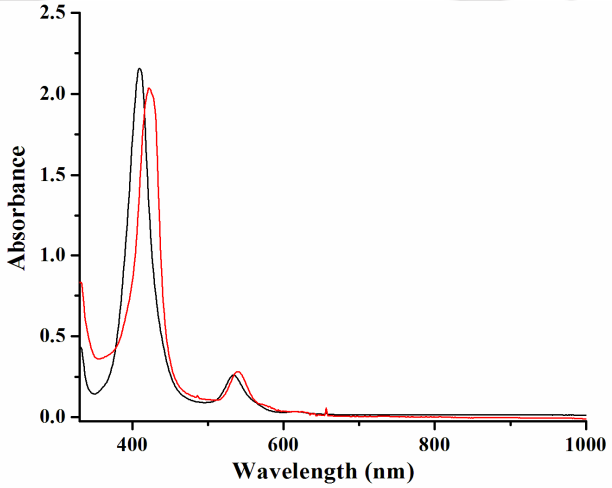

Figure A1.12. UV-visible spectra of complex **2.2** (11.38 µM) (black) and after addition of H_2O_2 to result in complex **2.3** (10.35 µM) (red) in THF at −80 °C.

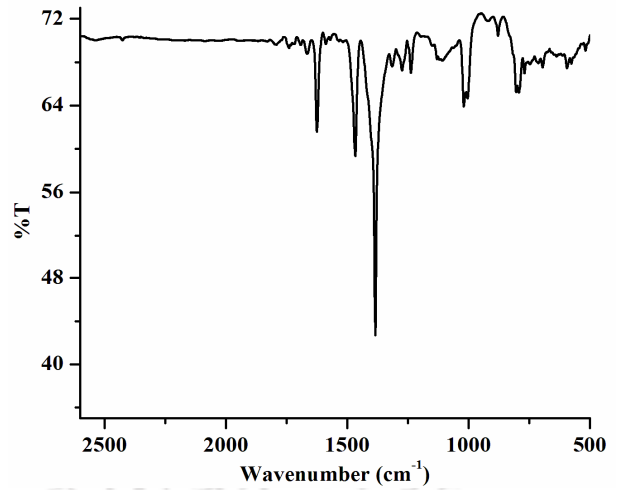

Figure A1.13. FT-IR spectrum of complex **2.3** in KBr.

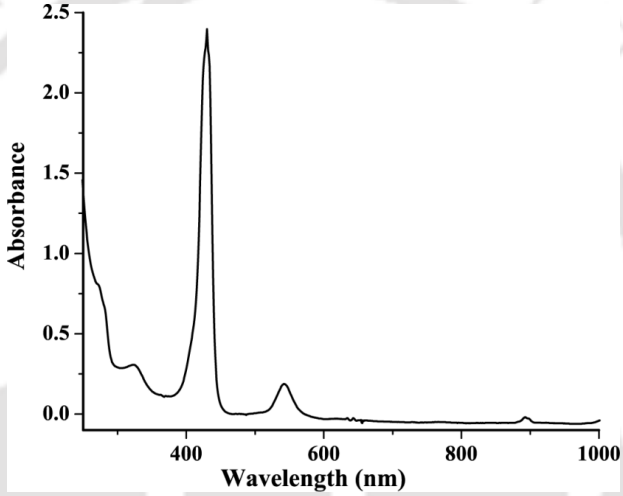

Figure A1.14. UV-visible spectrum of complex **2.3** in acetonitrile at −40 °C (10.46 µM).

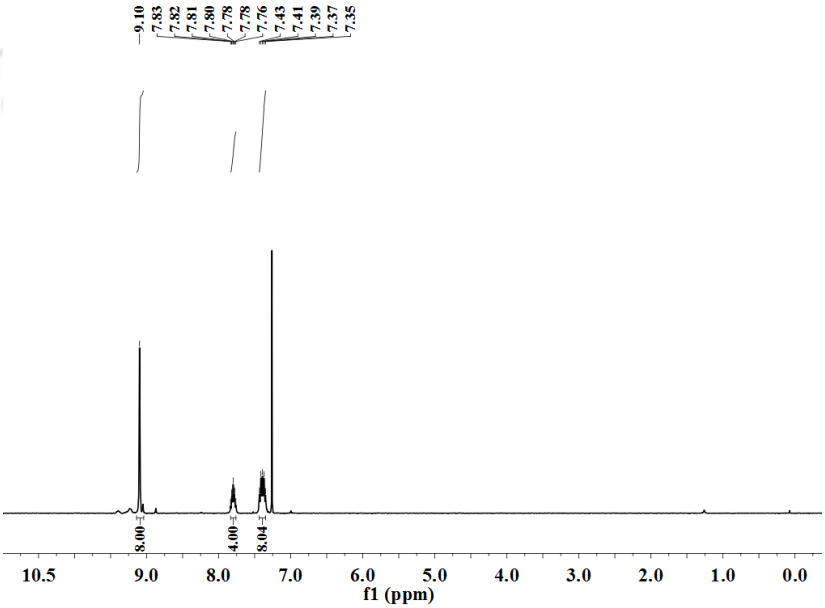

Figure A1.15. ^{1}H NMR spectrum of complex **2.3** in $CDCl_3$.

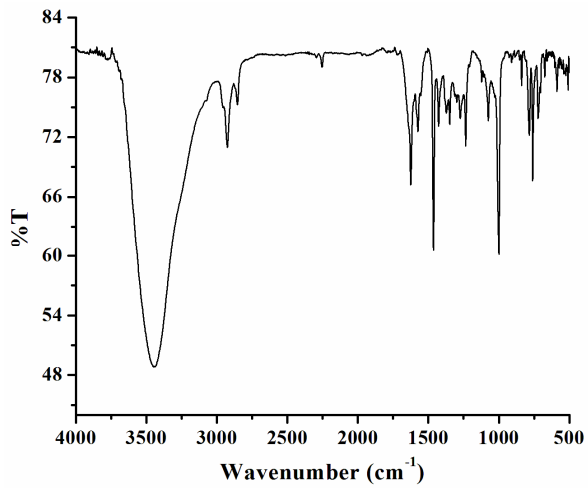

Figure A1.16. FT-IR spectrum of complex **2.4** in KBr.

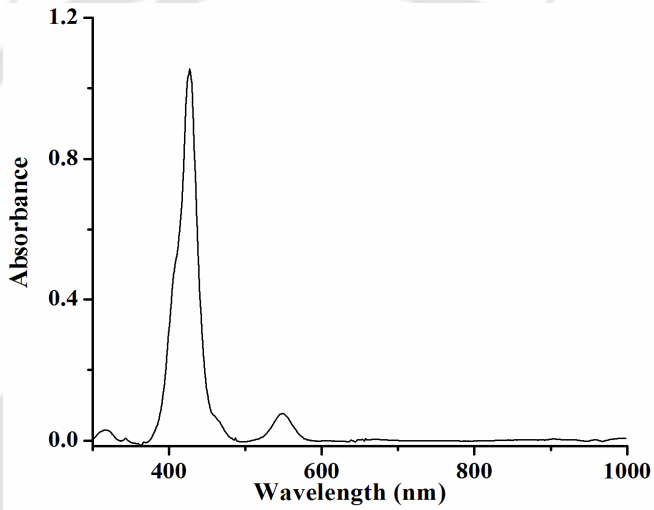

Figure A1.17. UV-visible spectrum of complex **2.4** in acetonitrile (5.49 μM).

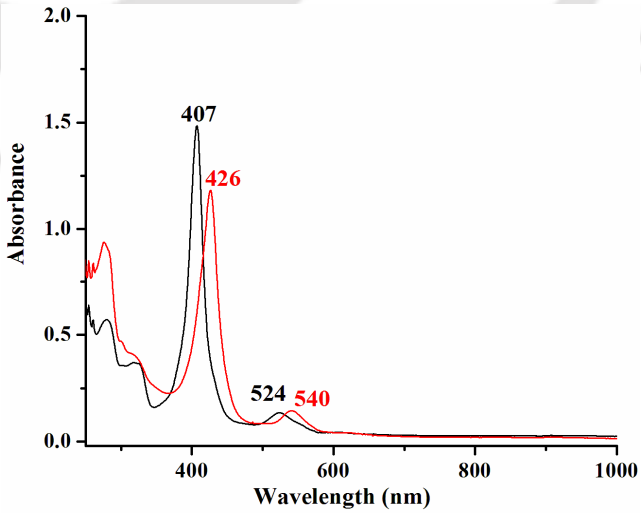

Figure A1.18. UV-visible spectra of complex **2.1** (8.26 μM) (black) and after addition of *m*CPBA (red line) in acetonitrile at –40 °C.

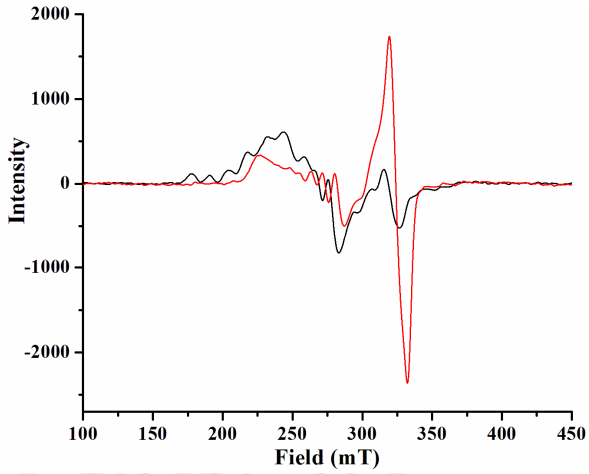

Figure A1.19. X-band EPR spectra of complex **2.1** (black) and after addition of *m*CPBA (red) in acetone at 77K.

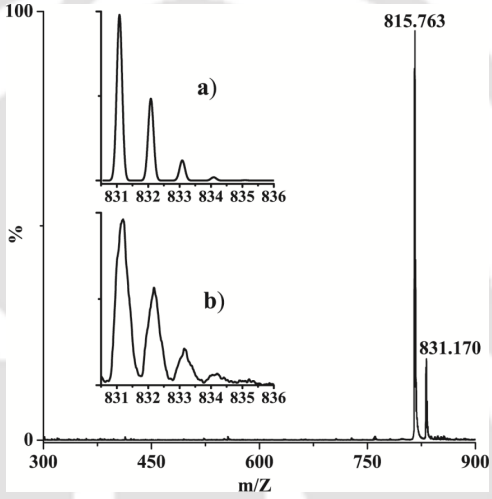

Figure A1.20. ESI-mass spectrum of the reaction mixture of complex **2.1** and *m*CPBA. [Inset: (a) simulated and (b) experimental isotopic distribution pattern].

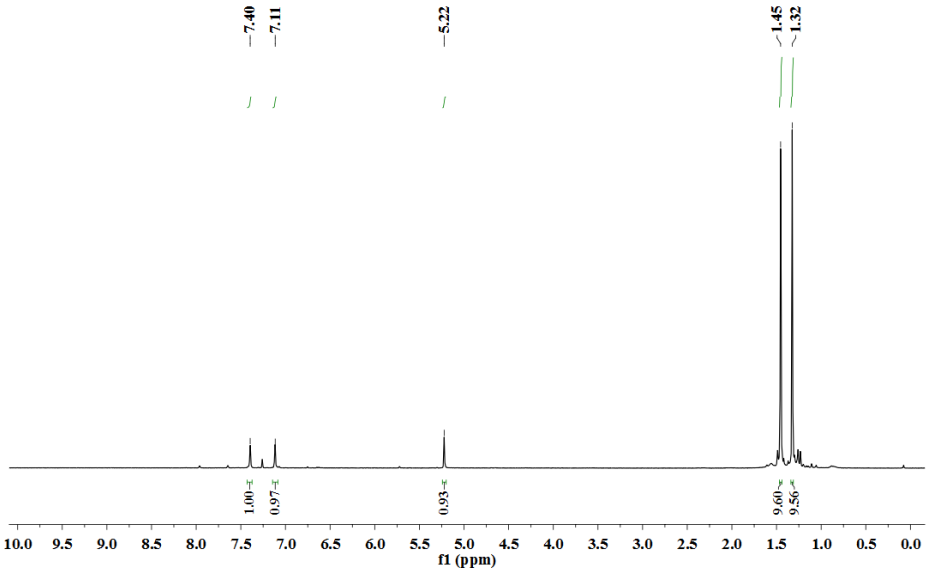

Figure A1.21. ^{1}H NMR spectrum of 2,4-di-*tert*-butyl-6-nitrophenol in $CDCl_3$.

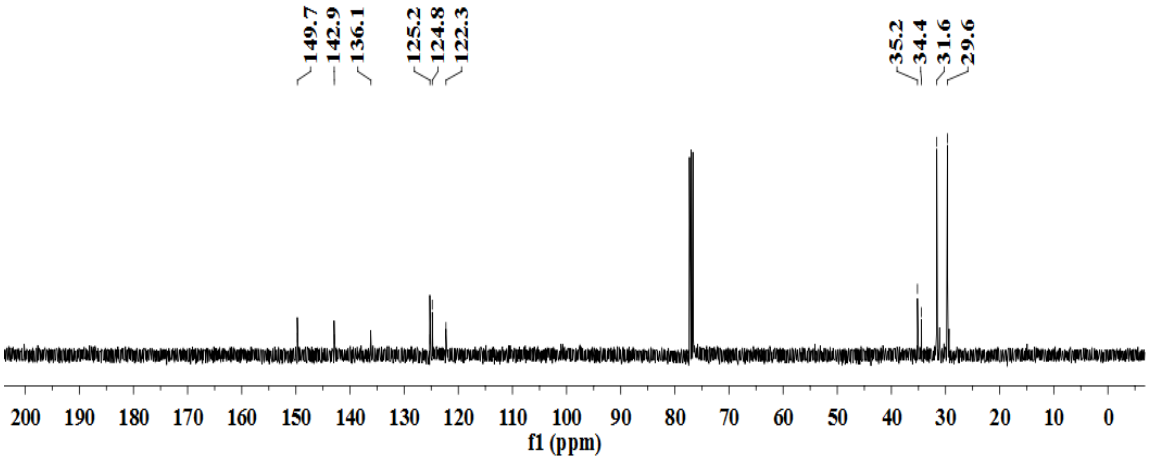

Figure A1.22. ^{13}C NMR spectrum of 2,4-di-*tert*-butyl-6-nitrophenol in $CDCl_3$.

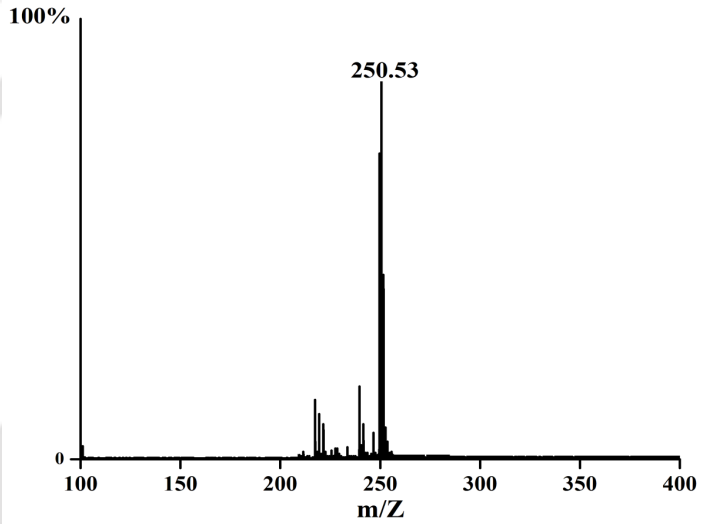

Figure A1.23. ESI-mass spectrum of 2,4-di-*tert*-butyl-6-nitrophenol in methanol.

Table A1.1. Selected bond lengths (Å) of ligand **L1H$_2$**, complexes **2.1** and **2.2**

Atoms	**L1H$_2$**	**2.1**	**2.2**
Co1–N3	-	-	1.894(10)
Co1–N1	-	1.974(3)	1.992(4)
Co1–N2	-	1.975(3)	1.997(4)
N3–O1	-	-	1.158(13)
C1-N1	1.367(3)	1.380(4)	1.374(7)
C1–C2	1.450(3)	1.433(5)	1.444(8)
C3-C4	1.446(3)	1.430(5)	1.441(8)
C4-C5	1.404(3)	1.382(5)	1.392(8)
C5-C6	1.501(3)	1.498(4)	1.492(8)
C7-F1	1.340(3)	1.350(5)	1.346(10)

Table A1.2. Selected bond angles (°) of ligand **L1H$_2$**, complexes **2.1** and **2.2**

Atoms	**L1H$_2$**	**2.1**	**2.2**
N1–Co1–N2	-	90.26(11)	90.59(18)
N1–Co1–N3	-	-	87.9(4)
N2–Co1–N3	-	-	93.9(4)
Co1-N3-O1	-	-	127.4(14)
Co1-N1-C1	-	128.1(2)	126.9(4)
N1-C1-C2	110.35(18)	110.8(3)	110.4(5)
C1-C2-C3	106.7(2)	106.8(3)	107.2(5)
C2-C3-C4	107.09(19)	107.7(3)	106.8(5)
C4-C5-C6	117.61(19)	118.1(3)	119.2(5)
F1-C7-C6	117.9(2)	117.5(3)	118.5(6)

Table A1.3. Crystallographic data for ligand **L1H$_2$**, complexes **2.1** and **2.2**

	L1H$_2$	**2.1**	**2.2**
Formulae	C_{44} H_{22} F_8 N_4	C_{46} H_{22} Cl_6 F_8 N_4 Co	C_{44} H_{20} F_8 N_5 Co O
Mol. wt.	758.66	1054.31	845.58
Crystal system	Monoclinic	Monoclinic	Monoclinic
Space group	P 21/c	C 2/c	P 21/n
Temperature /K	293(2)	293(2)	293(2)
Wavelength /Å	0.71073	0.71073	0.71073
a /Å	12.5453(6)	18.0573(4)	12.2731(7)
b /Å	11.4552(6)	16.8138(4)	12.5704(5)
c /Å	12.2023(5)	14.7268(3)	12.4945(7)
α/°	90.00	90.00	90.00
β/°	96.985(4)	97.453(2)	112.410(6)
γ/°	90.00	90.00	90.00
V/ Å^3	1740.56(14)	4433.46(17)	1782.05(16)
Z	2	4	2
Density/Mgm^{-3}	1.448	1.580	1.576
Abs. Coeff. /mm^{-1}	0.116	0.822	0.569
Abs. correction	Multi-scan	Multi-scan	Multi-scan
F(000)	772	2108	852
Total no. of reflections	3061	3908	3134
Reflections, $I > 2\sigma(I)$	2354	3258	2437
Max. 2θ/°	25.00	25.00	25.00
Ranges (h, k, l)	-14≤ h ≤14 -7≤ k ≤13 -14≤ l ≤ 13	-21 ≤ h ≤ 21 -16 ≤ k ≤ 19 -17 ≤ l ≤ 7	-14≤ h ≤8 -14≤ k ≤14 -12≤ l ≤ 14
Complete to 2θ (%)	99.8	99.8	99.9
Refinement method	Full-matrix least-squares on F^2	Full-matrix least-squares on F^2	Full-matrix least-squares on F^2

Goof (F^2)	1.018	0.938	0.871
R indices [$I > 2\sigma(I)$]	0.0477	0.0590	0.0884
R indices (all data)	0.0638	0.0684	0.1057

Appendix II

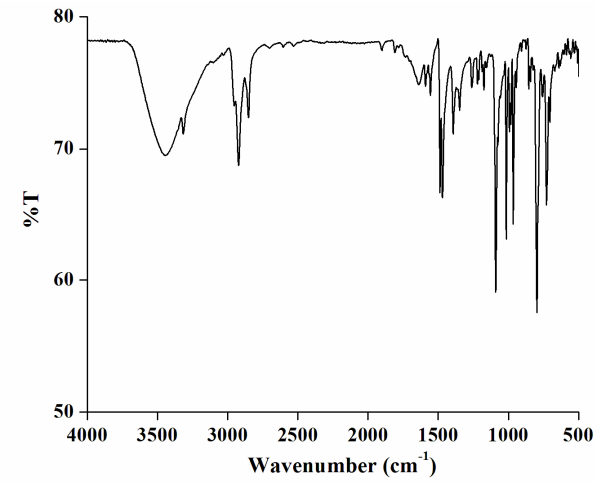

Figure A2.1. FT-IR spectrum of ligand **L2H$_2$** in KBr.

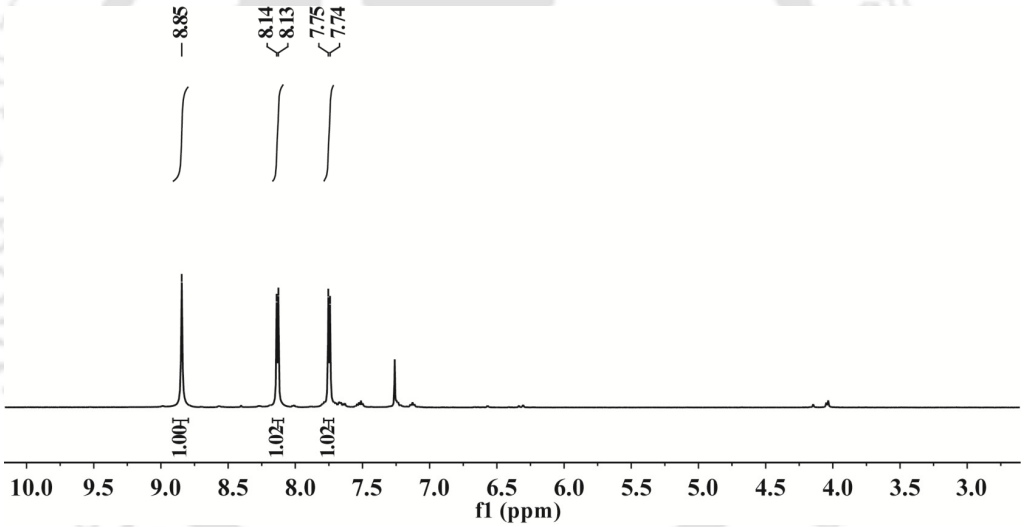

Figure A2.2. ^{1}H NMR spectrum of ligand **L2H$_2$** in $CDCl_3$.

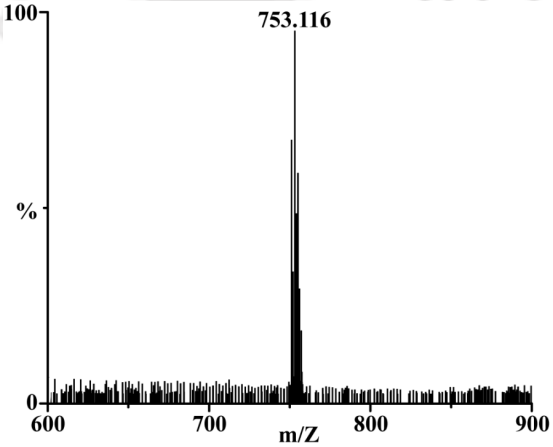

Figure A2.3. ESI-mass spectrum of ligand **L2H$_2$** in acetonitrile.

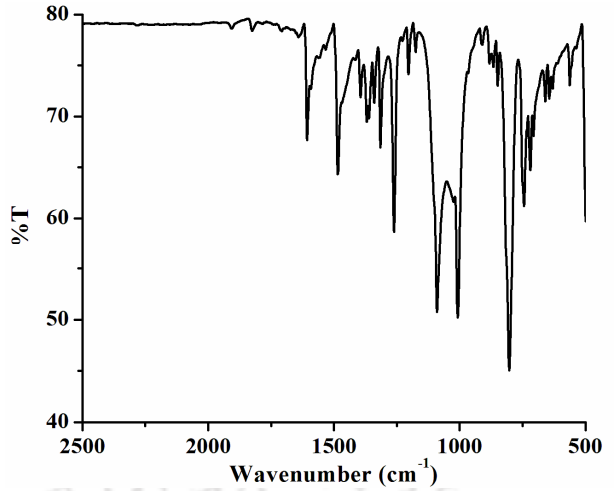

Figure A2.4. FT-IR spectrum of complex **3.1** in KBr.

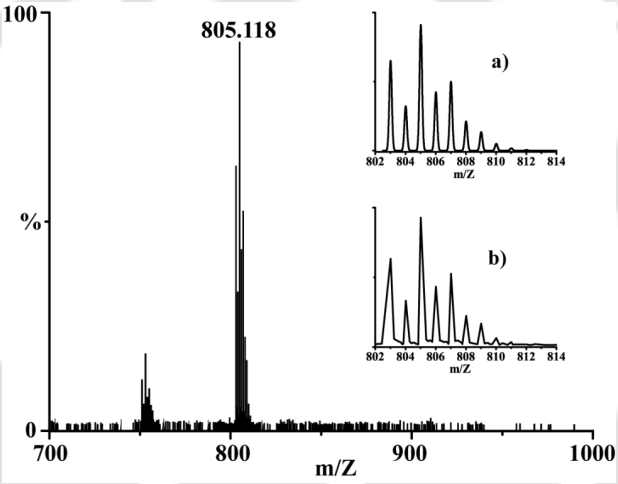

Figure A2.5. ESI-mass spectrum of complex **3.1** in acetonitrile. [Inset: (a) simulated and (b) experimental isotopic distribution pattern].

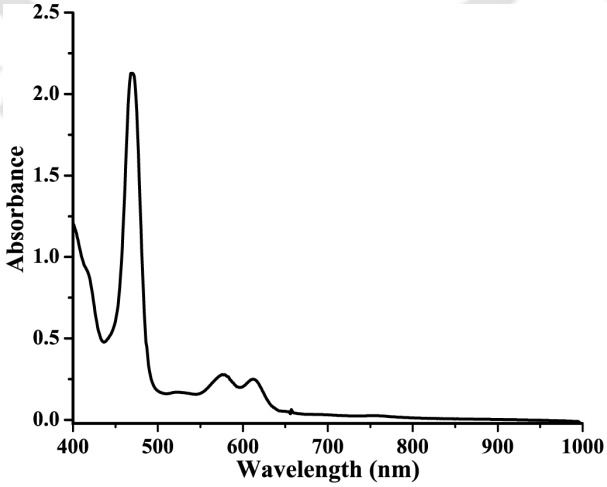

Figure A2.6. UV-visible spectrum of complex **3.1** in dichloromethane at room temperature. (35.21 μM)

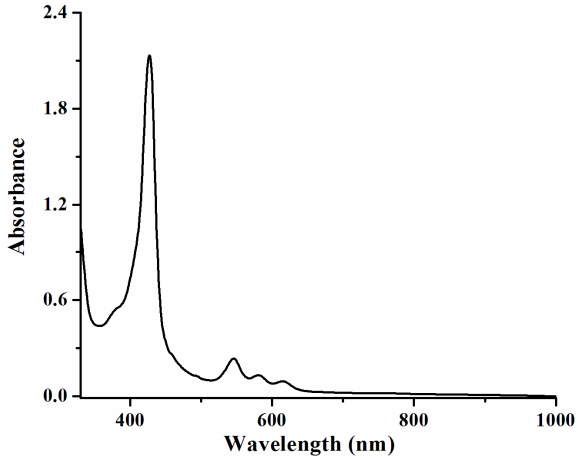

Figure A2.7. UV-visible spectrum of complex **3.2** in dichloromethane at −80 °C. (16.77 µM)

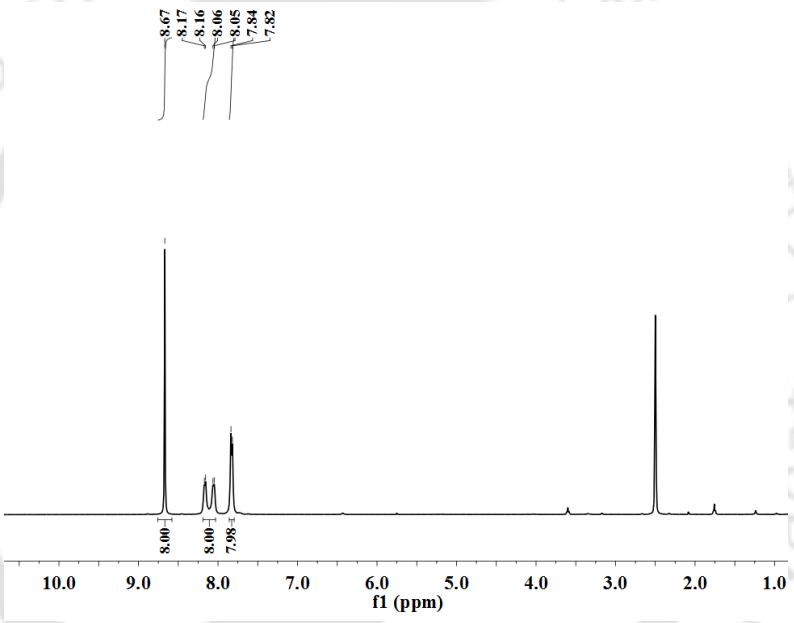

Figure A2.8. ^{1}H NMR spectrum of complex **3.2** in DMSO-d_6.

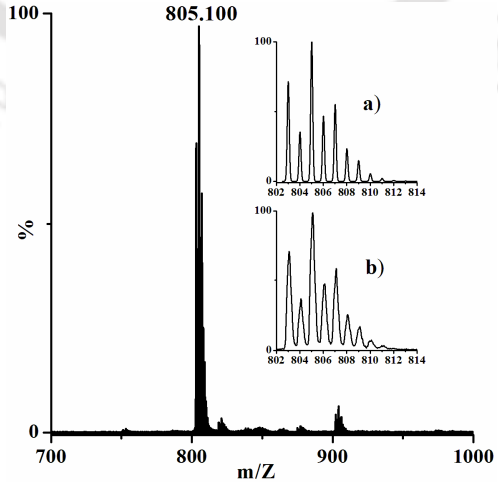

Figure A2.9. ESI-mass spectrum of complex **3.2** in acetonitrile. [Inset: (a) simulated and (b) experimental isotopic distribution pattern].

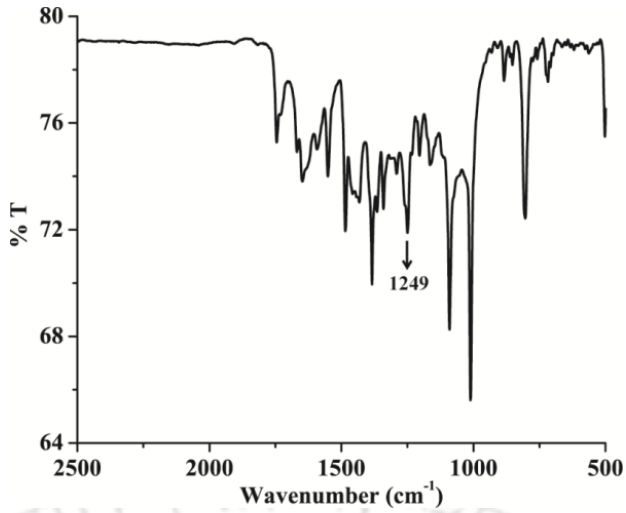

Figure A2.10. FT-IR spectrum of complex **3.3** in KBr.

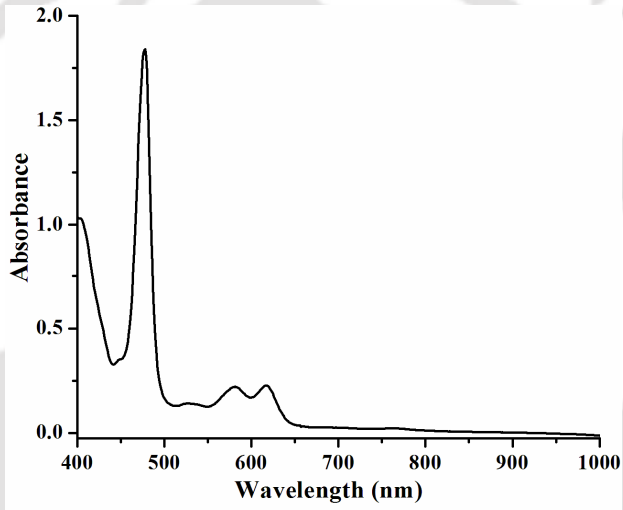

Figure A2.11. UV-visible spectrum of complex **3.3** in dichloromethane at −80 °C. (11.35 µM)

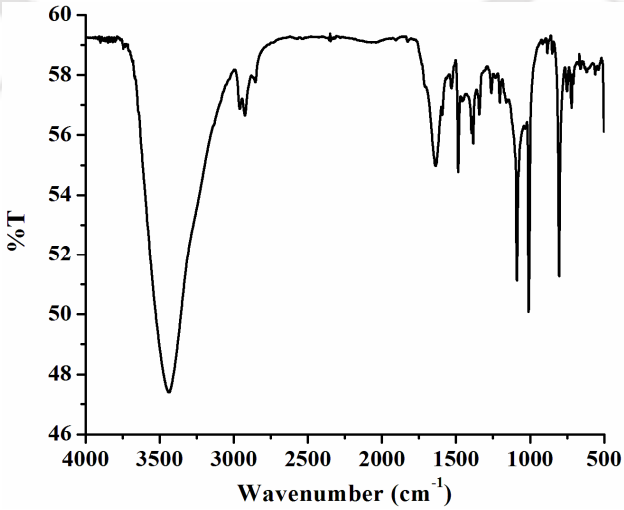

Figure A2.12. FT-IR spectrum of complex **3.4** in KBr.

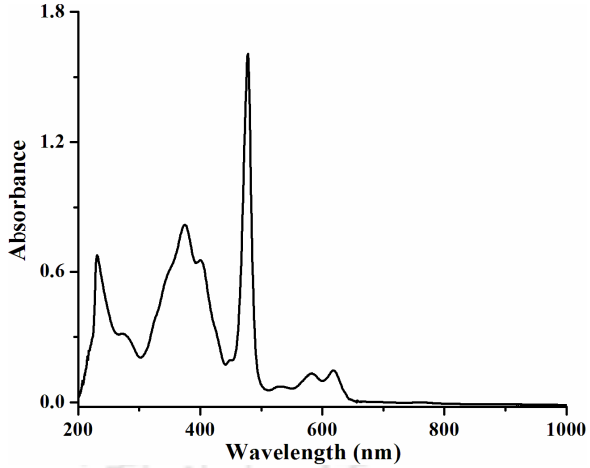

Figure A2.13. UV-visible spectrum of **3.4** in dichloromethane at room temperature. (9.69 µM)

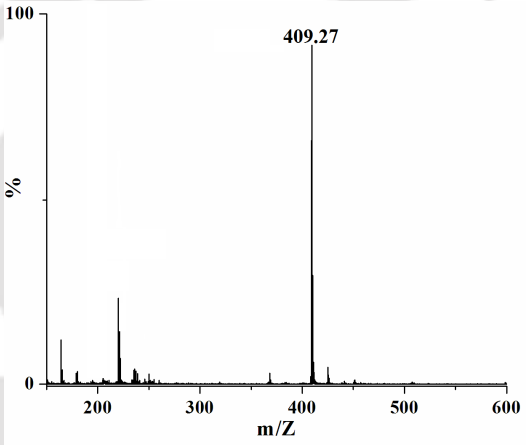

Figure A2.14. ESI-mass spectrum of 3,3',5,5'-tetra-*tert*-butyl-[1,1'-biphenyl]-2,2'-diol in acetonitrile.

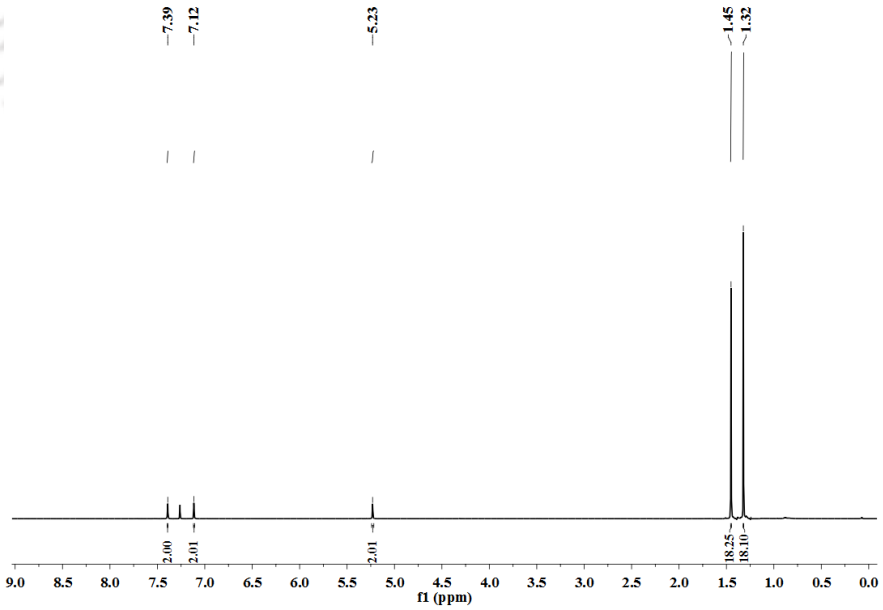

Figure A2.15. ^{1}H NMR spectrum of 3,3',5,5'-tetra-*tert*-butyl-[1,1'-biphenyl]-2,2'-diol in $CDCl_3$.

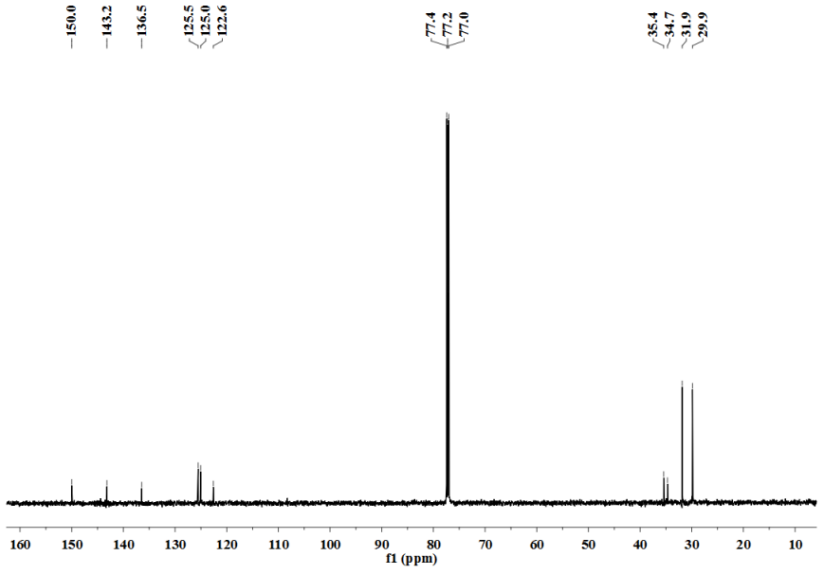

Figure A2.16. ^{13}C NMR spectrum of 3,3',5,5'-tetra-*tert*-butyl-[1,1'-biphenyl]-2,2'-diol in $CDCl_3$.

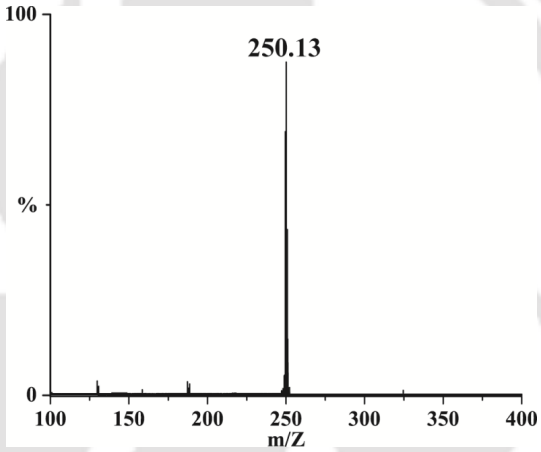

Figure A2.17. ESI-mass spectrum of 2,4-di-*tert*-butyl-6-nitrophenol in methanol.

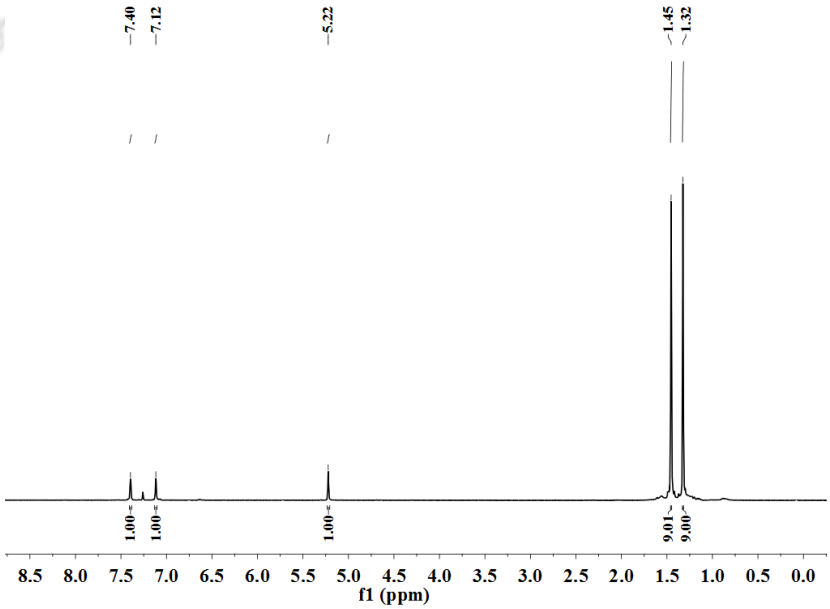

Figure A2.18. ^{1}H NMR spectrum of 2,4-di-*tert*-butyl-6-nitrophenol in $CDCl_3$.

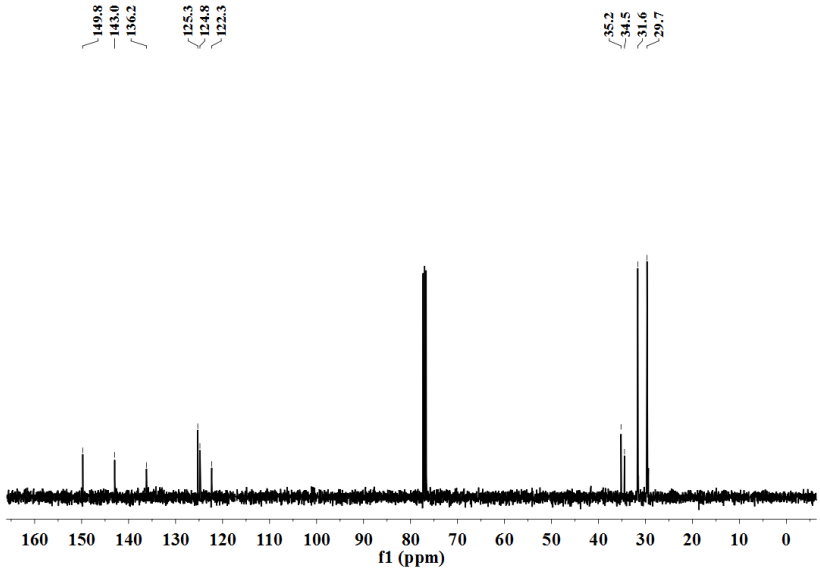

Figure A2.19. ^{13}C NMR spectrum of 2,4-di-*tert*-butyl-6-nitrophenol in $CDCl_3$.

Table A2.1. Selected bond lengths (Å) of complexes **3.1**, **3.2** and **3.3**.

Atoms	**3.1**	**3.2**	**3.3**
Mn1–N1	2.013(7)	2.013(4)	-
Mn1–N2	-	1.815(7)	-
Mn1–O4	-	-	2.167(2)
Mn2–O3	-	-	2.183(3)
Mn2–O2	-	-	2.193(3)
Mn3–O1	-	-	2.189(3)
Mn1–Cl2	2.581(10)	-	-
N2–O1	-	1.096(9)	-
N3–O2	-	-	1.221(4)
N3–O1	-	-	1.240(4)
C1–N1	-	1.371(6)	-
C1–C2	1.367(15)	1.436(6)	-
C3-C4	1.404(14)	1.440(6)	-
C4-C5	1.394(13)	1.373(6)	-

Table A2.2. Selected bond angles (°) of complexes **3.1**, **3.2** and **3.3**.

Atoms	**3.1**	**3.2**	**3.3**
N1–Mn1–N1	90.0	90.0	-
N1–Mn1–N2	-	90.0(1)	-
Mn1–N2–O1	-	180.0	-
Mn1–N1–C1	-	127.6(3)	-
N3–O2–Mn2	-	-	133.4(3)
N8–O4–Mn1	-	-	132.3(3)
O2–N3–O1	-	-	127.2(4)
O3–N8–O4	-	-	125.5(4)

N1–C1–C2	-	110.5(4)	-
C1–C2–C3	106.6(9)	106.6(4)	-
C2–C3–C4	122.8(9)	108.0(4)	-
C5–C4–C6	118.9(8)	-	-

Table A2.3. Crystallographic data of complexes **3.1**, **3.2** and **3.3**.

	3.1	**3.2**	**3.3**
Formulae	C_{44} H_{24} Cl_5 N_4 Mn	C_{44} H_{24} Cl_4 N_6 O_2 Mn	C_{88} H_{48} Cl_8 N_{10} O_4 Mn_2
Mol. wt.	840.86	865.43	1702.84
Crystal system	Tetragonal	Tetragonal	Monoclinic
Space group	I 4/m	I 4/m	P 21/n
Temperature /K	293(2)	101(1)	293(2)
Wavelength /Å	0.71073	0.71073	0.71073
a /Å	17.1994(12)	14.6282(13)	25.0821(10)
b /Å	17.1994(12)	14.6282(13)	16.7339(4)
c /Å	9.5386(17)	9.5602(17)	28.7679(12)
α/°	90.00	90.00	90
β/°	90.00	90.00	104.170(4)
γ/°	90.00	90.00	90
V/ $Å^3$	2821.7(6)	2045.7(5)	11707.1(8)
Z	2	2	4
Density/Mgm^{-3}	0.990	1.405	0.966
Abs. Coeff. /mm^{-1}	0.497	0.629	0.438
Abs. correction	Multi-scan	Multi-scan	Multi-scan
F(000)	852	878	3456
Total no. of reflections	1283	970	20597
Reflections, $I > 2\sigma(I)$	834	709	10819
Max. 2θ/°	24.997	25.000	25.000
Ranges (h, k, l)	$-17 \le h \le 12$ $-20 \le k \le 12$ $-10 \le l \le 11$	$-11 \le h \le 14$ $-11 \le k \le 17$ $-11 \le l \le 11$	$-26 \le h \le 29$ $-19 \le k \le 19$ $-30 \le l \le 34$
Complete to 2θ (%)	96.1	99.7	99.8
Refinement method	Full-matrix least-squares on F^2	Full-matrix least-squares on F^2	Full-matrix least-squares on F^2
Goof (F^2)	1.026	1.062	0.916
R indices [$I > 2\sigma(I)$]	0.1115	0.0528	0.0744
R indices (all data)	0.1441	0.0769	0.1204

Appendix III

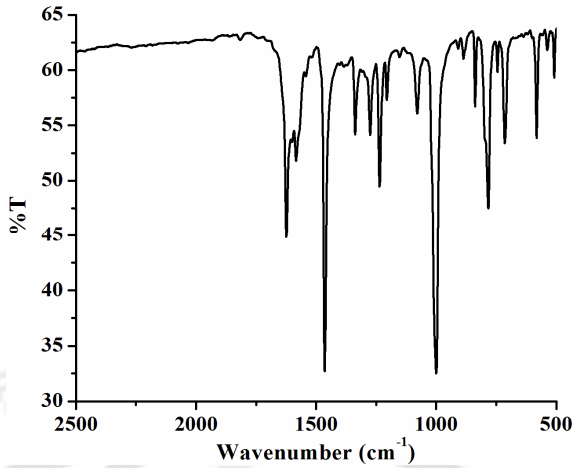

Figure A3.1. FT-IR spectrum of complex **4.1** in KBr.

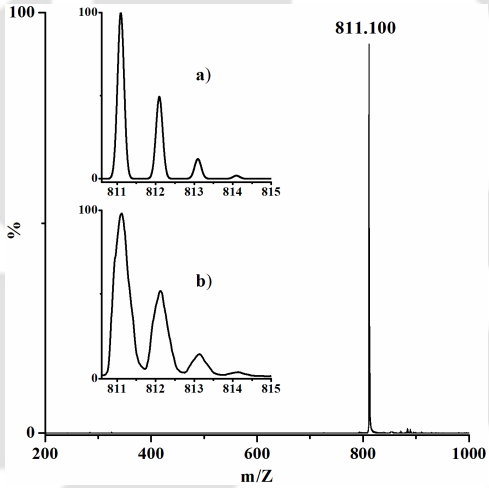

Figure A3.2. ESI-mass spectrum of complex **4.1** in acetonitrile. [Inset: (a) simulated and (b) experimental isotopic distribution pattern].

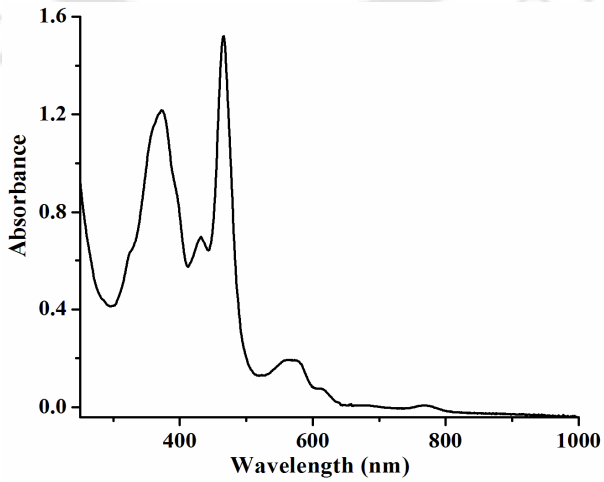

Figure A3.3. UV-visible spectrum of complex **4.1** in THF at room temperature (9.65 μM).

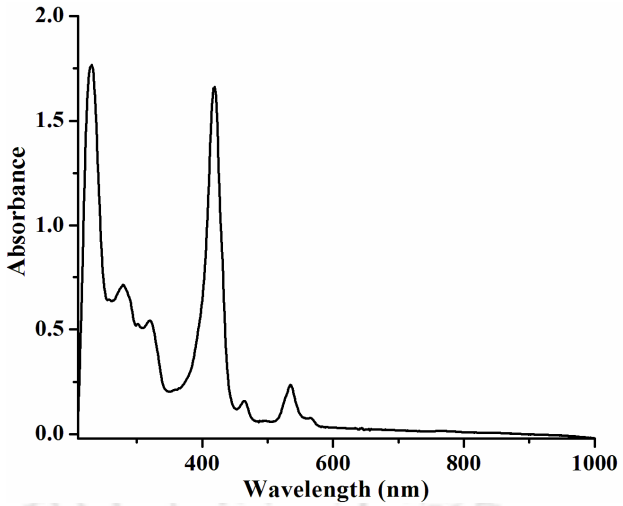

Figure A3.4. UV-visible spectrum of complex **4.2** in THF at −80 °C (9.14 µM).

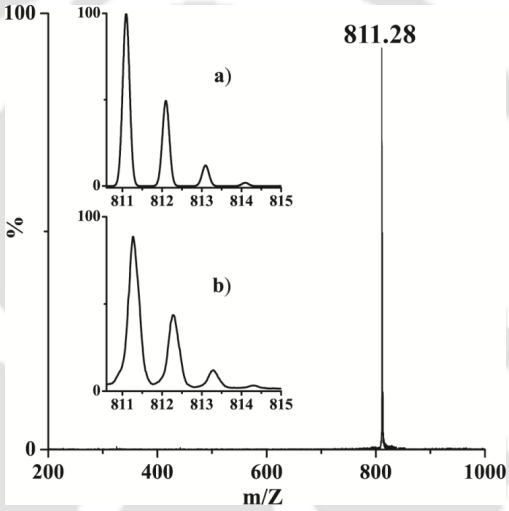

Figure A3.5. ESI-mass spectrum of complex **4.2** in acetonitrile. [Inset: (a) simulated and (b) experimental isotopic distribution pattern].

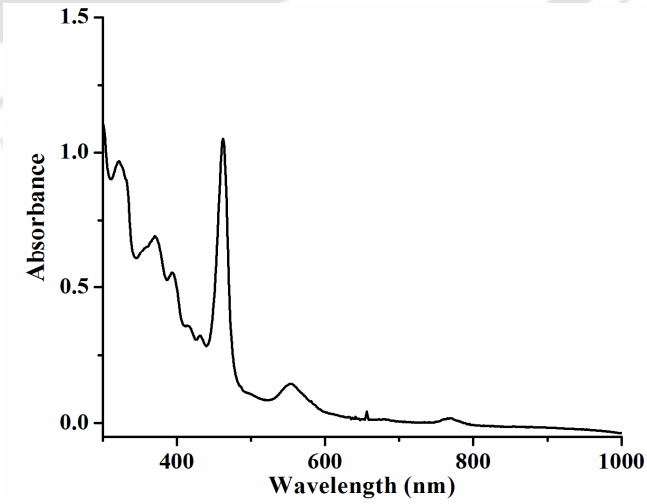

Figure A3.6. UV-visible spectrum of complex **4.3** in THF at −80 °C (8.40 µM).

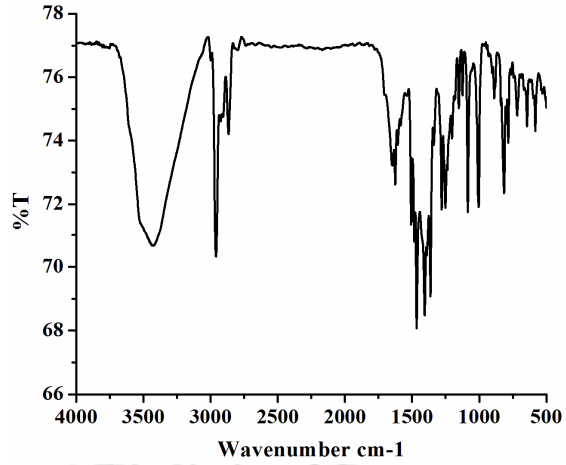

Figure A3.7. FT-IR spectrum of complex **4.4** in KBr.

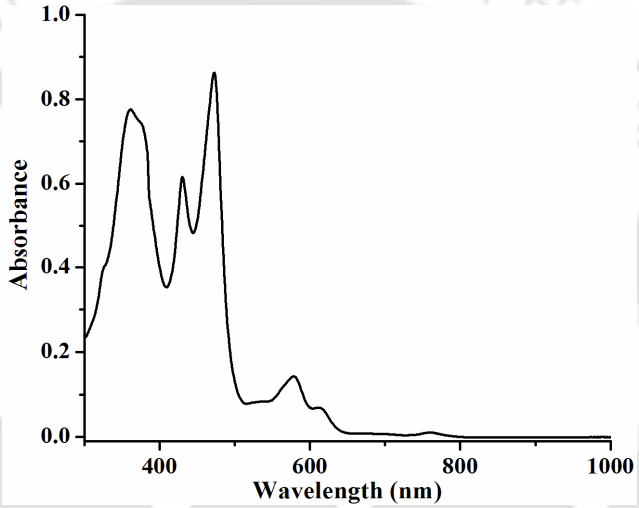

Figure A3.8. UV-visible spectrum of complex **4.4** in THF at room temperature (7.72 µM).

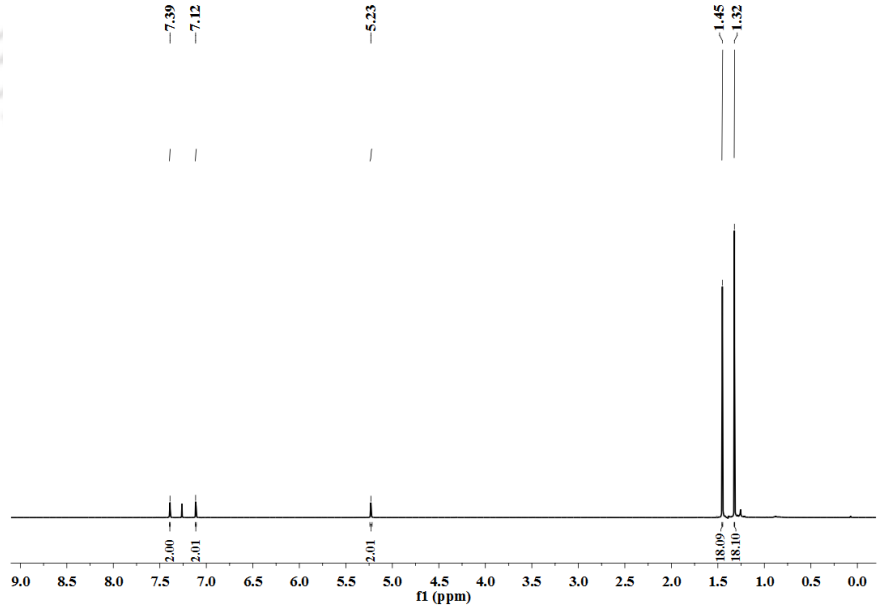

Figure A3.9. ^{1}H NMR spectrum of 3,3',5,5'-tetra-*tert*-butyl-[1,1'-biphenyl]-2,2'-diol in $CDCl_3$.

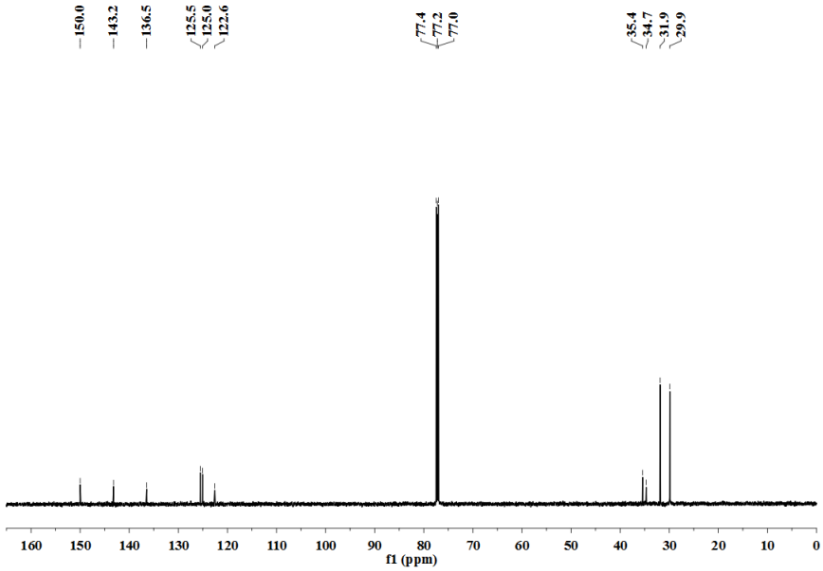

Figure A3.10. ^{13}C NMR spectrum of 3,3',5,5'-tetra-*tert*-butyl-[1,1'-biphenyl]-2,2'-diol in $CDCl_3$.

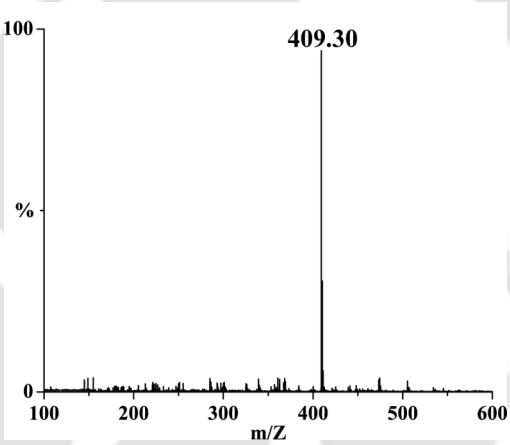

Figure A3.11. ESI-mass spectrum of 3,3',5,5'-tetra-*tert*-butyl-[1,1'-biphenyl]-2,2'-diol in acetonitrile.

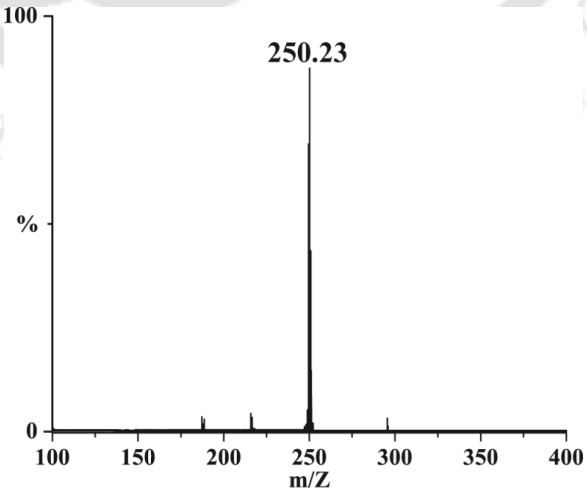

Figure A3.12. ESI-mass spectrum of 2,4-di-*tert*-butyl-6-nitrophenol in methanol.

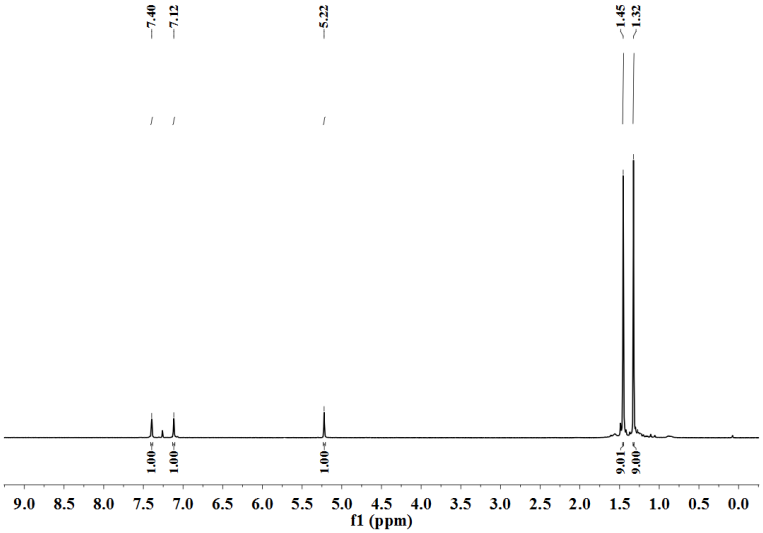

Figure A3.13. ^{1}H NMR spectrum of 2,4-di-*tert*-butyl-6-nitrophenol in $CDCl_3$.

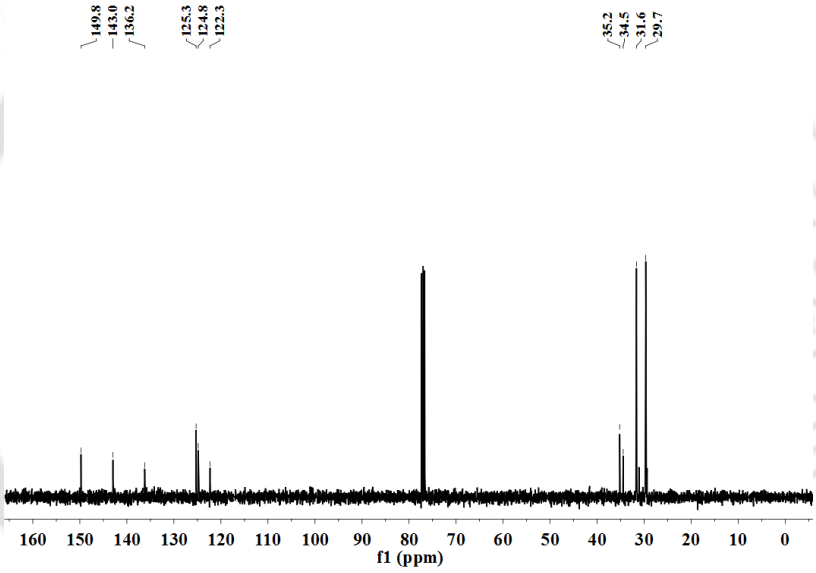

Figure A3.14. ^{13}C NMR spectrum of 2,4-di-*tert*-butyl-6-nitrophenol in $CDCl_3$.

Table A3.1. Selected bond lengths (Å) of complexes **4.1**, **4.2** and **4.3**

Atoms	**4.1**	**4.2**	**4.3**
Mn1–N1	2.030(8)	2.023(3)	2.005(4)
Mn1–N2	2.019(7)	2.026(3)	2.005(4)
Mn1–N3	-	1.844(4)	2.003(4)
Mn1–N4	-	-	2.011(3)
Mn1–O1	-	-	2.099(4)
Mn1–Cl1	2.223(7)	-	-
N3–O1	-	1.149(6)	-
N5–O1	-	-	1.219(6)
N5–O2	-	-	1.340(7)
N5–O3	-	-	1.163(6)

C1-N1	-	1.375(5)	1.395(5)
C1–C2	1.363(17)	1.434(5)	1.422(6)
C3-C4	1.390(13)	1.436(5)	1.432(6)
C4-C5	1.505(17)	1.402(6)	1.393(7)
C5-C6	1.374(10)	1.494(5)	1.494(6)

Table A3.2. Selected bond angles (°) of complexes **4.1**, **4.2** and **4.3**

Atoms	**4.1**	**4.2**	**4.3**
N1–Mn1–N2	90.3(3)	90.24(13)	89.23(15)
N1– Mn1–N3	-	91.66(15)	168.25(13)
N2– Mn1–N3	-	91.94(15)	89.48(15)
N3– Mn1–N4	-	-	88.99(15)
N1– Mn1–O1	-	-	101.51(16)
N2– Mn1–O1	-	-	91.65(17)
N3– Mn1–O1	-	-	90.20(16)
N4– Mn1–O1	-	-	100.05(17)
N1– Mn1–Cl1	91.0(3)	-	-
N2– Mn1–Cl1	91.6(3)	-	-
Mn1-N3-O1	-	171.0(5)	-
Mn1-O1-N5	-	-	130.7(5)
O1-N5-O3	-	-	124.7(6)
O1-N5-O2	-	-	112.2(5)
O2-N5-O3	-	-	123.0(5)
N1-C1-C2	-	109.5(3)	109.5(4)
C1-C2-C3	118.3(14)	107.7(4)	107.4(4)
C2-C3-C4	124.3(12)	106.9(3)	107.6(4)

Table A3.3. Crystallographic data for complexes **4.1**, **4.2** and **4.3**

	4.1	**4.2**	**4.3**
Formulae	C_{44} H_{20} Cl F_8 N_4 Mn	C_{44} H_{20} F_8 N_6 Mn O_2	C_{44} H_{20} F_8 N_5 Mn O_3
Mol. wt.	847.03	871.60	873.59
Crystal system	Orthorhombic	Monoclinic	Monoclinic
Space group	C 2221	P 21/n	P 21/c
Temperature /K	293(2)	100.02(18)	293(2)
Wavelength /Å	0.71073	0.71073	0.71073
a /Å	10.3830(8)	11.4272(8)	17.4734(15)
b /Å	21.0166(9)	12.7790(8)	10.9106(5)
c /Å	22.0740(8)	13.0588(7)	26.944(10)
α/°	90.00	90.00	90.00
β/°	90.00	112.456(7)	102.06(2)
γ/°	90.00	90.00	90.00
V/ $Å^3$	4816.9(5)	1762.4(2)	5023(2)
Z	4	2	4

Density/Mgm^{-3}	1.168	1.642	1.155
Abs. Coeff. /mm^{-1}	0.391	0.469	0.330
Abs. correction	Multi-scan	Multi-scan	Multi-scan
F(000)	1704	878	1760
Total no. of reflections	4094	3110	8826
Reflections, $I > 2\sigma(I)$	2809	2462	5279
Max. 2θ/°	25.00	24.99	24.99
Ranges (h, k, l)	-6≤ h ≤ 12 -14 ≤ k ≤ 24 -12 ≤ l ≤ 26	-12≤ h ≤ 13 -13≤ k ≤15 -15≤ l ≤ 9	-13≤ h ≤ 20 -12≤ k ≤12 -30≤ l ≤ 32
Complete to 2θ (%)	99.9	100.0	99.9
Refinement method	Full-matrix least-squares on F^2	Full-matrix least-squares on F^2	Full-matrix least-squares on F^2
Goof (F^2)	1.008	1.084	0.907
R indices [$I > 2\sigma(I)$]	0.0859	0.0603	0.0802
R indices (all data)	0.1114	0.0761	0.1124

Appendix IV

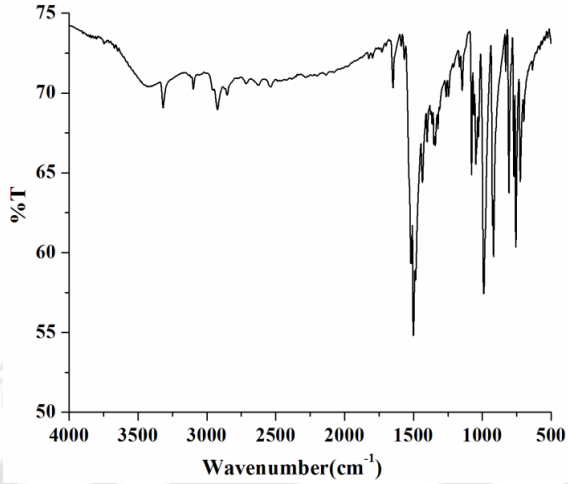

Figure A4.1. FT-IR spectrum of ligand **L3H$_2$** in KBr.

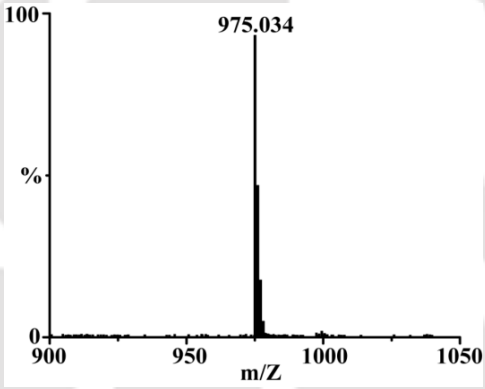

Figure A4.2. ESI-mass spectrum of ligand **L3H$_2$** in acetonitrile.

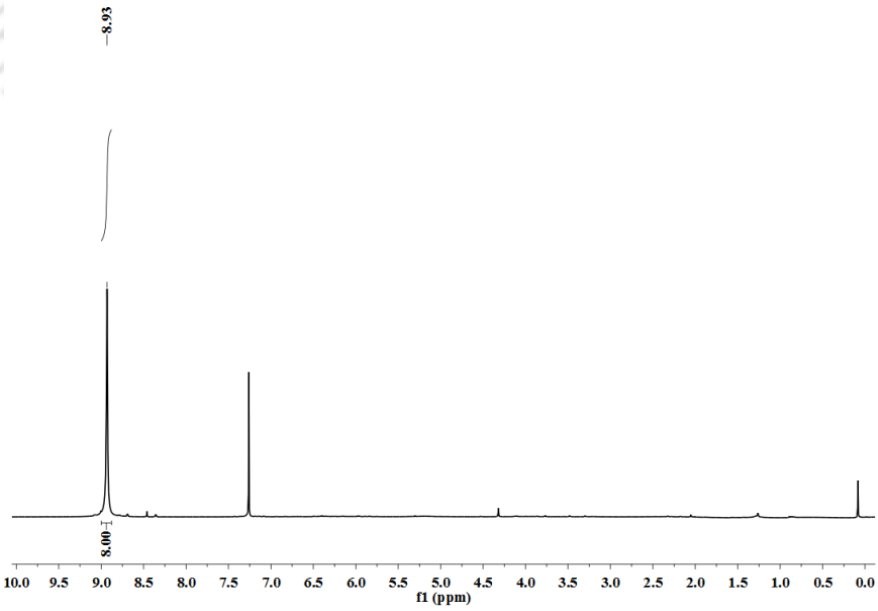

Figure A4.3. ^{1}H NMR spectrum of ligand **L3H$_2$** in $CDCl_3$.

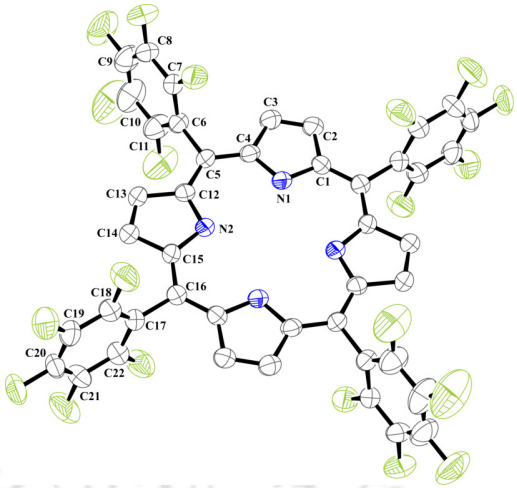

Figure A4.4. ORTEP diagram of ligand **L3H$_2$** (50% thermal ellipsoid plot, H-atoms are omitted for clarity).

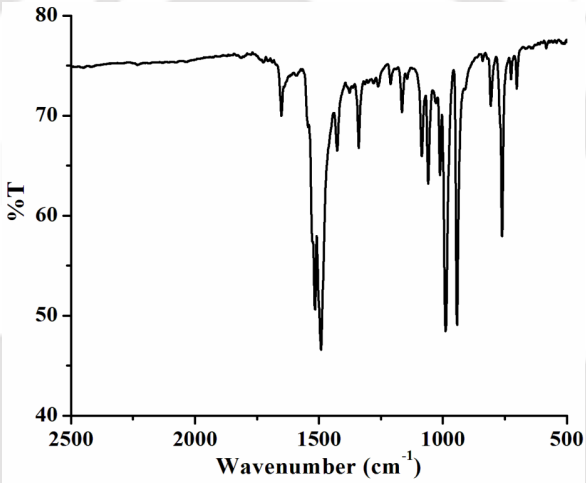

Figure A4.5. FT-IR spectrum of complex **5.1** in KBr.

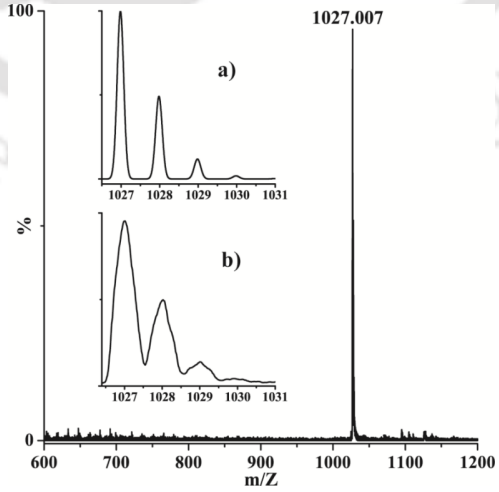

Figure A4.6. ESI-mass spectrum of complex **5.1** in acetonitrile. [Inset: (a) simulated and (b) experimental isotopic distribution pattern].

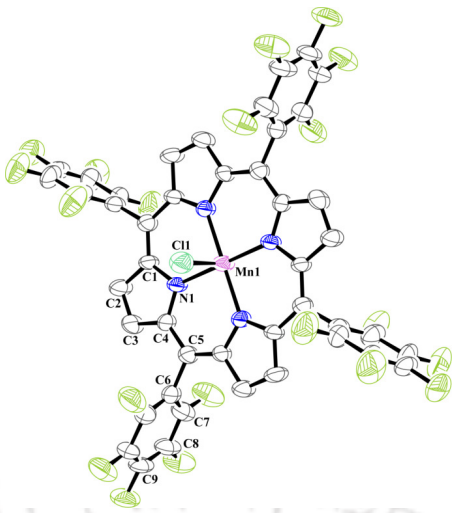

Figure A4.7. ORTEP diagram of complex **5.1** (50% thermal ellipsoid plot, H-atoms are omitted for clarity).

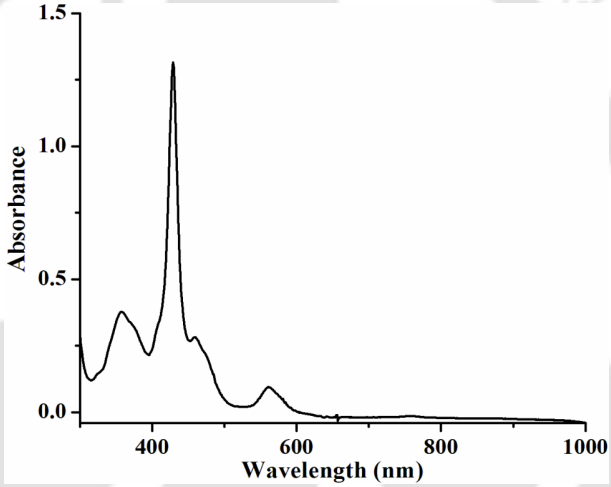

Figure A4.8. UV-visible spectrum of complex **5.1** in THF at room temperature (11.8 μM).

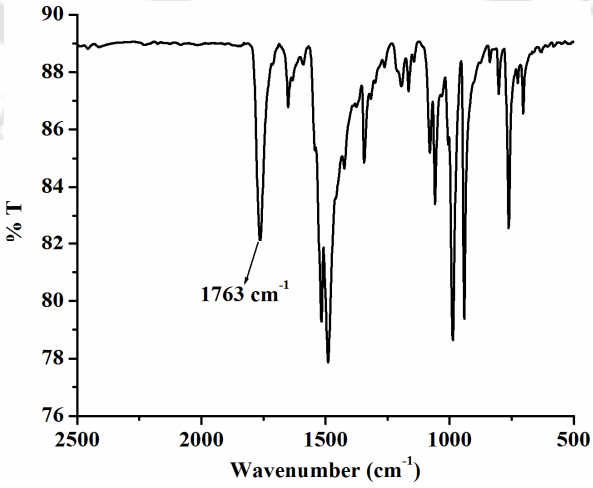

Figure A4.9. FT-IR spectrum of complex **5.2** in KBr.

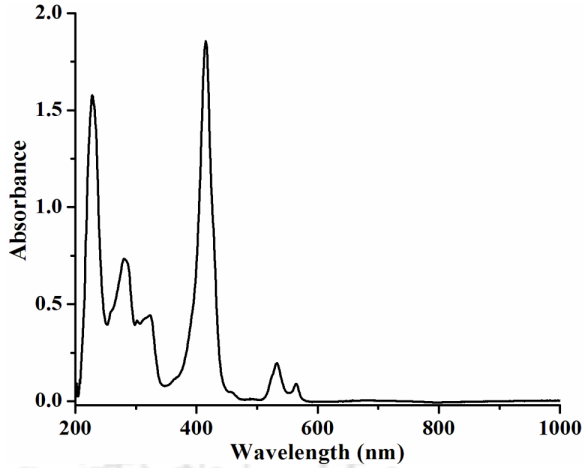

Figure A4.10. UV-visible spectrum of complex **5.2** in THF at −80 °C (17.44 µM).

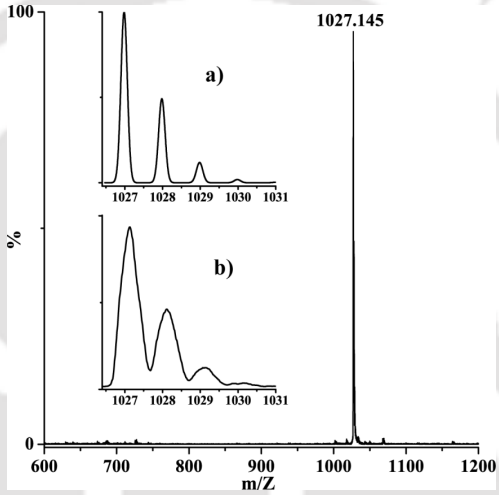

Figure A4.11. ESI-mass spectrum of complex **5.2** in acetonitrile. [Inset: (a) simulated and (b) experimental isotopic distribution pattern].

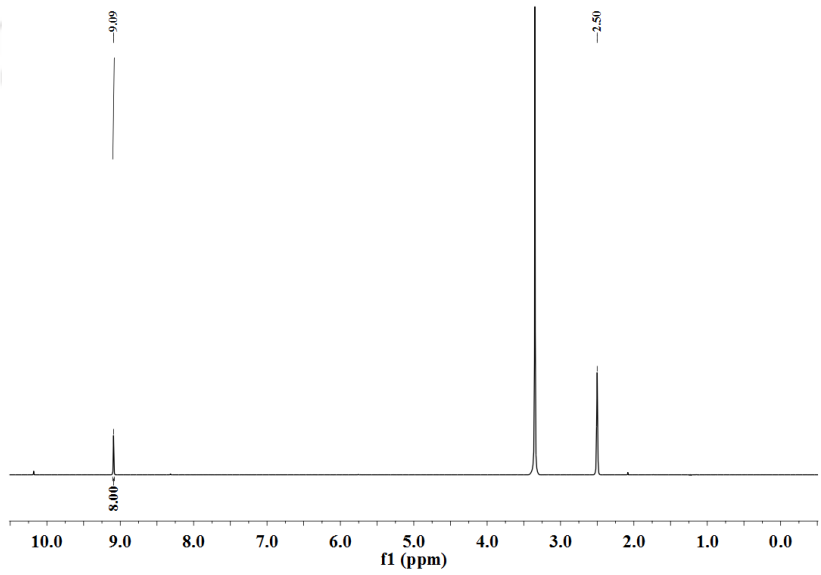

Figure A4.12. ^{1}H NMR spectrum of complex **5.2** in DMSO-d_6.

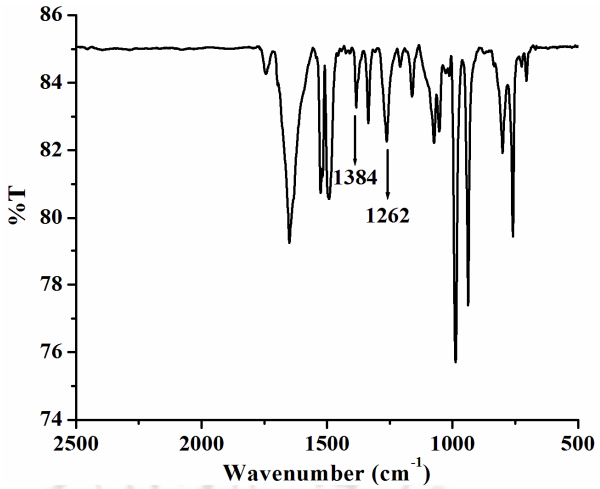

Figure A4.13a. FT-IR spectrum of complex **5.3** in KBr.

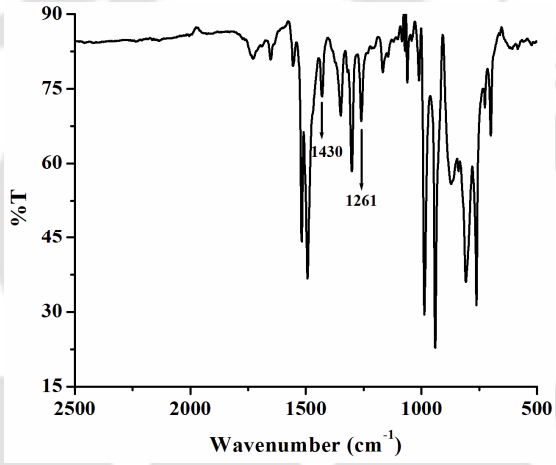

Figure A4.13b. Solution FT-IR spectrum of complex **5.3** in THF at room temperature.

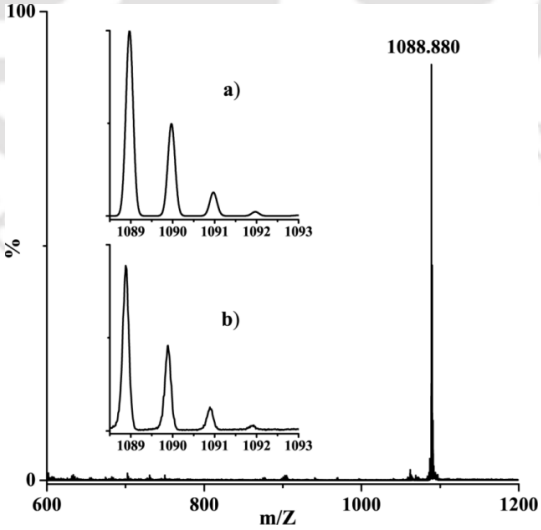

Figure A4.14. ESI-mass spectrum of complex **5.3** in acetonitrile. [Inset: (a) simulated and (b) experimental isotopic distribution pattern].

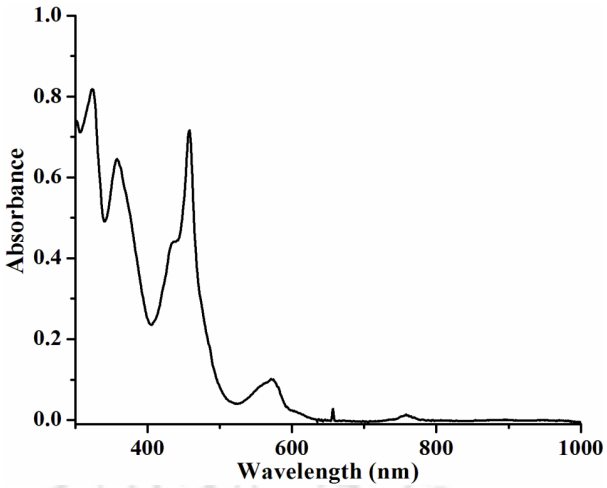

Figure A4.15. UV-visible spectrum of complex **5.3** in THF at −80 °C (13.08 µM).

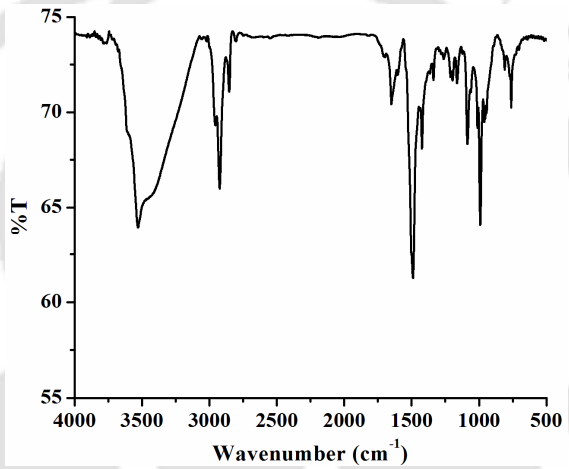

Figure A4.16. FT-IR spectrum of complex **5.4** in KBr.

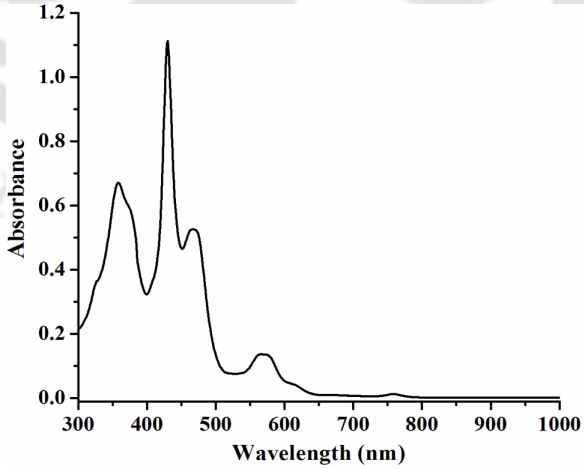

Figure A4.17. UV-visible spectrum of complex **5.4** in THF at room temperature (31.77 µM).

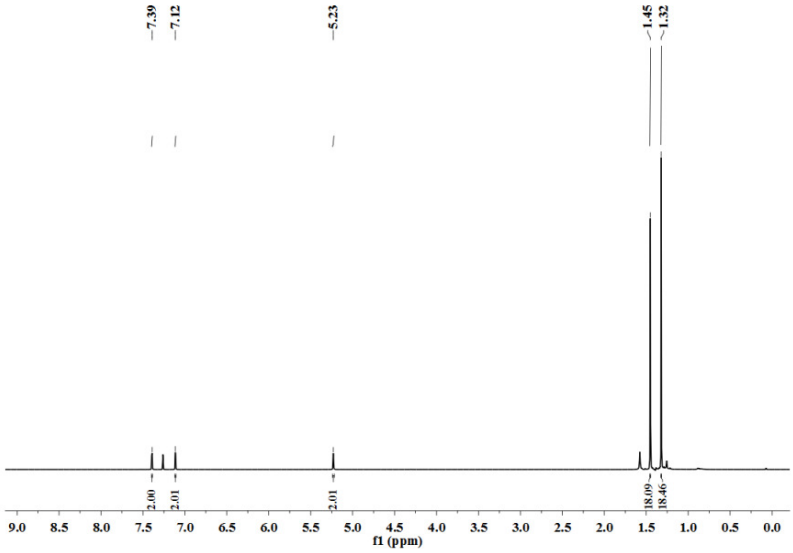

Figure A4.18. ^{1}H NMR spectrum of 3,3',5,5'-tetra-*tert*-butyl-[1,1'-biphenyl]-2,2'-diol in $CDCl_3$.

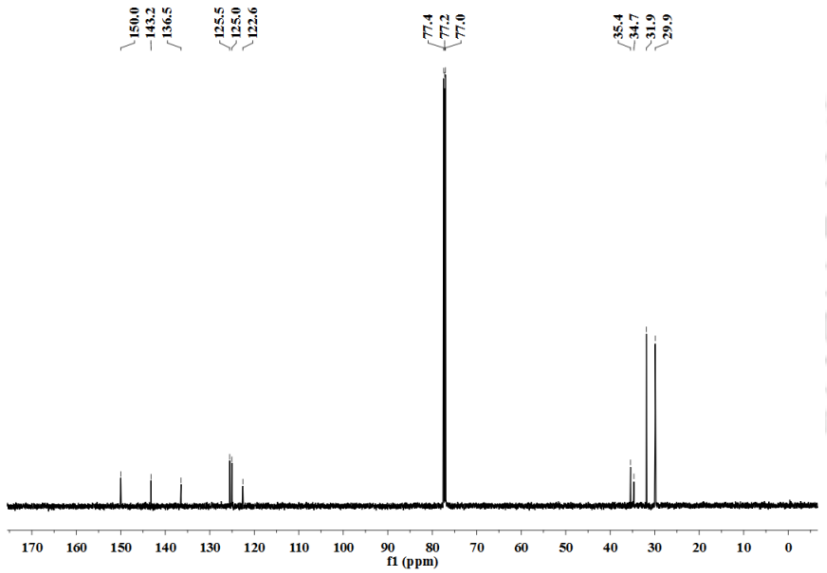

Figure A4.19. ^{13}C NMR spectrum of 3,3',5,5'-tetra-*tert*-butyl-[1,1'-biphenyl]-2,2'-diol in $CDCl_3$.

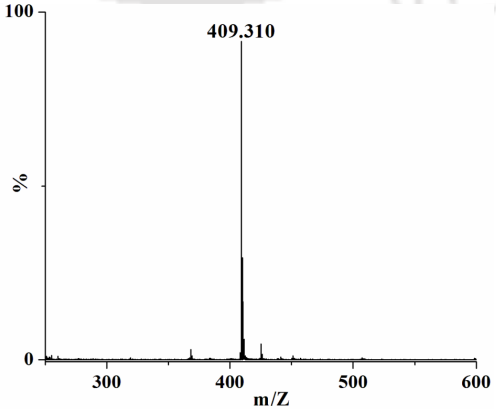

Figure A4.20. ESI-mass spectrum of 3,3',5,5'-tetra-*tert*-butyl-[1,1'-biphenyl]-2,2'-diol in acetonitrile.

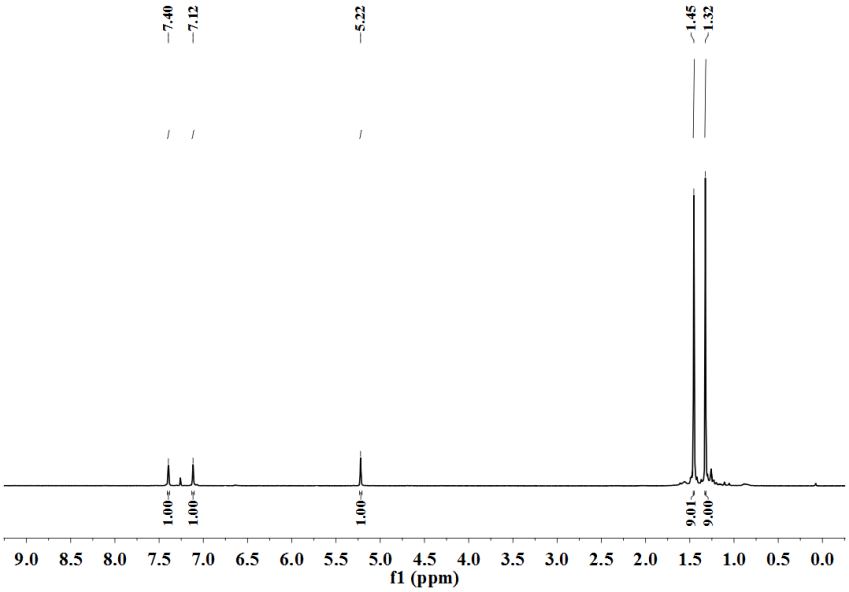

Figure A4.21. ^{1}H NMR spectrum of 2,4-di-*tert*-butyl-6-nitrophenol in $CDCl_3$.

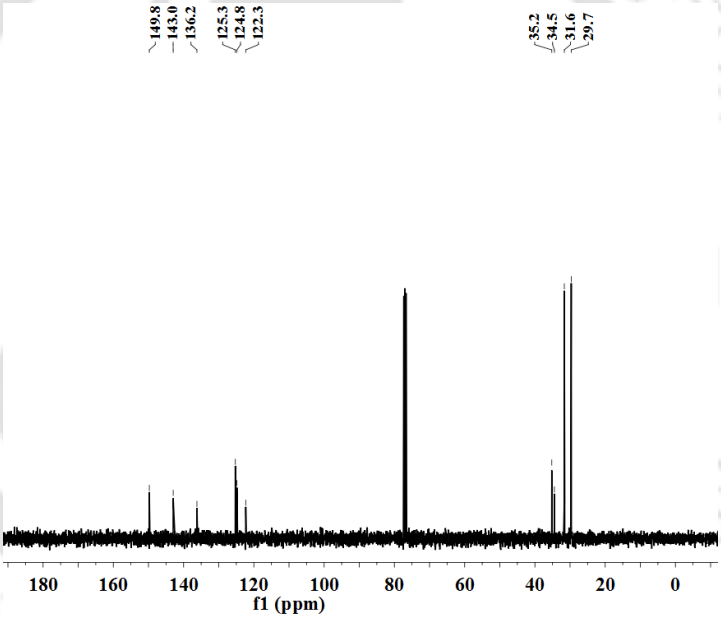

Figure A4.22. ^{13}C NMR spectrum of 2,4-di-*tert*-butyl-6-nitrophenol in $CDCl_3$.

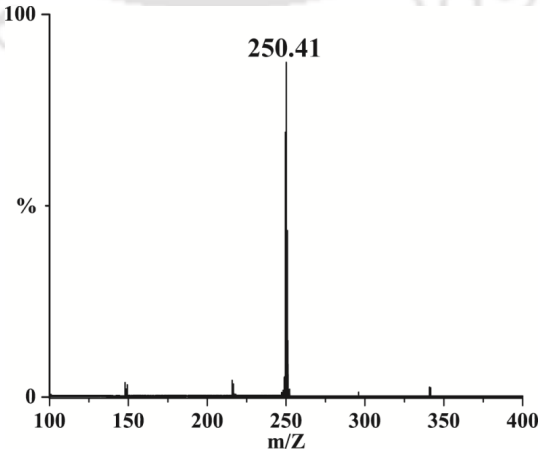

Figure A4.23. ESI-mass spectrum of 2,4-di-*tert*-butyl-6-nitrophenol in methanol.

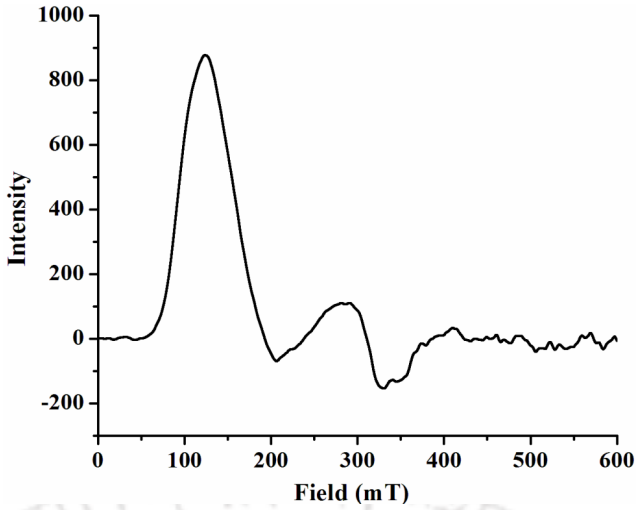

Figure A4.24. X-band EPR spectrum of [(L3)$Mn^{IV}O$] prepared in the reaction of complex **5.1** and *m*CPBA in THF at 77K.

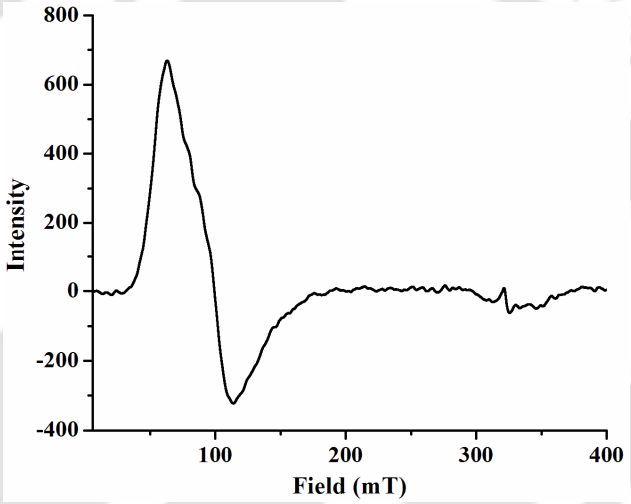

Figure A4.25. X-band EPR spectrum of [Mn^{II}(L3)] in THF at 77K. (g = 6.19, 2.02)

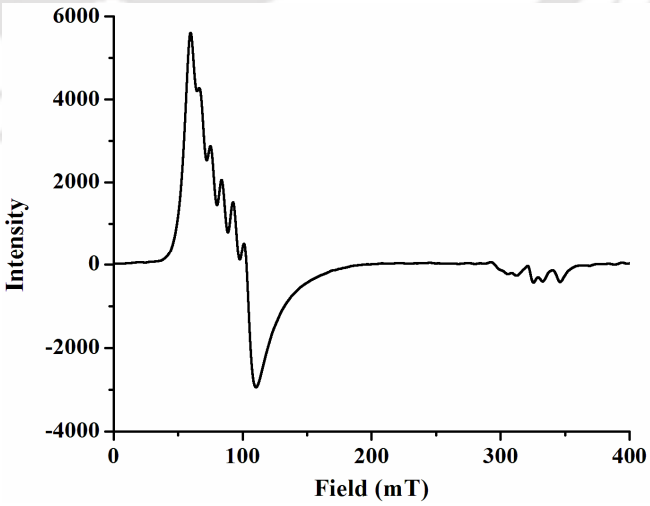

Figure A4.26. X-band EPR spectrum of [Mn^{II}(L3)] in acetonitrile at 77K. (g = 6.05, 2.00)

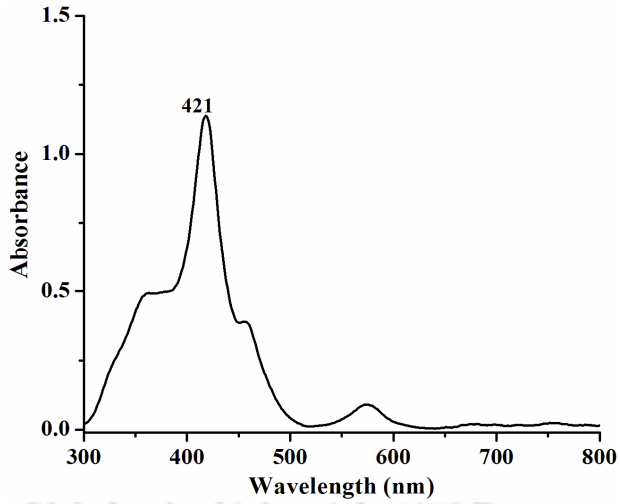

Figure A4.27. UV-visible spectrum of [(L3)$Mn^{IV}O$] generated during the reaction between complex **5.1** and *m*CPBA in THF at −80 °C.

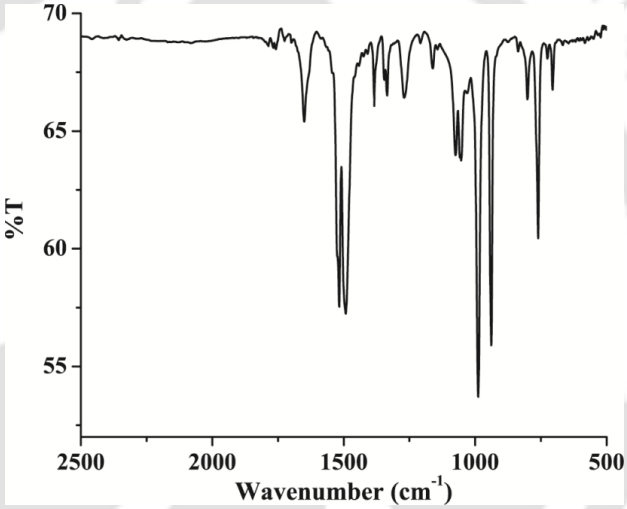

Figure A4.28. FT-IR spectrum of complex **5.3** formed in the reaction of [(L3)$Mn^{IV}O$] and NO_2 in KBr.

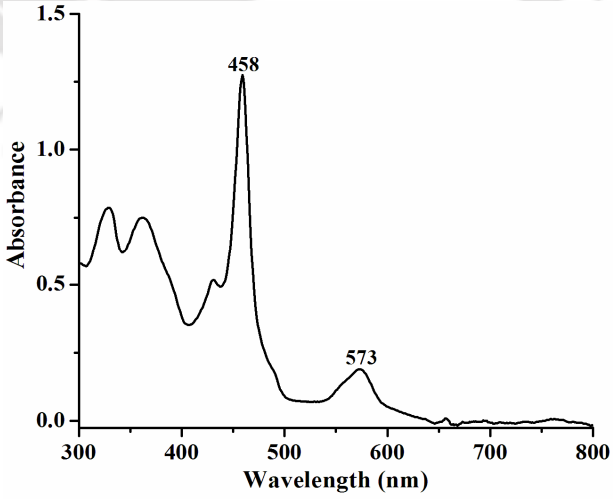

Figure A4.29. UV-visible spectrum of complex **5.3** formed in the reaction of [(L3)$Mn^{IV}O$] and NO_2 in THF at −80 °C.

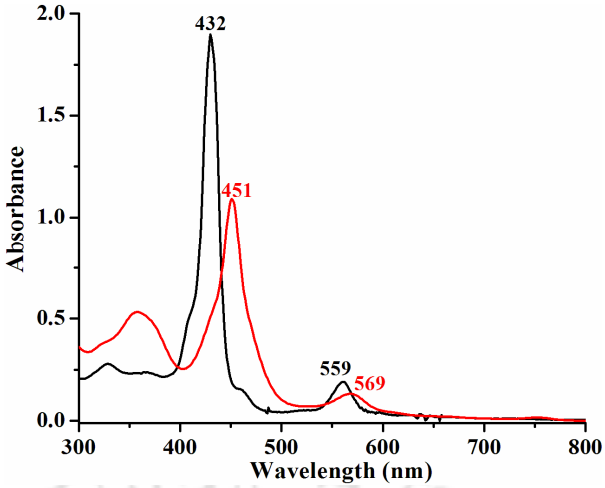

Figure A4.30. UV-visible spectra of [Mn^{II}(L3)] (black) and after addition of KO_2 (red) in THF at −80 °C.

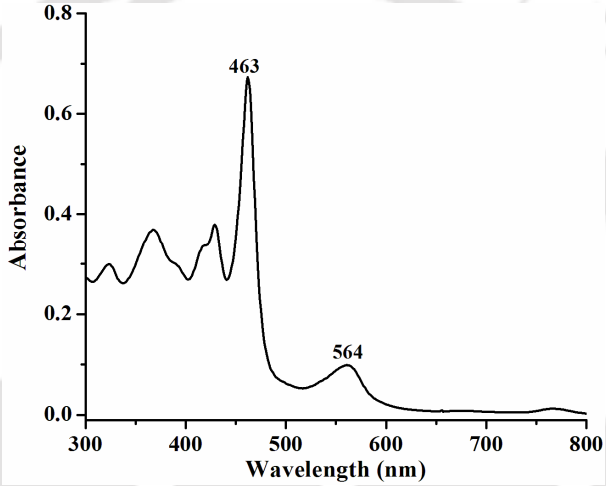

Figure A4.31. UV-visible spectrum of [Mn^{II}(L3)(Piperazine)(NO)] in THF at room temperature.

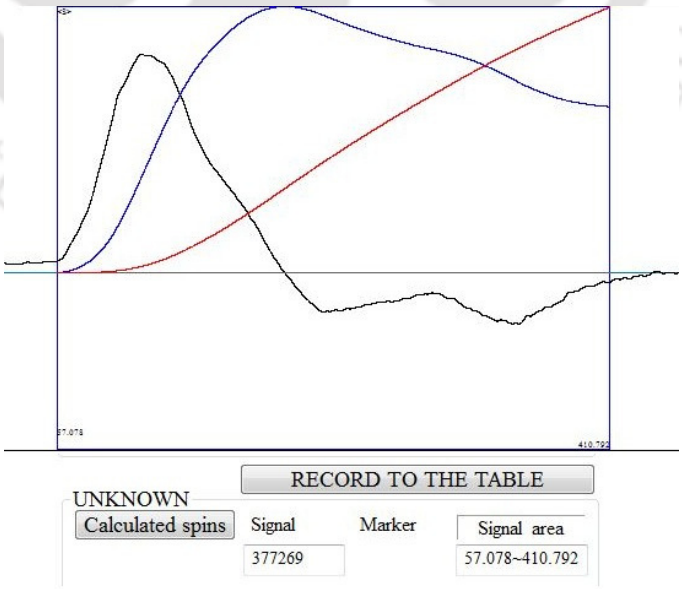

Figure A4.32a. Double integration of X-band EPR spectrum of the intermediate formed during the reaction between complex **5.2** and KO_2 in THF at 77K.

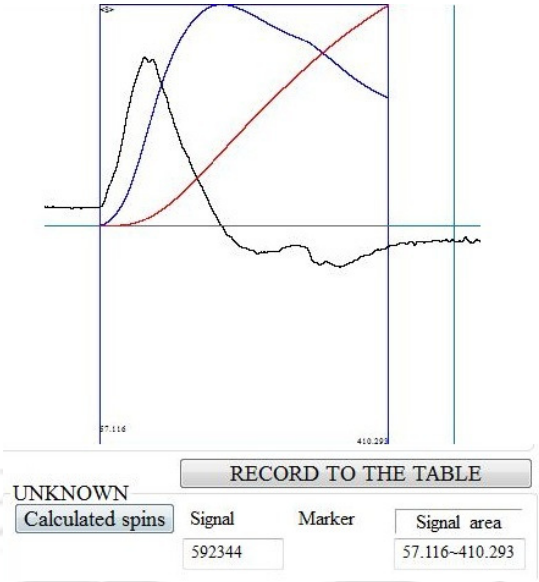

Figure A4.32b. Double integration of X-band EPR spectrum of [Mn^{IV}(L3)(O)] prepared in the reaction of complex **5.1** and *m*CPBA in THF at 77K.

Table A4.1. Crystallographic data for ligand **$L3H_2$**, complexes **5.1** and **5.2**

	$L3H_2$	**5.1**	**5.2**
Formulae	C_{44} H_{10} F_{20} N_4	C_{44} H_8 Cl F_{20} N_4 Mn	C_{48} H_{16} Cl_8 F_{20} N_6 O_2 Mn
Mol. wt.	974.56	1062.93	1427.21
Crystal system	Trigonal	Tetragonal	Tetragonal
Space group	R -3:H	I 4/m	I 4/m
Temperature /K	293(2)	293(2)	101(1)
Wavelength /Å	0.71073	0.71073	0.71073
a /Å	20.3568(13)	17.639(3)	16.8084(4)
b /Å	20.3568(13)	17.639(3)	16.8084(4)
c /Å	24.4679(14)	9.583(2)	9.5523(4)
α/°	90.00	90.00	90.00
β/°	90.00	90.00	90.00
γ/°	120.00	90.00	90.00
V/ $Å^3$	8781.0(12)	2981.6(12)	2698.74(17)
Z	9	2	2
Density/Mgm^{-3}	1.659	1.184	1.756
Abs. Coeff. /mm^{-1}	0.166	0.357	0.757
Abs. correction	Multi-scan	Multi-scan	Multi-scan
F(000)	4338	1044	1406
Total no. of reflections	3531	1399	1259
Reflections, $I > 2\sigma(I)$	1946	570	1126
Max. 2θ/°	25.234	24.983	24.996

Ranges (h, k, l)	-22 ≤ h ≤24 -11≤ k ≤21 -22≤ l ≤ 29	-20 ≤ h ≤ 17 -20 ≤ k ≤ 20 -11 ≤ l ≤ 6	-10 ≤ h ≤19 -9 ≤ k ≤19 -10 ≤ l ≤ 11
Complete to 2θ (%)	99.9	99.9	99.9
Refinement method	Full-matrix least-squares on F^2	Full-matrix least-squares on F^2	Full-matrix least-squares on F^2
Goof (F^2)	1.071	1.164	1.032
R indices [$I > 2\sigma(I)$]	0.0640	0.1247	0.0477
R indices (all data)	0.1244	0.1689	0.0535

Table A4.2. Selected bond lengths (Å) of ligand **L3H$_2$**, complexes **5.1** and **5.2**

Atoms	**L3H$_2$**	**5.1**	**5.2**
Mn1–N1	-	2.021(9)	2.028(3)
Mn1–N2	-	-	1.873(5)
N2–O1	-	-	1.132(10)
C1-N1	1.373(4)	1.414(13)	1.381(5)
C1–C2	1.426(5)	1.474(15)	1.455(5)
C3-C4	1.435(5)	1.427(15)	1.440(5)
C4-C5	1.392(5)	1.428(15)	1.402(5)
C5-C6	1.502(5)	1.545(16)	1.503(5)
C7-F1	1.341(4)	1.343(12)	1.348(3)

Table A4.3. Selected bond angles (˚) of ligand **L3H$_2$**, complexes **5.1** and **5.2**

Atoms	**L3H$_2$**	**5.1**	**5.2**
N1–Mn1–N1	-	90.0 (1)	180.0(17)
N1–Mn1–N2	-	-	90.0
Mn1-N2-O1	-	-	180.0
Mn1-N1-C1	-	125.9(7)	127.0(2)
N1-C1-C2	107.0(3)	110.1(9)	110.0(3)
C1-C2-C3	108.1(3)	105.1(10)	106.6(3)
C2-C3-C4	108.6(3)	108.3(11)	107.3(3)
C4-C5-C6	115.3(3)	114.7(9)	117.5(3)
F1-C7-C6	118.7(4)	121.7(8)	119.6(2)

List of Publications

(1) "Reaction of a nitrosyl complex of cobalt-porphyrin with hydrogen peroxide: Putative formation of peroxynitrite intermediate".

Saha, S.; Gogoi, K.; **Mondal, B.**; Ghosh, S.; Deka, H.; Mondal, B. *Inorg. Chem.* **2017**, *56,* 7781.

(2) "Reaction of a Co(III)-peroxo complex and NO: Formation of a putative peroxynitrite intermediate".

Saha, S.; Ghosh, S.; Gogoi, K.; Deka, H.; **Mondal, B.**; Mondal, B. *Inorg. Chem.* **2017**, *56*, 10932.

(3) "Dioxygenation reaction of a cobalt-nitrosyl: Putative formation of a cobalt–peroxynitrite via a $\{Co^{III}(NO)(O_2^{\bullet})\}$ intermediate".

Gogoi, K.; Saha, S.; Ghosh, S.; Deka, H.; **Mondal, B.**; Mondal, B. *Inorg. Chem.* **2017**, *56*, 14438.

(4) "Nitric Oxide Dioxygenase Activity of a Nitrosyl Complex of Cobalt(II) Porphyrinate in the Presence of Hydrogen Peroxide via Putative Peroxynitrite Intermediate".

Mondal, B.; Saha, S.; Borah, D.; Mazumdar, R.; Mondal, B. *Inorg. Chem.* **2019**, *58,* 1234.

(5) "Nitric Oxide dioxygenase activity of a nitrosyl complex of Mn(II)-porphyrinate in presence of superoxide: Formation of a Mn(IV)-oxo species through a putative peroxynitrite".

Mondal, B.; Borah, D.; Mazumdar, R.; Mondal, B. *Inorg. Chem.* **2019**, 00, 0000.

(6) "Reaction of a Nitrosyl Complex of Mn(II)-F_8TPP with Superoxide: Putative Formation of Peroxynitrite Intermediate".

Mondal, B.; Mondal, B. (communicated)